OCTOBER 1958 VOLUME 3 (1958) No. 4

GREGG M. SINCLAIR LIBRARY
UNIVERSITY OF HAWAII
8-7-63

NUCLEAR INSTRUMENTS

A JOURNAL ON ACCELERATORS, INSTRUMENTATION AND TECHNIQUES IN NUCLEAR PHYSICS

EDITOR: K. SIEGBAHN - UPPSALA

CONTENTS

GERALD A. BEHMAN, List of particle accelerator installations 181
A. ALBERIGI, C. BERNARDINI and I. F. QUERCIA, Proposal for an analog-to-digital electronic converter suited for nuclear pulse height analysis 201
WOLFGANG GRUHLE, Schneller Ringzähler als elektronischer Schalter 204
J. A. NORTHROP and JUDITH C. GURSKY, Relative scintillation efficiencies of noble gas mixtures 207
E. HUSTER und W. RAUSCH, Zur Herstellung sehr dünner elektrisch leitender Präparat-Unterlagen für absolute β-Zählung 213
U. FARINELLI, F. FERRERO and R. MALVANO, Measurement and automatic control of the energy of a 31 MeV betatron 218
G. CAGLIOTI, A. PAOLETTI and F. P. RICCI, Choice of collimators for a crystal spectrometer for neutron diffraction 223
N. E. BOOTH, F. L. HEREFORD and G. W. HUTCHINSON, Internally reflecting Čerenkov counter for high energy protons 229
R. L. CLARKE, New type of angular-distribution chamber 233
P. OHLIN, K. SIEGBAHN, T. SUNDSTRÖM and S. SVENNERSTEDT, Studies of neutron production in linear deuterium pinches 237

NORTH-HOLLAND PUBLISHING COMPANY - AMSTERDAM

NUCLEAR INSTRUMENTS

A journal on accelerators, instrumentation and techniques in nuclear physics

EDITOR: K. SIEGBAHN, UPPSALA

EDITORIAL BOARD:

J. B. ADAMS (CERN)
E. AMALDI (Rome)
H. L. ANDERSON (Chicago)
K. T. BAINBRIDGE (Cambridge, Mass.)
C. J. BAKKER (CERN)
P. R. BELL (Oak Ridge)
R. E. BELL (Montreal)
A. BERTHELOT (Saclay)
H. BRINKMAN (Groningen)
E. H. COOKE-YARBOROUGH (Harwell)
S. DE BENEDETTI (Pittsburgh)
M. DE HEMPTINNE (Louvain)
A. DE-SHALIT (Rehovoth)
M. DEUTSCH (Cambridge, Mass.)
S. DU TOIT (Pretoria)
B. S. DŽELEPOV (Leningrad)
W. GENTNER (CERN)
P. C. GUGELOT (Amsterdam)
H. HALBAN (Paris)
O. HAXEL (Heidelberg)
P. HUBER (Basel)
D. J. HUGHES (Brookhaven)
S. KIKUCHI (Tokyo)
J. KOCH (Copenhagen)
M. S. KOZODAEV (Moscow)
S. LIVINGSTON (Cambridge, Mass.)
E. M. MCMILLAN (Berkeley)
M. G. MEŠČERJAKOV (Moscow)
P. B. MOON (Birmingham)
M. L. OLIPHANT (Canberra)
W. PAUL (Bonn)
A. S. RAO (Bombay)
G. SALVINI (Rome)
P. SAVIĆ (Belgrade)
P. SCHERRER (Zürich)
CH. SCHMELZER (CERN)
H. W. B. SKINNER (Liverpool)
R. TANGEN (Blindern)
D. TAYLOR (Harwell)
V. I. VEKSLER (Moscow)
O. WERNHOLM (Stockholm)
G. VON DARDEL (CERN)
R. R. WILSON (Cornell)
S. D. WINTER (Saclay)

Contributions may be sent to the Editor, Professor K. Siegbahn, Institute of Physics, the University of Uppsala, either directly or through the intermediary of one of the members of the Editorial Board of the country of region in which the author is working. Contributions may be written in English, French or German, with an abstract in English.

Books for review should be sent to Professor Siegbahn.

Nuclear Instruments is published monthly. The subscription price of a volume of 360 pages is $ 17.00 (130 s), postage free.

Subscriptions should be sent to the publishers, North-Holland Publishing Company, P.O.Box 103, Amsterdam or to any subscription-agent.

No part of this issue may be reproduced in any form, by print, photoprint, microfilm or any other means without written permission from the publisher. Reprints, photoprints or microfilms are obtainable at cost from the publisher.

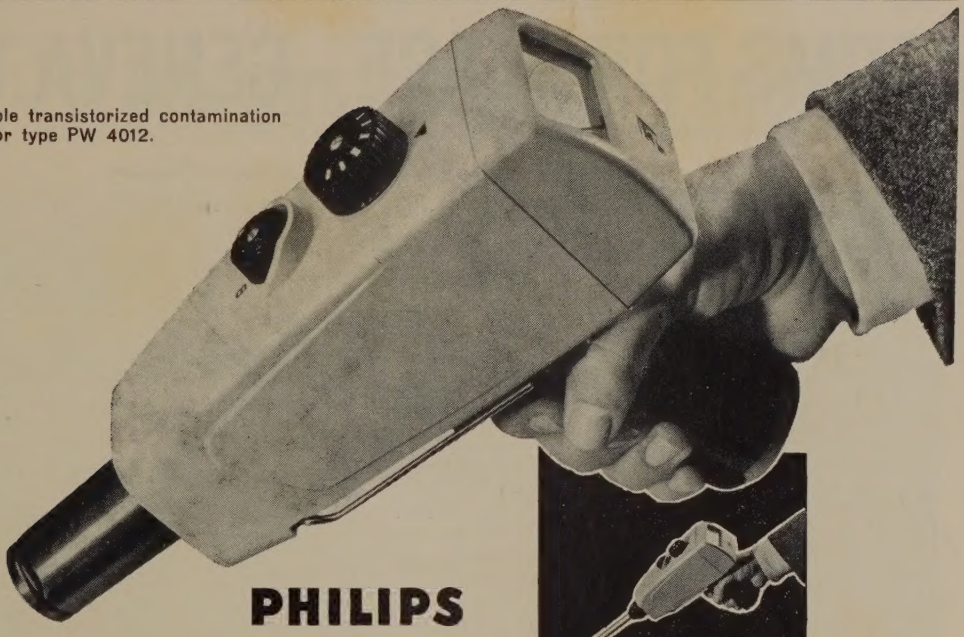

Portable transistorized contamination monitor type PW 4012.

PHILIPS

equipment for Nuclear Physics and Atomic Energy

This rugged, watertight and tropicallized battery-operated instrument incorporating the Philips G.M. counter tube type 18503 has been designed for the detection and measurement of radio-activity in such applications as:

- General radiation intensity checks in isotope laboratories, around isotope containers etc.
- Contamination checks of benches and apparatus.
- Radiation exposure measurements of personnel working with isotopes or X-rays.

It incorporates the following features:

- Three measuring ranges resp. 0-1, 0-10 and 0-100 mr/h (Ra γ).
- Compensation for voltage drop during battery life ensures maintenance of accuracy.
- Provision to insert probe extension.
- Beta sensitive G.M. tubes 18504 (2-3 mgr/cm²) and 18505 (1.5-2 mgr/cm²) can be used as well.
- Large, easy readable and shock-proof measuring instrument.

PW 4012
with probe extension.

- Synchro-cyclotrons for various final energies.
- Cockcroft-Walton accelerators.
- Generators for very high d.c. voltages.
- Linear electron accelerators.
- Reactor control instrumentation
- Radiation measuring and detection equipment.
- Civil defence instruments.
- Area monitoring instrumentation.
- Geiger counter tubes.
- Photomultipliers.
- Radio-active isotopes.
- Air & gas liquefiers.

PHILIPS

Nuclear Equipment

For further information please apply to:

N.V. PHILIPS' GLOEILAMPENFABRIEKEN,
Scientific Equipment Department, Eindhoven-Holland
RESEARCH & CONTROL INSTRUMENTS LTD.
Instrument House, 207/215, King's Cross Road, London WC 1

PHILIPS

NZO

ATOMS FOR PEACE - GENEVA 1958

The **"Presentation Set"** given to official delegates at Geneva by the U.S.A.

JUST PUBLISHED by Addison-Wesley

PROJECT SHERWOOD – THE U.S. PROGRAM IN CONTROLLED FUSION
By Amasa S. Bishop, *U.S. Atomic Energy Commission*

The first detailed account of "Project Sherwood"—the search for means of harnessing the energy of thermonuclear reactions. Written for the thoughtful layman as well as for scientists and engineers, this book parallels the historic "Smyth Report." 228 pp, 53 illus, 1958 — $ 5.75

U.S. RESEARCH REACTOR OPERATION AND USE
Edited by Joel W. Chastain, Jr., *Battelle Memorial Institute*

Describes the basic types of research reactors, and the uses for which each is best suited; also discusses operating, administrative, legal and cost problems. 384 pp, 181 illus, 1958 — $ 7.50

RADIATION BIOLOGY AND MEDICINE: Selected Reviews in the Life Sciences
Edited by Walter D. Claus, *U.S. Atomic Energy Commission*

More than 50 distinguished authors review advances in the uses and effects of nuclear radiation in biology, medicine, and agriculture. Among the topics covered are radioisotopes in medicine and agriculture, mutations permissible dosages, and mathematical biology. 968 pp, 198 illus, 1958 — $ 11.50

URANIUM ORE PROCESSING. Edited by J. W. Clegg and D. D. Foley, *Battelle Memorial Institute*

For the first time in book form, a condensed but essentially complete description of current practices in the winning of uranium from its ores. 450 pp, 118 illus, 1958 — $ 7.50

THORIUM PRODUCTION TECHNOLOGY. By F. L. Cuthbert, *National Lead Company of Ohio*

Contains virtually all of the information currently available on thorium production technology. The organization of the book follows the natural production flow from minerals in the ground to the fabricated slug. 320 pp, 84 illus, 1958 — $ 6.50

SOLID FUEL REACTORS. By J. R. Dietrich and W. H. Zinn, *General Nuclear Engineering Corporation*

Reviews the basic concepts, present state of development, and technical and economic outlooks of five projected solid fuel nuclear power reactor types; fast-neutron power breeders, heavy-water reactors, gas-cooled reactors, organic moderated and cooled reactors, and a thermal reactor for recycling plutonium. 864 pp, 385 illus, 1958 — $ 10.75

PHYSICAL METALLURGY OF URANIUM
By A. N. Holden, *General Electric Company, Vallecitos Atomic Laboratory*

A comprehensive and unified treatment which places emphasis upon interpretation in terms of fundamental properties and mechanisms, and relates the metallurgical behavior of uranium to that of other metals. 272 pp, 190 illus, 1958 — $ 5.75

BOILING WATER REACTORS. By Andrew W. Kramer, Editor, *Atomics* and formerly Editor, *Power Engineering*

This valuable reference work on the history and technology of boiling water reactors includes detailed descriptions of the Experimental Boiling Water Reactor (EBWR), the Vallecitos reactor, and the various BORAX experiments. 592 pp, 292 illus, 1958 — $ 8.50

FLUID FUEL REACTORS
Edited by J. A. Lane and H. G. MacPherson, *Oak Ridge National Laboratory*, and Frank Maslan, *Brookhaven National Laboratory*

A through treatment of three basic types of fluid fuel reactors; aqueous homogeneous reactors, fused salt systems, and liquid metal fuel reactors. 1008 pp, 338 illus, 1958 — $ 11.50

THE TRANSURANIUM ELEMENTS. By Glenn T. Seaborg, *University of California*

This book provides a complete summary of the chemical and nuclear properties of the known synthetic transuranium elements, as well as the prospects for future elements. 354 pp, 73 illus, 1958 — $ 7.00

SODIUM GRAPHITE REACTORS. By Chauncey Starr and R. W. Dickinson, *Atomics International*

A unified and coherent presentation of sodium graphite reactor technology. While emphasis has been placed on the design and development of the Sodium Reactor Experiment (SRE), the authors have wherever possible included information applicable to sodium graphite systems and, in many cases, to reactor design in general. 304 pp, 99 illus, 1958 — $ 6.50

THE SHIPPINGPORT PRESSURIZED WATER REACTOR
Written by personnel of the *Naval Reactor Branch, Division of Reactor Development, U.S. Atomic Energy Commission; Westinghouse Electric Corp., Bettis Plant; and Duquesne Light Company*

A complete account of the first large-scale central station nuclear power plant to be built and operated in the western hemisphere, written by the scientists and engineers who designed, developed, constructed, and tested the plant. 600 pp, 163 illus, 1958 — $ 9.50

Special price for complete set of 12 volumes – $84.00

These prepublication prices good only until December 1, 1958

A-W Representative, Continental Europe: W. S. HALL & Co. - 696 Keizersgracht, Amsterdam

ADDISON-WESLEY PUBLISHING COMPANY, INC.
READING, MASSACHUSETTS, U.S.A.

New- a low cost neutron generator

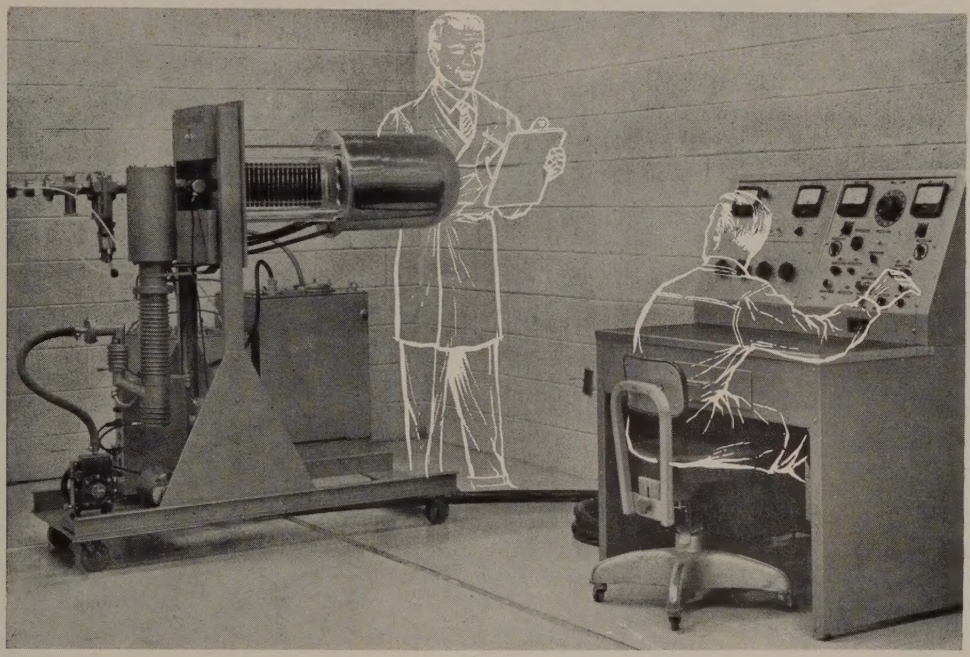

Facts and Features:

Output up to 10^{10} neutrons/sec continuous, Remote Operation, Mobile, No special building facilities required, Easily operated and maintained.

Designed for...

- **Activation Analysis**
- **Neutron Scattering and Nuclear Reaction Research**
- **Radiation damage studies**
- **Biological Studies**
- **Training of Nuclear Scientists**
- **Instrument calibration**
- **Well Logging Research**
- **Model 100-I pictured at left, complete with targets and installed, $ 20,000. F.O.B, Austin.**

For further information, write:

TEXAS NUCLEAR CORPORATION

P. O. BOX 9267 • AUSTIN 17, TEXAS

INTERNATIONAL

advertise

YOUR NUCLEAR PRODUCTS IN

sell

YOUR NUCLEAR PRODUCTS

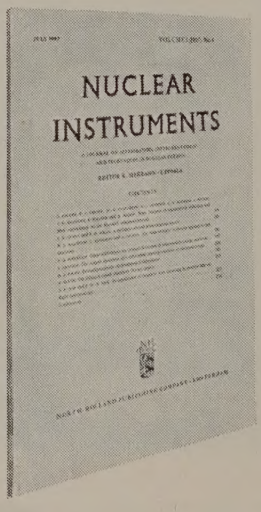

reap

YOUR NUCLEAR SALES
REWARDS

world wide

KEY NUCLEAR MANAGEMENT
NUCLEAR SCIENTISTS
NUCLEAR ENGINEERS
NUCLEAR PRODUCTION
PERSONNEL

SUBSCRIBE TO

you reach

THE WHOLE
NUCLEAR SALES WORLD IN

Entirely international in scope Nuclear Instruments is the one nuclear scientific journal that has an established subscription clientele through-out the whole world-where-ever nuclear men are at work—they want your nuclear products—they need your nuclear products—advertise in Nuclear Instruments and tell them WHAT – HOW – WHERE they can get your nuclear products

GO INTERNATIONAL WITH YOUR SALES PROGRAM TODAY WRITE

WILLIAM F. BAARS - ADVERTISING MANAGER NORTH-HOLLAND PUBLISHING COMPANY

P.O. BOX 103 – AMSTERDAM, HOLLAND

INTERNATIONAL

MARSHALL

PULSE HEIGHT ANALYSER

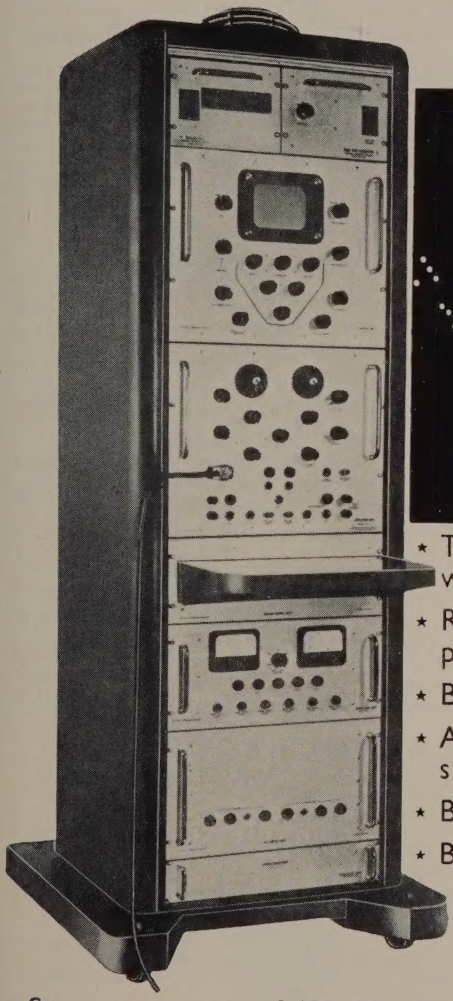

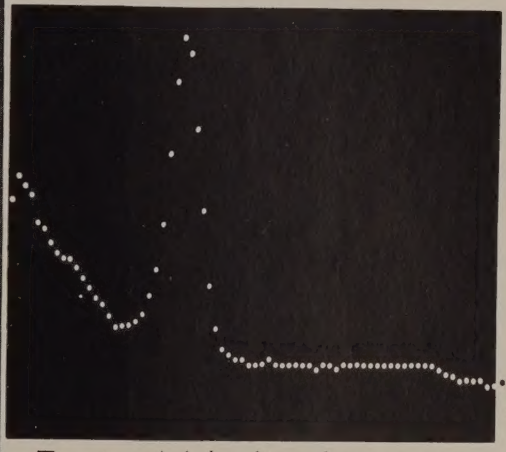

* Torsional delay line data storage with computor reliability.
* Resolution constant or proportional to amplitude.
* Background subtraction.
* Analysis of pulses of either sign from 1 mV to 50 V.
* Binary and decimal storage.
* Both digital and analogue display.

* Storage capacity 2400 digits.
* Analogue readout and automatic printout using either adding machine or electric typewriter.
* High stability and linearity.
* Total count scaler.
* Accurate live time integrator.
* Built-in precision test pulse generator.

MARSHALL
THE AIRPORT CAMBRIDGE, ENGLAND
TELEPHONE CAMBRIDGE 56291 TELEGRAMS AND CABLES MARFLY CAMBRIDGE

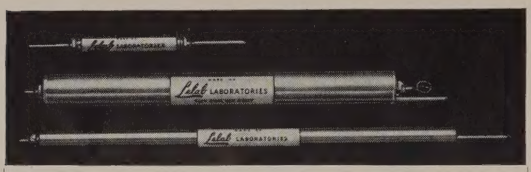

LELAB METAL-WALLED G-M TUBES

for anti-coincidence applications where uniformity counts !

Lelab Counter Tubes are individually constructed, filled, and tested. Each is fabricated almost entirely of metal. All components are confined within the diameter of the tube shell to permit close stacking.

Compare our low prices on these superior tubes!

(Makers of Lelab [Robinson-Selverstone Type] Probe Counters for neurosurgery and where a fine needle-like probe for highly localized measurements is useful.)

Write for complete information

H. W. Leighton Laboratories

York & Sunset Lane-Hatboro, Pa. U.S.A.

MODEL 412 MERCURY RELAY

PRECISION SLIDING PULSER

for Precise Calibration of Single & Multi-Channel Pulse Height Analyzers

Determines Window Widths Using Principle of *Constant Angular Velocity* — **AUTOMATICALLY** **10 × more accurately** **40 × faster than conventional pulsers**

Incorporates Both Manual Control and Precision Motor Drive

Simulates Pulses from Scintillation, Proportional or Geiger Counters

RISE TIME—Less than .003 usec.

DECAY TIME CONSTANT—1, 10, 100, 350, usec.

LINEARITY—0.1% 10 turn potentiometer with 5″ dial.

CALIBRATION—Self contained standard cell and null balance circuit for precision adjustment.

MERCURY PULSER, Model 401

Featuring Versatility and Precision

Specifically designed for the Nuclear Physics Laboratory

RISE TIME—Less than .003usec

DECAY TIME CONSTANT—1, 10, 100 usec

Fast rise and exponential decay simulates scintillation, proportional or geiger counter pulses for test and calibration of amplifiers, pulse height analyzers, scalers, etc.

MODEL 412 . . . $450.00 — MODEL 401 . . . $125.00

RADIATION INSTRUMENT CO.

P. O. BOX 733, SILVER SPRING, MARYLAND, U.S.A.

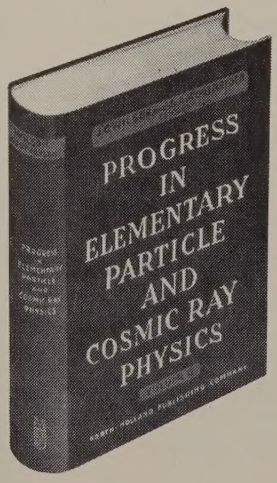

PROGRESS IN ELEMENTARY PARTICLE AND COSMIC RAY PHYSICS VOL. IV

Editors

J. G. WILSON, *Professor of Physics, University of Leeds*

and

S. A. WOUTHUYSEN, *Professor of Physics, University of Amsterdam*

6 × 9″ XII + 482 p. 110 illus. Guilders 45.00 (90 s)

CONTENTS

1. *Some Theoretical Aspects of the Strong Interactions of the New Particles* (B. D'Espagnat and J. Prentki). 2. *The Properties and Production of K-mesons* (W. D. Walker). 3. *The Interaction of μ-Mesons with Matter* (G. N. Fowler and A. W. Wolfendale). 4. *The Primary Cosmic Radiation and its Time Variations* (S. F. Singer). 5. *The Origin of Cosmic Radiation* (V. L. Ginzburg).

Sole Agency for U.S.A.: Interscience Publishers, Inc. — New York

NORTH-HOLLAND PUBLISHING COMPANY - AMSTERDAM

Send your order to your bookseller or directly to us

Check the many ways ANTON can serve your nuclear needs

☐ **Anton's Electrically Compensated Ion Chambers and BF_3 Counter Tubes**

(Enriched, normal or depleted in B^{10}) for detection of either slow or fast neutrons are widely-used in reactor control and monitoring, oil well logging and neutron survey. Available in a wide range of diameters, sensitive lengths and wall thicknesses in 2S aluminum or stainless steel.

☐ **Anton End Mica Window Counters**

Alpha, beta, gamma counters are halogen quenched, stainless steel. Also available with special organic as well as other rare gas fills. Window thicknesses available from 1 mg/cm². Tubes vary from subminiature to standard conventional sizes and are based with standard RMA connectors. JAN types available.

☐ **Anton Thin Wall Counter Tubes**

Stainless steel, halogen quenched counter tubes for beta, gamma studies are extremely sensitive and can meet all JAN-MIL specifications. They are the only commercial metal thin wall tubes available with a stainless steel 30 mg/cm² wall which will not dent or collapse. Instruments using groups of these tubes exceed in sensitivity and stability most scintillation units.

☐ **Anton's Pancake Tubes**

Halogen quenched, sensitive beta-gamma detectors with end mica window. These units are designed for low intensity measurement and are widely used in facilities doing low-count work. Flat pancake design offers advantage of large diameter window without large volume and high background count.

Anton high efficiency tubes are Platinized*. This process provides sensitivity beyond that of standard tubes.

*Reg. pending

☐ **229 Ratemeters**

The most precise laboratory ratemeter available, Anton's 229 Series has 7 scales, including a single log scale from 300-50,000 cpm with accuracy of better than ±2% of meter reading above ⅓ scale. It has dual range input sensitivity and provides precise and efficient measurement of radioactivity in industry, research and medicine.

☐ **700 Survey Meter**

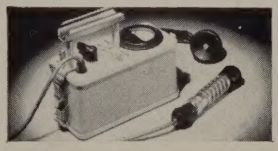

Portable laboratory or field survey meter (.5; 5; 50 mr/hr full scale) is built to FCDA specifications – the only CDV-700 type survey meter which can be exposed continuously to high intensity radiation without detector failure. Probe uses Anton halogen quenched, very thin wall, stainless steel counter tube. Accuracy assured from −55°C to +75°C.

☐ **44 Ratemeter**

Low-cost, accurate, dual range (0-5000; 0-50,000 cpm) . . . exclusive input design. Supplied with Anton long-lived, stainless steel, halogen quenched, thin wall (30 mg/cm²) counter tube or a wide range of other tubes. Unit features a jack for external meters, terminal board construction and oscilloscope connections.

☐ **6001 Sample Changer**

For quick, accurate measurement of low intensity radiation. Designed for use of one or two Anton pancake type, high beta sensitivity, low background counter tubes. Provides 2″ lead plus 3/16″ aluminum shielding in all directions, lowering the background count by a factor of from two to four. Makes possible counting geometry of nearly 100%.

☐ **High Pressure Reactor Connectors**

Anton's stainless steel, hermetically sealed reactor heater-end connector withstands 2000 PSI at temperatures of 636°F, with terminals capable of carrying a load of 16 amperes with a potential drop of less than 10 milliwatts. A wide variety of conventional and specialized connectors is available.

☐ **Medical Eye, Brain And Ingestion Probes**

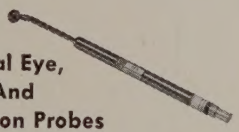

These tubes are rugged, sensitive alpha, beta, gamma radiation detectors specifically designed for reliable, low count medical tracer work. They can be cold sterilized and their pulse intensity obviates the need for a preamplifier.

☐ **Air Particle Monitors**

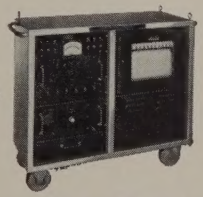

Monitoring systems for aerosol contamination (alpha, beta, gamma) are available in a full range of moving filter paper, fixed filter paper and impact instruments. Rack mounted, cart mounted and portable instruments available.

☐ **Corona Discharge V-R Tubes (300V-30KV)**

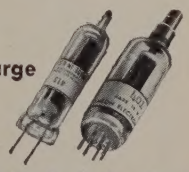

Anton is licensed under the basic patents in this field. Valuable data available concerning this low-cost solution to high voltage low current regulation problems.

. . . and many more. SEND FOR FREE DATA CONCERNING YOUR SPECIFIC NUCLEAR INSTRUMENT, TUBE OR COMPONENT NEEDS.

ANTON ELECTRONIC LABORATORIES, INC.

A subsidiary of United States Hoffman Machinery Corporation

1226 FLUSHING AVE., BROOKLYN 37, N. Y.

Versatile Research Accelerator

3-Mev Model K *Van de Graaff*®

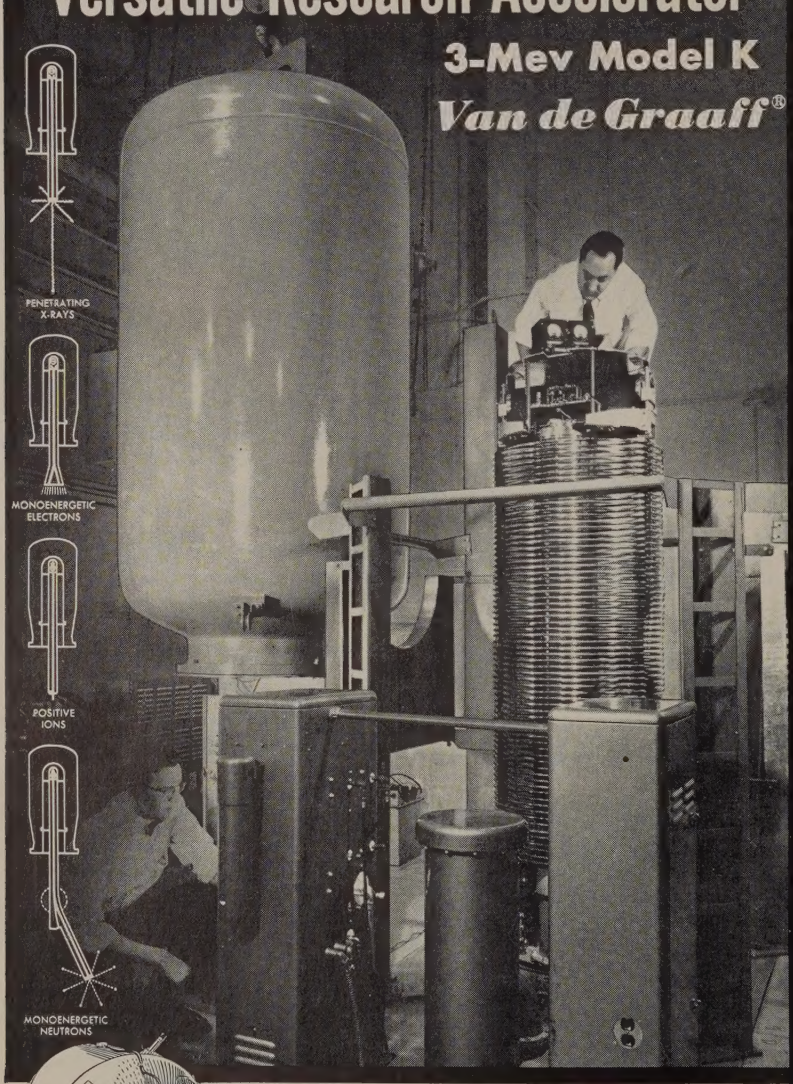

Photos Courtesy of Gulf Research and Development Company

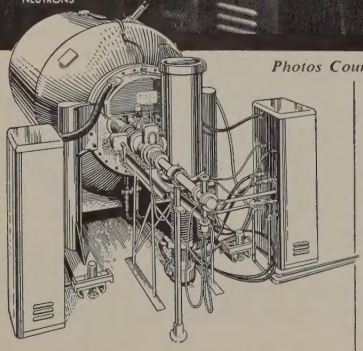

The 3-Mev, Model K Van de Graaff can be furnished for horizontal installation as illustrated above.

ELECTRONS:
1 microampere to 1 milliampere. (Use of maximum current requires beam scanning).

X-RAYS:
900 R per minute at one meter. (Equivalent to 20,000 curies of Cobalt-60).

POSITIVE IONS:
10 to 200 microamperes.

NEUTRONS:
6 x 10^{11} neutrons per second.

Both voltage and current output are stable, precisely controlled, and continuously variable.

This powerful multi-particle accelerator — proved in the field — is the basic tool for a broad program of fundamental or applied radiation research.

Now in use for:

Nuclear physics
Radiation processing
Polymerization
Radiation chemistry
Reactor engineering
Sterilization
Radiation damage
Biology
Particle injection
Radiography

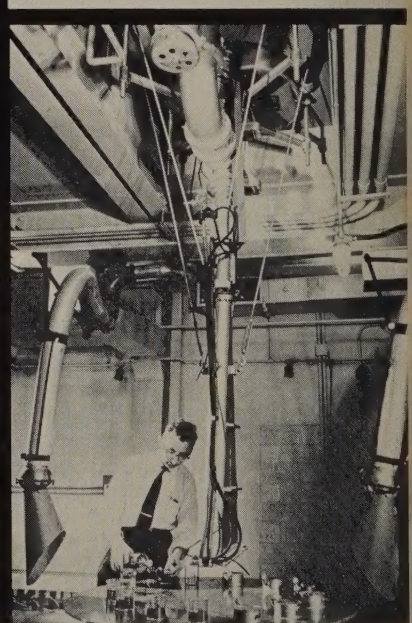

HIGH VOLTAGE ENGINEERING
CORPORATION
BURLINGTON MASSACHUSETTS

Write our Technical Sales Department for more information on the Model K, 3-Mev Van de Graaff.

NUCLEAR INSTRUMENTS 3 (1958) 181–200; NORTH-HOLLAND PUBLISHING CO. – AMSTERDAM

LIST OF PARTICLE ACCELERATOR INSTALLATIONS†

GERALD A. BEHMAN

Radiation Laboratory, University of California, Berkeley, California

Received 1 August 1958

Accelerator installations throughout the world are listed here with the types of particles accelerated and the energy and other characteristics of the machines. Geographical distribution of these accelerators by type of accelerator and country is tabulated, as is the distribution of the machines in the United States according to type of machine and primary activity of the organization.

1. Introduction

This list is intended to include data on all accelerators throughout the world and supersedes similar lists by Cushman[1]), by Shewchuck[2]), and by Frost and Putnam[3]). Data presented here have been acquired in most instances by direct response to a questionnaire sent by the author to the individual installations or, in the case of some countries, to the scientific attachés of the various embassies. In a few cases, it was necessary to acquire the data indirectly through the technical literature or by reference to manufacturers' data.

Of the 411 questionnaires sent out, 224 went to installations in the United States, while 187 went to other countries. Replies were received from 89% of the installations polled in the United States, and from 74% of the installations in other countries. Questionnaires submitted to Argentina, Brazil, Chile, China, Mexico, Rumania, and Turkey were not answered. A time interval of ten months was arbitrarily set for response to the questionnaire. In some instances, not all of the desired information was furnished on the returned questionnaire; these cases are indicated in the list by n.a. (not available).

For rapid and ready reference, the information is classified, first, according to the type of accelerator and, second, according to the address of the installation. Each accelerator group is grossly separated into those machines located in the United States and those located elsewhere in the world.

† This work was performed under the auspices of the United States Atomic Energy Commission.

The general types of accelerators included are direct-current (dc) machines, induction machines, and resonance accelerators. The dc machines comprise cascade rectifiers (Cockcroft-Walton), electrostatic generators (Van de Graaff), and certain transformer-rectifier combinations. The primary example of an accelerator operating on the principle of induction is the betatron. Resonance accelerators include both traveling- and standing-wave linear accelerators as well as magnetic accelerators of the cyclotron or synchrotron type. In this survey, the category *cyclotron* includes continuous-wave (CW) and frequency-modulated (FM) machines. The synchrotron group includes proton, electron, and fixed-field alternating-gradient (FFAG) machines.

For the convenience of the reader, the distribution of these machines throughout the world is summarized by type of accelerator and country in table 1. The distribution of types of establishments having accelerators in the United States is analyzed in table 2 according to type of machine and primary activity of the organization.

Every effort has been made to avoid duplication or omission of information. The author will appreciate notification of such errors.

[1]) Bonnie E. Cushman, Bibliography of Particle Accelerators: July 1948 to December 1950, UCRL-1238 (March 1951).

[2]) Sergey Shewchuck, Bibliography of Particle Accelerators (for) January to December 1951, UCRL-1951 (Sept. 1952).

[3]) Frederick E. Frost and Jane M. Putnam, Particle Accelerators. I. Bibliography. II. List of High-Energy Installations, UCRL-2672 (Nov. 1954).

TABLE 1

Distribution of Machines by Type and Country

Country	D. C. Machines	Induction Machines	Resonance Machines			Total
		Betatrons	Linear Accelerators	Magnetic Accelerators		
				Cyclotrons	Synchrotrons	
United States	134	39	32	36	18	259
Outside the United States	135	37	28	39	29	268
Argentina				1		1
Australia	4			2	3	9
Belgium	7		3	1		11
Brazil		1				1
Canada	8	2	1	2	1	14
Denmark	3			1		4
Formosa	1					1
France	15	2	4	1	1	23
Germany	8	6		4	2	20
Great Britain	26	2	15	8	5	56
India	2					2
Iran	1					1
Israel	1			1		2
Italy	5	2			1	8
Japan	17	11	1	5	6	40
Mexico	1					1
Netherlands	5			1	1	7
New Zealand		1				1
Norway	6	1				7
Poland	1					1
Portugal	1					1
Spain	2					2
Sweden	8	2		3	2	15
Switzerland	5	2	1	2	2	12
Union of South Africa	1			1		2
Union of Soviet Socialist Republics	3	4	3	5	5	20
Yugoslavia	4	1		1		6

TABLE 2

Distribution of Establishments Reporting Accelerators in the United States According to Type of Machine and Activity

Type of Machine	Type of Establishment					Total
	Colleges and Universities	Federal † Government	Hospitals	Private Firms	Nonprofit Organizations	
D. C. Machines	31	11	9	33	4	88
Betatrons	9	7	5	14	0	35
Linear Accelerators	14	1	3	2	1	21
Cyclotrons	23	2	0	1	1	27
Synchrotrons	11	1	0	1	0	13
Total	88	22	17	51	6	184

† Atomic Energy Commission contractors are classified according to the type of establishment holding the contract.

LIST OF ACCELERATOR INSTALLATIONS

I. DIRECT CURRENT MACHINES

In the United States

Location	Type	Dimensions	Particles Accelerated	Energy (MeV)
[1]Argonne Cancer Research Hospital, University of Chicago, Chicago, Ill.	Van de Graaff	7-ft tank length	e	2
[1]Argonne National Laboratory, Lemont, Ill.	Van de Graaff	18-ft accelerating tube	p, d	3.6
	Van de Graaff	9-ft tank length	e	1.0
[1]Arkansas, University, Fayetteville, Ark.	High-voltage rectifier	≈10-ft accelerating tube	p, d, α	0.4
[1]Atomics International, Canoga Park, Calif.	Van de Graaff	4-ft accelerating tube	e	1.6
[2]Austenal, Inc., Chicago, Ill.	Van de Graaff	n.a.	X-rays	1
[2]Babcock and Wilcox, Lynchburg, Va.	Van de Graaf	n.a.	X-rays	1
[2]Union Carbide and Carbon Corp., Bakelite Division, Bloomfield, N.J.	Van de Graaff	n.a.	e	2
[1]Bartol Research Foundation of the Franklin Institute, Swarthmore, Pa.	Cockcroft-Walton	4-ft accelerating tube	d	0.135
	Van de Graaff	21-ft accelerating tube	p	5.5
	Van de Graaff	6-ft accelerating tube	d	1.7
[2]Baylor University, College of Medicine, Houston, Tex.	Van de Graaff	n.a.	X-rays	2
[1,2]Bell Telephone Laboratories, New York, N.Y.	Van de Graaff	n.a.	e	1
	*Van de Graaff	n.a.	e	1
[1,2]Brookhaven National Laboratory, Upton, Long Island, N.Y.	Van de Graaff	8-ft accelerating tube	p, d, He^3, α	4
	Van de Graaff	3-ft accelerating tube	e	2
	Van de Graaff	3-ft accelerating tube	e	2
	Van de Graaff	12-ft accelerating tube	p	4
[1]California Institute of Technology, Pasadena, Calif.	Van de Graaff	2.25-ft accelerating tube	p, d, α, He^3	0.6
	Van de Graaff	8-ft accelerating tube	p, d, α, He^3	1.8
	Van de Graaff	9-ft accelerating tube	p, d, α, He^3	3.0
[2]California Research Corporation, Richmond, Calif.	Van de Graaff	n.a.	e	2
[1]California, University, Radiation Laboratory, Berkeley, Calif.	Cockcroft-Walton	4-ft accelerating tube	p	0.5
	Cockcroft-Walton	4-ft accelerating tube	gaseous ions	0.5
	Van de Graaff	27-ft tank length	p, d, α	4
[1]California, University, Radiation Laboratory, Livermore, Calif.	Van de Graaff	1.7-ft accelerating tube	p, d	1
	Cockcroft-Walton	6-ft accelerating tube	p, d, α	0.5
[1]Carnegie Institution of Washington, Washington, D.C.	Van de Graaff	n.a.	α	7
[2]Chicago Bridge and Iron Company, Birmingham, Ala.	Van de Graaff	n.a.	X-rays	2
	Van de Graaff	n.a.	X-rays	1
[1]Chicago, University, Chicago, Ill.	Cockcroft-Walton	7.5-ft accelerating tube	p, d	0.45
[3]College of Agriculture and Mechanics, Ames, Ia.	Cockcroft-Walton	5-ft accelerating tube	p, d, α	0.3

* Under construction.

[1]) Information obtained from response to questionnaire.

[2]) Information from High Voltage Engineering Company, Burlington, Massachusetts.

[3]) Information from E. H. Krause, Particle Accelerators, in American Institute of Physics Handbook (McGraw-Hill, New York, 1957) pp. 8-184 to 8-201.

[4]) Information from Allis-Chalmers Company, Milwaukee, Wisconsin.

[5]) Information from Varian Associates, Palo Alto, California.

[6]) Information from W. K. H. Panofsky, Some Comments on Soviet Physics Based on a Visit of 14-26 May, 1956. Internal Memorandum, High-Energy Physics Laboratory, Stanford University, Stanford, California (May 31, 1956).

[7]) E. P. Rosenbaum, Physics in the U.S.S.R., Sci. American 195, No. 2 (1956) 29.

Location	Type	Dimensions	Particles Accelerated	Energy (MeV)
[1]Columbia University, Pupin Cyclotron Laboratories, New York, N.Y.	Van de Graaff	12-ft accelerating tube	p, d, α	6.5
[1]Connecticut, University, Storrs, Conn.	Cockcroft-Walton	3-ft accelerating tube	positive ions	0.25
[2]Cooper Alloy Corporation, Hillside, N.Y.	Van de Graaff	n.a.	X-rays	1
[2]Cornell University, Ithaca, N.Y.	Van de Graaff	n.a.	e	2
[1]Dow Chemical Company, Midland, Mich.	Van de Graaff	4.6-ft accelerating tube	p, d, e	2
	Van de Graaff	n.a.	e	2
[1]Dow Chemical Company, Western Division, Pittsburg, Calif.	Van de Graaff	n.a.	e	2.5
[1]Duke University, Durham, N.C.	Van de Graaff	25-ft tank length	p, d, α	4
[2]E. I. Dupont de Nemours, Inc., Wilmington, Del.	Van de Graaff	n.a.	e	2
	Van de Graaff	n.a.	e	3
[2]Eugene Talmadge Memorial Hospital ,Augusta, Ga.	Van de Graaff	2.7-ft accelerating tube	X-rays	2
[1]Ethicon, Inc., Somerville, N.J.	Van de Graaff	n.a.	e	2.5
[1]Evans Signal Laboratory, Belmar, N.J.	Van de Graaff	n.a.	p, d, e	2
[1]Florida, University, Gainesville, Fla.	Van de Graaff	5-ft accelerating tube	p, d	1
[2]Florida State University, Tallahassee, Fla.	Van de Graaff (tandem)	n.a.	p, α	10
[1]Foster-Wheeler Corporation, Mountaintop, Pa.	Van de Graaff	3.7-ft accelerating tube	X-rays	2
[1]General Electric Company, Hanford Laboratories, Richland, Wash.	Van de Graaff	5.3-ft tank length	e	2.0
	Van de Graaff	6.3-ft tank length	p, d	2.0
[1]General Electric Company, Aircraft Nuclear Propulsion Department, Cincinnati, O.	Van de Graaff	3.6-ft accelerating tube	e	2
[1]Arnold Greene, Inc., Cambridge, Mass.	Van de Graaff	n.a.	X-rays	1
[2]Gulf Research and Development Company, Pittsburgh, Pa.	Van de Graaff	n.a.	p, d, α, e	3
[1]Humble Oil and Refining Company, Houston, Tex.	Van de Graaff	3.25-ft accelerating tube	e	2
[1]Iowa State University, Iowa City, Ia.	Cockcroft-Walton	5-ft accelerating tube	p, d, α	0.5
	Van de Graaff	20-ft accelerating tube	p, d, α	4
[2]Johns Hopkins University, Baltimore, Md.	Van de Graaff	6-ft accelerating tube	p, d	3
[1]Kansas, University, Lawrence, Kan.	Van de Graaff	7-ft accelerating tube	p, d	3
[1]Kentucky, University, Lexington, Ky.	Van de Graaff	7.5-ft accelerating tube	p, d	2.2
	Cockcroft-Walton	2-ft accelerating tube	d	0.12
[1]Lemuel Shattuck Hospital for Chronic Diseases, Boston, Mass.	Van de Graaff	n.a.	X-rays	2
[1]Lockheed Aircraft Corporation, Missile Systems Division, Palo Alto, Calif.	Van de Graaff	3.5-ft accelerating tube	p, d, α	3
[1]Los Alamos Scientific Laboratory, Los Alamos, N. Mex.	Cockcroft-Walton	6.3-ft accelerating tube	p, d	0.50
	Cockcroft-Walton	3.3-ft accelerating tube	p, d	0.25
	Van de Graaff	20-ft accelerating tube	p, d, α	8
	Van de Graaff	5-ft accelerating tube	p, d, t, He^3, α	2.5
	Van de Graaff	5-ft accelerating tube	p, d, t, He^3, α	2.5
[2]Los Angeles Tumor Clinic, Los Angeles, Calif.	Van de Graaff	3-ft accelerating tube	X-rays	2
[1]Magnolia Petroleum Company, Dallas, Tex.	Van de Graaff	1.2-ft accelerating tube	p, d	0.5
	Van de Graaff	3-ft accelerating tube	p, d, He^3, α	2
[1]Massachusetts Institute of Technology, Laboratory for Nuclear Science, Cambridge, Mass.	Van de Graaff	18-ft accelerating tube	p, d, α	8.5
	Van de Graaff	9-ft accelerating tube	p, d	4
[2]Massachusetts General Hospital, Boston, Mass.	Van de Graaff	2.7-ft accelerating tube	X-rays	2.0

Location	Type	Dimensions	Particles Accelerated	Energy (MeV)
[2]Mellon Institute, Pittsburgh, Pa.	Van de Graaff	n.a.	e	3
[3]Minnesota, University, Minneapolis, Minn.	Van de Graaff	20-ft accelerating tube	p, d	3.5
[2]Monsanto Chemical Company, Dayton, O.	Van de Graaff	n.a.	e	2
[1,2]National Bureau of Standards, Washington, D.C.	A-C Rectifier	2.25-ft each section	e	1.4
	Cockcroft-Walton	5-ft accelerating tube	p, d	0.25
	Van de Graaff	n.a.	p, d, α	2
[1]National Institutes of Health, Public Health Service, Bethesda, Md.	Van de Graaff	n.a.	e	2
	Van de Graaff	n.a.	e	2
	Van de Graaff	n.a.	e	3
[1]Nebraska, University, Lincoln, Neb.	Cockcroft-Walton	n.a.	positive ions	0.4
[1]Northwestern University, Evanston Ill.	Van de Graaff	12-ft accelerating tube	p, α, e	5
[1]Notre Dame, University, Notre Dame, Ind.	Van de Graaff	12-ft accelerating tube	p, d, α, e	4
[1]Oak Ridge National Laboratory, Union Carbidge Nuclear Company, Oak Ridge, Tenn.	Cascade	8.5-ft accelerating tube	p, d, α	0.6
	Cockcroft-Walton	3-ft accelerating tube	d	0.25
	Van de Graaff	12-ft accelerating tube	p, d, α	6.3
	Van de Graaff	4.7-ft accelerating tube	p, d	3
	Van de Graaff	2.7-ft accelerating tube	X-rays	2.0
[1]Pennsylvania, University, Philadelphia, Pa.	Van de Graaff	12-ft accelerating tube	p, d	3
[2]Pondville State Hospital, Wrentham, Mass.	Van de Graaff	n.a.	X-rays	2
[1]Princeton University, Princeton, N.J.	Van de Graaff	n.a.	p, d, α	3
[1]Radio Corporation of America, Princeton, N.J.	Van de Graaff	n.a.	e	1
[1]Redstone Arsenal, Huntsville, Ala.	Van de Graaff	22-ft tank length	p, d	2
[1,2]Rensselaer Polytechnic Institute, Troy, N.Y.	Cockcroft-Walton	3.5-ft accelerating tube	p, d	0.25
	Van de Graaff	n.a.	p, d	1
[1]Rice Institute, Houston, Tex.	Cockcroft-Walton	2-ft accelerating tube	p, d	0.2
	Van de Graaff	18-ft accelerating tube	p, d, t, He^3, α	6
[1]Sandia Corporation, Albuquerque, N.Mex.	Van de Graaff	n.a.	p, d, e	2
[1]Shell Development Company, Houston, Tex.	Van de Graaff	n.a.	p, d	2
[1]Shell Development Company, Emeryville, Calif.	Van de Graaff	7-ft accelerating tube	e	3
[2]Socony-Vacuum Oil Company, Paulsboro, N.J.	Van de Graaff	n.a.	e	2
[1]Swedish Hospital, Seattle, Wash.	Van de Graaff	4-ft accelerating tube	X-rays, e	2
[1]Stanford Research Institute, Palo Alto, Calif.	Van de Graaff	n.a.	p, d	2
	Resonant Transformer	n.a.	e	1
[2]Texas Oil Company, New York, N.Y.	Van de Graaff	n.a.	p, d, α	3
[2]Texas Nuclear, Austin, Tex.	Van de Graaff	n.a.	p, d, α	2
[1]Texas, University, Austin, Tex.	Van de Graaff	10-ft accelerating tube	p, d, t, α	4
	Full-wave, four-tube rectifier	1.6-ft accelerating tube	d	0.1
[1]University Hospital, Cleveland, O.	Van de Graaff	6.5-ft tank length	X-rays	2
[1]Upjohn Company, Kalamazoo, Mich.	Van de Graaff	n.a.	e	2
[1]U.S. Air Force, Air Material Command, Wright-Patterson Air Force Base, O.	Van de Graaff	n.a.	p	2
[1]U.S. Army Chemical Center, Chemical and Radiological Laboratory, Army Chemical Center, Md.	Van de Graaff	n.a.	e	0.3

Location	Type	Dimensions	Particles Accelerated	Energy (MeV)
[1,2]U.S. Army Quartermaster Corps, Natick, Mass.	Van de Graaff	n.a.	p, d, α	1
[1]U.S. Naval Hospital, Bethesda, Md.	Van de Graaff	14-ft tank length	e	2
[1]U.S. Naval Postgraduate School, Monterey, Calif.	Van de Graaff	n.a.	p, d, α, e	2
[1]U.S. Naval Radiological Defense Laboratory, San Francisco, Calif.	Van de Graaff	n.a.	p, d, α, e	2
[1]U.S. Naval Research Laboratory, Washington, D.C.	Cockcroft-Walton	4.5-ft accelerating tube	p, d	0.50
	Cockcroft-Walton	3.3-ft accelerating tube	p, d	0.25
	Van de Graaff	2.5-ft accelerating tube	p, d, He^3, α	2.1
	Van de Graaff	3-ft accelerating tube	e, p	2.0
	Van de Graaff	4-ft accelerating tube	e	2.0
	Van de Graaff	15.5-ft accelerating tube	p, d, He^3, α	6.0
[2]Virginia, University, Charlottesville, Va.	Van de Graaff	3-ft accelerating tube	p, d, α	1.5
[1]Watertown Arsenal, Watertown, Mass.	Van de Graaff	n.a.	p, d	2
[1]Wells Surveys, Inc., Tulsa, Okla.	Van de Graaff	n.a.	p, d	0.65
[1]Westinghouse Electric Corporation, Commerical Atomic Power, Pittsburgh, Pa.	Van de Graaff	6-ft tank length	p, d, e	2
	Van de Graaff	6-ft tank length	p, d, e	2
	Van de Graaff	37-ft tank length	p, d, e	2
	Van de Graaff	22.5-ft tank length	p, d, e	6
[1,2]Wisconsin, University, Madison, Wis.	Van de Graaff	n.a.	p, d, α	4.5
	Van de Graaff	n.a.	p, d, α	2
	Van de Graaff (tandem)	n.a.	p, α	10

Outside the United States

Location	Type	Dimensions	Particles Accelerated	Energy (MeV)
Australia				
[1]Australian National University, Canberra	Cockcroft-Walton	9-ft accelerating tube	p, d	0.5
	Cockcroft-Walton	14-ft accelerating tube	p, d, α	1.25
[1]Melbourne, University, Victoria	Van de Graaff	10-ft accelerating tube	p, d	1.0
	Van de Graaff	6.5-ft accelerating tube	e	0.7
Belgium				
[1]Centre de Physique Nucleaire, Ecole Royale Militaire, Bruxelles	Cockcroft-Walton	n.a.	p	1.4
[1]Centre de Physique Nucleaire, Louvain	Van de Graaff	3.5-m accelerating tube	p, d	1.8
[1]Institut Interuniversitaire des Sciences Nucleaire, Faculte Polytechnique, Mons	Cockcroft-Walton	6-m accelerating tube	p, d, α	1.3
[1]Laboratoire de Radioactivite et de Physique Nucleaire, Université de Liège, Liège	Cockcroft-Walton	n.a.	p, d	1
	Van de Graaff	n.a.	p, d	2
	Electrostatic-charge transport by airblown dust particles	n.a.	p, d	0.8
[1]Universite Libre de Bruxelles, Bruxelles	Cockcroft-Walton	n.a.	p, d	0.85

Location	Type	Dimensions	Particles Accelerated	Energy (MeV)
Canada				
[1]Atomic Energy of Canada, Ltd., Chalk River, Ontario	*Van de Graaff (tandem)	Two accelerators end-to-end	p, d, t, α	10
[1]British Columbia, University, Vancouver, B.C.	Van de Graaff	16-ft accelerating tube	p, d, α	2.25
[2]Canadian Defense Research Board, Alberta	Van de Graaff	n.a.	p, d, α	2
[2]Canadian Department of Defense Production, Montreal	Van de Graaff	n.a.	e	3
[1]Montreal, University, Montreal	Cockcroft-Walton	4.5-ft tank length	p, d	0.5
[3]National Research Council, Ottawa	Van de Graaff	1.4-ft accelerating tube	e	0.6
	Van de Graaff	9-ft accelerating tube	p	4
[1]Ontario Cancer Institute, Toronto	Van de Graaff	n.a.	p, d, α	3
Denmark				
[1]Institute for Theoretical Physics, Copenhagen	Transformer-Rectifier	2.6-m accelerating tube	p, d	1
	Van de Graaff	4.4-m accelerating tube	p, d, α	4
	Van de Graaff	3.0-m accelerating tube	p, d, α	2.2
Formosa				
[2]National Tsing Hua University	Van de Graaff	n.a.	p, d, e	3
France				
[1]Centre d'Études Nucleaires, Grenoble, Isére	Van de Graaff	n.a.	p, e	0.6
	Van de Graaff	n.a.	e	0.6
	*Van de Graaff	n.a.	p, d, α, e	1.4
[1]Centre d'Études Nucleaires de Saclay, Saclay	Van de Graaff	3.0-m accelerating tube	p, d	2
	Van de Graaff	7.0-m accelerating tube	p, d, α	5
[2,3]Ecole Normal Superieure, Paris	Cockcroft-Walton	2.1-m accelerating tube	d	0.6
	Van de Graaff	2.1-m accelerating tube	p, d, e	2
[2]Ecole Polytechnique, Paris	Van de Graaff	n.a.	p, d	2
[3]Institute Interuniversitaire des Sciences Nucleaire, Mons	Cockcroft-Walton	5-m accelerating tube	p, d	1.4
[1]Institute of Nuclear Research, University of Strasbourg, Strasbourg	Cockcroft-Walton	5-m accelerating tube	p, d, α	1.5
	*Van de Graaff	n.a.	p, d, α	6
[1]Laboratoire de Physique Atomique et Moleculaire, College de France, Paris	Van de Graaff	1.6-m accelerating tube	d→n	0.6
	Van de Graaff	1.25-m accelerating tube	d→n	0.15
[3]Laboratoire de Synthese Atomique, Ivry	Cockcroft-Walton	n.a.	d	0.9
[2]Lyons, University, Lyons	Van de Graaff	n.a.	p, d, α, e	2
Germany				
[1]Institut für Kernphysik der Universität Frankfurt am Main	Cockcroft-Walton	n.a.	p, d	1.5
[1]Institut für Physik im Max-Planck-Institut für Med. Forschung, Heidelberg	Van de Graaff	3-m accelerating tube	p, d, α, e	1
[2]Institut für Strahlen und Kernphysik, University of Bonn, Bonn	Van de Graaff	n.a.	e	3
[1,2]Max-Planck-Institut für Chemie, Mainz	*Van de Graaff	3.5-m accelerating tube	p, d, α, e	5
	Cockcroft-Walton	4.25-m accelerating tube	p, d	1.5
[3]Max-Planck-Institute for Physics of the Stratosphere, Hechingen	Van de Graaff	5.5-m accelerating tube	p, d, α, e	1.5
[1]Physikalisches Institut der Universität Freiberg, Freiberg	Van de Graaff	n.a.	p, d	6
[1]Physical Institute, Free University Berlin-Dahlen	Van de Graaff	2-m accelerating tube	e	1

Location	Type	Dimensions	Particles Accelerated	Energy (MeV)
Great Britain				
[1]Associated Electrical Industries, Ltd., Aldermaston, England	Van de Graaff	9-ft accelerating tube	p, d	3.8
	Van de Graaff	4.5-ft accelerating tube	p, d	0.6
[1]Atomic Energy Research Establishment, Harwell, England	Cockcroft-Walton	n.a.	p, d, t	0.5
	*Van de Graaff (tandem)	14-ft accelerating tube	p, d, O^{16}	10
	Van de Graaff	13-ft accelerating tube	p, d, He^3, α	4.5
	Van de Graaff	4ft accelerating tube	e	2.25
[2]British Insulated Callender's Cables, Ltd., London, England	Van de Graaff	n.a.	e	2
[1,3]Cambridge, University, Cambridge, England	Cockcroft-Walton	12-ft accelerating tube	p, d	1
	Cockcroft-Walton	16-ft accelerating tube	p, α	1.4
[1,3]Clarendon Laboratory, Oxford University, Oxford, England	Cockcroft-Walton	12-ft accelerating tube	p, d, α	1.1
	Cockcroft-Walton	6-ft accelerating tube	p, d, α	0.5
[1,3]Edinburgh, University, Edinburgh, Scotland	Cockcroft-Walton	12-ft accelerating tube	p, d, α	1.0
[1]Hammersmith Hospital, London, England	Van de Graaff	7.5-ft accelerating tube	d, e	2.0
[1]Liverpool, University, Mt. Pleasant, Liverpool, England	Cockcroft-Walton	n.a.	p, d	1
[3]London, University, London, England	Van de Graaff	n.a.	e	2
[1]Medical Research Council Radiobiological Research Unit, Harwell England	Cockcroft-Walton	2-m accelerating tube	p, d	1
[2]National Physical Laboratory, Teddington, England	Van de Graaff	n.a.	X-rays	2
[1]Physical Laboratories, The University, Manchester, England	Van de Graaff	12.7-ft accelerating tube	p, d, t, He^3, α, He^{4++}	6
	Van de Graaff	6-ft accelerating tube	p, d, α	3
[1]Royal Cancer Hospital, London,	Van de Graaff	4.5-ft accelerating tube	e	2
[2]Royal Infirmary, Edinburgh, Scotland	Van de Graaff	n.a.	X-rays	2
[2]Sheffield National Center for Radiotherapy, Sheffield, England	Van de Graaff	n.a.	X-rays	2
[2]Standard Telecommunication Laboratories, Ltd., Enfield, Middlesex, England	Van de Graaff	n.a.	p, d, α, e	2
[2]Tube Investments Research Laboratory, Cambridge, England	Van de Graaff	n.a.	p, d, α, e	2
	Van de Graaff	n.a.	e	1
[1]Westminster Hospital, London, England	Van de Graaff	n.a.	e→X-rays	2
India				
[1]Atomic Energy Establishment, Bombay	Cockcroft-Walton	n.a.	d	1.2
[1]Tata Institute of Fundamental Research, Bombay	Cockcroft-Walton	n.a.	d	1.2
Iran				
[2]Teheran, University, Teheran	Van de Graaff	n.a.	p, d, α, e	3.0
Israel				
[1,2]Weizmann Institute, Rehovoth	Van de Graaff	n.a.	p, d, α	3.0
Italy				
[2]Bologna, University, Bologna	Van de Graaff	n.a.	X-rays	2.0
[1]Instituto di Fisica Universita Catania, Catania	Van de Graaff	n.a.	p, d	2.0

Location	Type	Dimensions	Particles Accelerated	Energy (MeV)
[3]CISE Laboratory, Milan	Cockcroft-Walton	1-m accelerating tube	d	0.4
[1]Instituto Superior di Sanita, Rome	Cockcroft-Walton	3-m accelerating tube	p, d	1.0
[2]Pirelli, Milan	Van de Graaff	n.a.	e	2.0
Japan				
[1]Central Research Laboratory,	Cockcroft-Walton	n.a.	n.a.	0.3
Hitachi, Ltd., Tokyo	Van de Graaff	n.a.	n.a.	1.5
[1]Electrotechnical Laboratory, Tokyo	Cockcroft-Walton	n.a.	n.a.	0.8
	Van de Graaff	n.a.	n.a.	3.0
[1,2]Japan Atomic Energy Research Inst., (Ibaraki Pref.)	Van de Graaff	n.a.	p, d, α, e	2.0
[2]Japanese Chemical and Fiber Association, Osaka	Van de Graaff	n.a.	e	2.0
[1]Konan University, Kobe	Cockcroft-Walton	n.a.	p, d, t, α	0.4
[1]Kyoto University, Kyoto	Cockcroft-Walton	n.a.	p, d	0.6
[1]Kyushu University, Fukuoka	Van de Graaff	9-m tank length	p, d	5.0
[1]Osaka University, Osaka	Cockcroft-Walton	n.a.	p, d	0.6
	Van de Graaff	n.a.	n. a.	2.5
[1]Rikkyo University, Tokyo	Cockcroft-Walton	n.a.	n.a.	0.2
[1]Scientific Research Institute, Tokyo	Van de Graaff	n.a.	n.a.	2.0
[1]Tohoku University, Sendai	Van de Graaff	7-m tank length	p,d	2.0
[1]Tokyo Institute of Technology, Tokyo	*Cockcroft-Walton	n.a.	d	0.44
[1]Tokyo Shibaura Electric Company, Ltd., Tokyo	Cockcroft-Walton	n.a.	n.a.	0.15
[1]Tokyo, University, Tokyo	Van de Graaff	n.a.	n.a.	1.6
Mexico				
[2,3]National University of Mexico, Mexico 20, D.F.	Van de Graaff	4.2-ft accelerating tube	p, d, e	2.0
Netherlands				
[1]Delft Institute of Technology, Delft	Van de Graaff	n.a.	p, d	2.5
[1]Natuurkundig Laboratorium der	Cockcroft-Walton	3-m accelerating tube	d	0.6
Rijksuniversiteit, Groningen	Cockcroft-Walton	1.6-m accelerating tube	p, d	0.6
[1]State University of Utrecht, Utrecht	Cockcroft-Walton	8-ft accelerating tube	p, d	0.7
	Van de Graaff	n.a.	p, d, α	3.0
Norway				
[1]Fysisk Institutt, Bergen University, Bergen	Van de Graaff	7-m accelerating tube	p, d, α	1.2
[1,3]Municipal Hospital, Bergen	Van de Graaff	n.a.	e	1.5
	Van de Graaff	n.a.	p	1.5
[1,3]Norges Tekniske Högskole, Trondheim	Van de Graaff	3.6-m accelerating tube	p, d	4.0
[1]Oslo, University, Blindern	Van de Graaff	3.6-m accelerating tube	p	2.0
	Van de Graaff	1.5-m accelerating tube	p	0.5
Poland				
[1]Danzig, University, Danzig	Van de Graaff	1.1-m accelerating tube	p, d	0.5
Portugal				
[2]Junta de Energia Nuclear, Lisbon	Van de Graaff	n.a.	p, d, e	2.0
Spain				
[1,2]Junta de Energia Nuclear, Madrid	Cockcroft-Walton	n.a.	p, d	0.6
	Van de Graaff	n.a.	p, d, t, α, e	2.0
Sweden				
[1]A. B. Atomenergi, Stockholm	*Van de Graaff	n.a.	p, d, α	5.5

Location	Type	Dimensions	Particles Accelerated	Energy (MeV)
[1]Chalmer's University of Technology Göteborg	Van de Graaff	4-m accelerating tube	p, d, t, α	4.0
[1]Försvarets Forskningsanstalt, Stockholm	Van de Graaff	2.25-m accelerating tube	p, d, e	3.0
	Van de Graaff	1.0-m accelerating tube	e	1.5
[3]Fysika Institutionen, Lund	Van de Graaff	4.0-m accelerating tube	p, d	4.0
[1]Nobel Institute for Physics, Stockholm	Cockcroft-Walton	7-m accelerating tube	p, d, α	1.2
[1]Radiofysiska Istitutionen. Karolinska Sjukhuset Stockholm	Cockcroft-Walton	3.5-m tank length	e→X-rays	1.2
[1]Fysiska Institutionen, Uppsala	Van de Graaff	1.5-m accelerating tube	e	0.8
Switzerland				
[1]Physikalisches Institut der Eidg. Technischen Hochschule, Zürich	Cockcroft-Walton	n.a.	p, d, α	1.2
	Cockcroft-Walton	n.a.	p	2.0
[1]Physikalisches Institut der Universität Basel, Basel	Cockcroft-Walton	3-m accelerating tube	p, d	1.0
	Cockcroft-Walton	4-m accelerating tube	p, d, α	4.0
[1]Physikalisches Institut der Universität Zürich, Zürich	Van de Graaff	1.2-m accelerating tube	p, d, α	1.7
Union of South Africa				
[1]Diamond Research Laboratory, Johannesburg	Cockcroft-Walton	n.a.	p, d, α, e	2.0
Union of Soviet Socialist Republics				
[3]Physico-Technical Institute, USSR Academy of Sciences, Kharkov	Van de Graaff	n.a.	e	1.0
	Van de Graaff	n.a.	p, d, e	3.0
	Van de Graaff	n.a.	p, d, e, α	5.0
Yugoslavia				
[1]Institute "J. Stefan", Ljubljana	Van de Graaff	1.6-m accelerating tube	p	2.0
[1]Insitute of Nuclear Sciences, Belgrade	Cockcroft-Walton	5-m accelerating tube	p, d	1.5
	Cockcroft-Walton	1-m accelerating tube	p, d	0.2
[1]Institute "Rudjer Boskovic", Zagreb	Cockcroft-Walton	n.a.	d	0.2

II. INDUCTION MACHINES: BETATRONS

In the United States

Location	Orbit Radius	Particles Accelerated	Energy (MeV)
[1,4]Allis-Chalmers, Milwaukee, Wis.	8.20 in.	e	28
[1,4]Anderson Hospital and Tumor Institute, University of Texas, Houston, Tex.	9.5 in.	e	24
[1,4]Baldwin-Lima-Hamilton Corporation, Lima, O.	8.22 in.	e↔X-rays	24
[4]Birdsboro Steel Foundry, Birdsboro, Pa.	7.5 in.	e↔X-rays	24
[4]Bonney-Floyd Steel Castings Company, Columbus, O.	7.5 in.	e↔X-rays	24
[1]Case Institute of Technology, Cleveland, O.	17.25 cm	e	30
[3]Chicago, University, Chicago, Ill.	33 in.	e	100
[4]Continental Foundry and Machine Company, Coraopolis, Pa.	8.13 in.	e↔X-rays	24
[4]Continental Foundry and Machine Company, East Chicago, Ind.	7.5 in.	e↔X-rays	24
[1]Detroit Arsenal, Ordnance Corps, Center Line, Mich.	5.5 in.	e	15
[1,3,4]Electric Steel Foundry Company, Portland, Oreg.	8 in.	e↔X-rays	22
	11.5 in.	e	50
	33 in.	e	100
[1]General Electric Research Laboratory, Schenectady, N.Y.	5.25 in.	e	11.7
[4]General Steel Castings Company, Eddystone, Pa.	7.5 in.	e	24
[4]General Steel Castings Company, Granite City, Ill.	7.5 in.	e	24
[1,4]Illinois, University, Urbana, Ill.	8 in.	e	24
	10 in.	e	80
	46 in.	e	340
[1,4]Illinois, University, Medical School, Chicago, Ill.	20 in.	e	24
[1]Knolls Atomic Power Laboratory, General Electric Company Schenectady, N.Y.	33 in.	e	100
[1,4]Los Alamos Scientific Laboratory, Los Alamos, N.Mex.	19.3 cm	e	24
[1,4]Madison Radiation Center, Madison, Wis.	8.5 in.	e	24
[1,4]Memorial Center, New York, N.Y.	20 cm	e	24
[4]Mesta Machine Company, Homestead, Pa.	7.5 in.	e↔X-rays	24
[4]Michigan, University, Ann Arbor, Mich.	7.5 in.	e↔X-rays	24
[4]Mt. Sinai Hospital, New York, N.Y.	7.5 in.	e↔X-rays	24
[3]National Bureau of Standards, Washington, D.C.	115 in.	e	50
[4]Ohio Steel Castings Company, Lima, O.	7.5 in.	e	24
[1,4]Pennsylvania, University, Philadelphia, Pa.	19.1 cm	e	24
[1,4]Picatinny Arsenal, Dover, N.J.	8 in.	e	24
[1,4]Pittsburgh Steel Foundry Corporation, Glassport, Pa.	8.22 in.	e	24
[1,4]Presbyterian Hospital, New York, N.Y.	7.5 in.	e↔X-rays	25
[1]Rensselaer Polytechnic Institute, Troy, N.Y.	11.5 in.	e	31
[3]U.S. Naval Ordnance Laboratory, Silver Spring, Md.	5.2 in.	e	10
[1,4]U.S. Naval Research Laboratory, Washington, D.C.	7.3 in.	e	21
[1,4]U.S. Navy Electronics Laboratory, San Diego, Calif.	8.2 in.	e	26
[1,4]Washington University, School of Medicine, St. Louis, Mo.	19 cm	e	24
[4]Watervliet Arsenal, Watervliet, N.Y.	7.5 in.	e	24

Outside the United States

Location	Orbit Radius	Particles Accelerated	Energy (MeV)
Brazil			
[4]Sao Paulo, University, Sao Paulo	7.5 in.	e	24
Canada			
[1, 4]Ontario Cancer Institute, Toronto	7.5 in.	e→γ	25
[1, 4]Saskatchewan, University, Saskatoon, Saskatchewan	20 cm	e	25
France			
[1]Institute Gustave Roussy, Paris	19 cm	e	22
[4]Ministry of Health, Paris	19 cm	e→γ	24
Germany			
[1]Physikalisches Institut der Technischen Hochschule, Karlsruhe	24 cm	e	31
[1]Siemens-Reiniger-Werke, Erlangen	10 cm	e	15
	21 cm	e	35
[1]Universität Frankfurt, Frankfurt	21 cm	e	35
Universität Heidelberg, Heidelberg	19.2 cm	e	35
Universität Würzburg, Würzburg	20 cm	e	35
Great Britain			
[1]Christie Hospital and Holt Radium Institute, Withington, Manchester, England	19 cm	e	20
[1]Metropolitan-Vickers, Manchester, England	20 cm	e	20
Italy			
[1]Clinica Medica, Universita Torino, Turin	26 cm	e	31
[1]Instituto Nazionale di Fisica Nucleare, Universita Torino, Turin	24.5 cm	e	31
Japan			
[1]Central Research Laboratory, Hitachi Ltd., Tokyo	7 cm	e	3.5
	22 cm	e	20
[1]Electrotechnical Laboratory, Tokyo	13.5 cm	e	10
[1]Osaka University, Osaka	8 cm	e	6
	19 cm	e	24
[1]Research Laboratory, Mitsubishi Electric Company, Amagasaki	18 cm	e	30
[1]Shimadzu Seisakusho, Ltd., Kyoto	8 cm	e	6
	12.5 cm	e	15
[1]Tokyo Shibaura Electric Company, Ltd., Mazda Research Laboratory, Kawasaki	10 cm	e	15
[1]Tokyo University of Education, Tokyo	8.5 cm	e	6
	29 cm	e	30
New Zealand			
[1, 4]Dunedin Hospital, Dunedin, New Zealand	19 cm	e	24
Norway			
[1]Bergen University, Bergen	40 cm	e	47
Sweden			
[1]Royal Institute of Technology, Stockholm	8 cm	e	5
[1]Radiumhemmet, Karolinska Sjukhuset, Stockholm	20 cm	e	15
Switzerland			
[1]Roentgeninstitut, Inselspital, Bern	25 cm	e	31
[1]Physikalisches Institut der Universität Zürich, Zürich	30 cm	e	31

Location	Orbit Radius	Particles Accelerated	Energy (MeV)
Union of Soviet Socialist Republics			
[6]Lebedev Institute, Moscow	n.a.	e	30
[6]Moscow State University, Moscow	n.a.	e	n.a.
[6]Tomsk	n.a.	e	100
[6]Tomsk	n.a.	e	20
Yugoslavia			
[1]Institute "J. Stefan", Ljubljana	25 cm	e	31

III. RESONANCE MACHINES

Linear Accelerators

In the United States

Location	Type	Accelerator Length	Particles Accelerated	Energy (MeV)
[1]Argonne Cancer Research Hospital, University of Chicago, Chicago, Ill.	Traveling-wave	16 ft	e	60
[1]Bartol Research Foundation of the Franklin Institute, Swarthmore, Pa	n.a.	3 ft	e	1.4
[1]Brookhaven National Laboratory, Upton, Long Island, N.Y.	n.a.	110 ft	p	50
[1]Brown University, Providence, R.I.	n.a.	3 ft	p, d	0.2
[1]California, University, Radiation Laboratory, Berkeley, Calif.	Traveling-wave	3.3 ft	e	5
	Traveling-wave	3.3 ft	e	5
	Standing-wave	40 ft	p	32
	Standing-wave	18.2 ft	p	9.8
	Standing-wave	120 ft	heavy ions to Ne^{20}	10 MeV/ nucleon
[1,5]California, University, Radiation Laboratory, Livermore, Calif.	*Traveling-wave	14 ft	e	16
	Traveling-wave	11 ft	p	3.75
	Traveling-wave	11 ft	d	7.5
	Traveling-wave	11 ft	α	15
[1]California, University, Radiation Laboratory, Site 300, Livermore, Calif.	Traveling-wave	6.7 ft	e	10
[4]Columbia University, New York, N.Y.	n.a.	9.5 ft	e	15
[1]Ethicon, Inc., Somerville, N.J.	Traveling-wave	10 ft	e	7
[1]General Atomic, Division of General Dynamics, San Diego, Calif.	n.a.	12 ft	e	33
[1]Massachusetts Institute of Technology, Laboratory for Nuclear Science, Cambridge, Mass.	n.a.	21 ft	e	17
[1]Michael Reese Hospital, Chicago, Ill.	n.a.	10 ft	e	35
[1]Minnesota, University, Institute of Technology, Minneapolis, Minn.	n.a.	120 ft	p	68
[1]Montana State University, Missoula, Mont.	Traveling-wave	3.78 ft	e	8
[1]Purdue University, Lafayette, Ind.	n.a.	10 ft	e	5.5
	n.a.	2.5 ft	e	1.7
[1]Stanford Hospital, San Francisco, Calif.	Traveling-wave	6 ft	e→X-rays	5

Location	Type	Accelerator Lentgh	Particles Accelerated	Energy (MeV)
[1]Stanford University, Stanford, Calif.	Traveling-wave	12 ft	e	38
	Traveling-wave	260 ft	e	700
	Traveling-wave	20 ft	e	75
[1]Stanford University, Microwave Laboratory, Stanford, Calif.	Traveling-wave	2 ft	e	6
[1]U.S. Army Ionizing Radiation Center, Lathrop, Calif.	*Traveling-wave	15 ft	e	24
[1]Virginia, University, Charlottesville, Va.	n.a.	1 ft	e	0.75
[1]Yale University, New Haven, Conn.	n.a.	20 ft	e	7
	n.a.	138 ft	heavy ions to A^{40}	10 MeV/ nucleon

Outside the United States

Location	Type	Accelerator Length	Particles Accelerated	Energy (MeV)
Belgium				
[1]Ecole Royale Militaire, Centre de Physique Nucleaire, Brussels	Helix	5 m	p	10
[1]Ghent, University, Ghent	n.a.	2 m	e	4
	*n.a.	n.a.	n.a.	15
Canada				
[1]McGill University, Montreal	*n.a.	10 ft	e	10
France				
[1]Centre d'Etudes Nucleaires de Saclay, Saclay	n.a.	6.30 m	e	28
[1]Centre Anticancereaux, Nancy	n.a.	2 m	e	4
[1]Curie Foundation, Paris	n.a.	3 m	e	4
[1]Paris, University, Laboratoire d'Electronique et de Radioelectricite, Paris	Traveling-wave	1 m	e	2
Great Britain				
[1]Associated Electrical Industries, Ltd., Aldermaston, England	Helix	1 m	p	4
[1]Atomic Energy Research Establishment, Harwell, England	Traveling-wave	6 m	e	15
	*n.a.	100 ft	p	50
	Traveling-wave	6 m	e	28
[1]Christie Hospital and Holt Radium Institute, Manchester, England	n.a.	1 m	e	4
[1]Hammersmith Hospital, London, England	n.a.	3 m	e	8
[1]Liverpool Radium Institute, Clatterbridge Hospital, Liverpool, England	n.a.	1.5 m	e	4
[1]Metropolitan-Vickers, Manchester, England	Traveling-wave	1 m	e	4
	Traveling-wave	1 m	e	4
[1]Ministry of Supply, London, England	n.a.	1 m	e	5
[1]Mount Vernon Hospital, Northwood, London, England	Traveling-wave	100 cm	e	3.9
[1]Mullard Research Laboratories, Surrey, England	n.a.	1 m	e	4
Newcastle General Hospital, Newcastle-upon-Tyne, England	Standing-wave	1 m	e	4.3
[1]St. Bartholomew's Hospital, London, England	n.a.	6 m	e	17
[1]Western General Hospital, Edinburgh, Scotland	n.a.	1 m	e	4

Location	Type	Accelerator Length	Particles Accelerated	Energy (MeV)
Japan				
[1]Central Research Laboratory, Hitachi Ltd., Tokyo	*n.a.	2 m	e	6
Switzerland				
[1]European Council for Nuclear Research, Geneva	*n.a.	n.a.	p	50
Union of Soviet Socialist Republics				
[6]Big Volga Laboratories, Bolshoya Volga	n.a.	n.a.	p	9
[6]Moscow Physical Institute, Moscow	n.a.	n.a.	p	40
[6]Ukrainian Technical Institute, Kharkov	n.a.	n.a.	p	21

Magnetic Accelerators: Cyclotrons

In the United States

Location	Type	Pole-piece Diameter	Particles Accelerated	Energy (MeV)
[1]Argonne National Laboratory, Lemont, Ill.	CW	62 in.	p	10.8
			d	21.6
			α	43.2
[1]Brookhaven National Laboratory, Upton, Long Island, N.Y.	n.a.	18 in.	p	3
			d	2
	n.a.	60 in.	p	11
			d	22
			α	44
[1]California, University, Radiation Laboratory, Berkeley, Calif.	CW	72 in.	p	12
			d	24
			α	48
	FM	184 in.	p	720
			d	430
			α	880
[1]California, University, Radiation Laboratory, Livermore, Calif.	CW (variable energy)	90 in.	p	14
			d	12
			α	24
[1]Carnegie Institute of Technology, Pittsburgh, Pa.	FM	70.8 in.	p	450
[1]Carnegie Institution of Washington, Washington, D.C.	CW	60 in.	p	8
			d	16
			α	32
[1]Chicago, University, Enrico Fermi Institute for Nuclear Studies, Chicago, Ill.	FM	170 in.	p	450
[1]Columbia University, Pupin Cyclotron Laboratory, New York, N.Y.	CW	36 in.	p	15
			d	10
[1]Columbia University, Nevis Cyclotron Laboratories, Irvington-on-Hudson, N.Y.	FM	164 in.	p	400
[1]Harvard University, Cyclotron Laboratory, Cambridge, Mass.	FM	95 in.	p	160
[1]Illinois, University, Urbana, Ill.	n.a.	47 in.	p	6
			d	12
			α	24
[1]Indiana University, Bloomington, Ind.	CW	45 in.	d	11.4
			He^{++}	27.8

Location	Type	Pole-piece Diameter	Particles Accelerated	Energy (MeV)
[1]Lewis Flight Propulsion Laboratory, National Advisory Committee for Aeronautics, Cleveland, O.	CW	60 in.	d	20
[1]Los Alamos Scientific Laboratory, Los Alamos, N. Mex.	CW	42 in.	p	9
	(variable		d	16
	energy)		α	32
[1]Massachusetts Institute of Technology, Laboratory for Nuclear Science, Cambridge, Mass.	n.a.	42 in.	p	7.5
			d	15
			α	30
[1]Michigan, University, Ann Arbor, Mich.	CW	42 in.	p, d, α	10
[1]Oak Ridge National Laboratory, Oak Ridge, Tenn.	CW	86 in.	p	25
	CW	63 in.	N^{3+}	27
	CW	44 in.	p	5
	CW	48 in.	N^{5+}	80
[1]Oregon State College, Corvallis, Oreg.	CW	37 in.	d	7.5
[1]Pittsburgh, University, Radiation Laboratory, Pittsburgh, Pa.	n.a.	47 in.	p	9.5
			d	19
			α	38
[1]Princeton University, Palmer Physical Laboratory, Princeton, N.J.	FM	35 in.	p	20
[1]Purdue University, Lafayette, Ind.	n.a.	37 in.	d	9.7
			α	19.4
[1]Rochester, University, Rochester, N.Y.	n.a.	27 in.	p	7
			d	4.3
			α	7
	FM	130 in.	p	240
[1]Stanford University, Stanford, Calif.	CW	27 in.	d	2.8
[1]U.S. Naval Research Laboratory, Washington, D.C.	n.a.	6 in.	e	1
	n.a.	6 in.	e	3
	n.a.	6 in.	e	3
	n.a.	6 in.	e	6
[1]Washington University, St. Louis, Mo.	CW	45 in.	p	5.1
			d	10.2
			α	20.4
[1]Washington, University, Seattle, Wash.	CW	72 in.	p	11.5
[1]Yale University, Sloane Physics Laboratory, New Haven, Conn.	CW	28 in.	d	4.2
			α	7.6

Outside the United States

Location	Type	Pole-piece Diameter	Particles Accelerated	Energy (MeV)
Argentina				
[3]n.a.	FM	n.a.	n.a.	n.a.
Australia				
[1]Australian National University, Canberra	n.a.	30 in.	p	8
[1]Melbourne, University, Melbourne	variable	40 in.	p	12.5
	energy		d	6.25
			α	12.5

Location	Type	Pole-piece Diameter	Particles Accelerated	Energy (MeV)
Belgium				
[1,3]Centre de Physique Nucleaire, Louvain	CW	94 cm	d	13.35
Canada				
[1]McGill University, Montreal, Quebec	FM	82 in.	p	100
[1]Western Ontario, University, London, Ontario	n.a.	35 cm	e	4.5
Denmark				
[1]Institute for Theoretical Physics, Copenhagen	CW	90 cm	p	5.5
			d	11
			α	22
			also C, N, O	
France				
[1]Centre d'Etudes Nucleaires de Saclay, Saclay	n.a.	160 cm	d	20
			α	45
			N^{6+}	120
			O^{6+}	120
Germany				
[1]Institut für Strahlen- Und Kernphysik, Universität Bonn, Bonn	FM	190 cm	d	35
			α	70
[1]Institut für Physik im Max-Planck-Institut für Med. Forschung, Heidelberg	CW	101 cm	d	13
[1]Universität Braunschweig, Braunschweig	n.a.	50 cm	e	5
[1]Universität Mainz, Mainz	n.a.	50 cm	e	10
Great Britain				
[1]Atomic Energy Research Establishment, Harwell, England	FM	110 in.	p	175
[1,3]Birmingham, University, Birmingham, England	CW	61.5 in.	p	10
			d	20
			H_2^+	
			He^3	
			α	40
			also C, N, O	
[1,3]Cambridge, University, Cambridge, England	n.a.	35.5 in.	p	
			d	8
			α	
[1]Hammersmith Hospital, London, England	CW	50 in.	p	7.5
			d	15
			α	30
[1]Liverpool, University, Mt. Pleasant, Liverpool, England	CW	37 in.	p	4.5
			d	8.9
	FM	156 in.	p	410
[1]University College, London, England	n.a.	20 in.	e	4.5
	n.a.	80 in.	e	25
Israel				
[1]Hebrew University, Jerusalem	n.a.	n.a.	p	1
Japan				
[1]Kyoto University, Kyoto	n.a.	105 cm	d	16
[1]Osaka University, Osaka	n.a.	111.8 cm	d	12
[1]Scientific Research Institute, Tokyo	n.a.	66 cm	d	4
Tokyo, University, Institute of Science and Technology, Tokyo	n.a.	40 cm	d	2
			p	4

Location	Type	Pole-piece Diameter	Particles Accelerated	Energy (MeV)
[1]Tokyo, University, Institute for Nuclear Study, Tokyo	n.a.	160 cm	p	65 (FM)
			d	22 (CW)
			p	16 (CW)
Netherlands				
[1]Instituut voor Kernphysisch Onderzoek, Amsterdam	FM	180 cm	d	26
			α	52
Sweden				
[1]Nobel Institute for Physics, Stockholm	CW	80 cm	p	3.5
			d	7.
			α	14
	CW	225 cm	p	11 MeV/ nucleon
			d	11 MeV/ nucleon
			α	11 MeV/ nucleon
			ions to Ne^{6+}	11 MeV/ nucleon
[1]Gustaf Werner Institute for Nuclear Chemistry, Uppsala	FM	230 cm	p	192
Switzerland				
[1]Physikalisches Institut der Universität Zürich, Zürich	FFAG	33 in.	p	7.5
			d	10
			α	20
[1]European Council for Nuclear Research, Geneva	FM	50 cm	p	600
Union of South Africa				
[1]South African Council for Scientific and Industrial Research, Pretoria	CW	113 cm	d	15.5
Union of Soviet Socialist Republics				
[1,6]Big Volga Laboratories, Bolshoya Volga	FM	6 m	n.a.	680
[6]Institute for Thermal Studies, Moscow	CW	1.5 m	n.a.	n.a.
[6]Moscow Physical Institute, Moscow	n.a.	1.5 m	n.a.	n.a.
[6]Peking	CW	n.a.	n.a.	25
[1]Radium Institute, USSR Academy of Sciences, Leningrad	n.a.	14 in.	d	1.8
Yugoslavia				
[1]Institute "Rudjer Boskovic", Zagreb	*n.a.	140 cm	p	8
			d	16
			heavy ions	

Magnetic Accelerators: Synchrotrons

In the United States

Location	Type	Orbit Radius	Particles Accelerated	Energy (MeV)
[1]Brookhaven National Laboratory, Upton, Long Island, N.Y.	proton	30 ft	p	3 000
	*proton	421.45 ft	p	30 000
[1]California, University, Medical Center, San Francisco, Calif.	electron	29 cm	e	70
[1]California, University, Radiation Laboratory, Berkeley, Calif.	electron	3.3 ft	e	340
	proton	50 ft	p	6 300
[1]California Institute of Technology, Pasadena, Calif.	electron	376 cm	e	1 200
[1]Cornell University, Laboratory of Nuclear Studies, Ithaca, N.Y.	electron	12.5 ft	e	1 000
[1]General Electric Company, Schenectady, N.Y.	electron	2 ft	e	300
[1]Iowa State College, Ames, Ia.	electron	1 ft	e	90
	electron	1 ft	e	90
[1]Massachusetts Institute of Technology, Cambridge, Mass.	electron	3.3 ft	e	350
[1]Michigan, University, Ann Arbor, Mich.	electron	3.3 ft	e	100
[1]Midwestern Universities Research Association, Madison, Wis.	FFAG	60 cm	e	0.4
	FFAG	60 cm	e	0.4
	FFAG	150 cm	e	40
[1]Purdue University, Lafayette, Ind.	electron	100 cm	e	340
[1]U.S. Naval Research Laboratory, Washington, D.C.	*electron	77 cm	e	100
[1]Virginia, University, Charlottesville, Va.	electron	30 cm	e	75

Outside the United States

Location	Type	Orbit Radius	Particles Accelerated	Energy (MeV)
Australia				
[1]Australian National University, Canberra	*proton	480 cm	p	10 600
	electron	10 cm	e	33
[1]Melbourne, University, Melbourne	electron	10 cm	e	18
Canada				
[1]Queens University, Kingston, Ontario	electron	29.3 cm	e	70
France				
[1]Centre d'Etudes Nucleaires de Saclay, Saclay	proton	8.40 m	p	4 000

Location	Type	Orbit Radius	Particles Accelerated	Energy (MeV)
Germany				
[1]Physikalisches Institut, Freie Universität, Berlin-Dahlen	electron	7.5 cm	e	12
[1]Physikalisches Institut der Universität Bonn, Bonn	electron	170 cm	e	500
Great Britain				
[1]Birmingham, University, Birmingham, England	proton	450 cm	p	1 000
[1]Cambridge, University, Cambridge, England	electron	10 cm	e	33
[1]Oxford University, Oxford, England	electron	46.7 cm	e	125
[1]Glasgow, University, Glasgow, Scotland	electron	125 cm	e	340
[1]Royal Cancer Hospital, London, England	electron	10 cm	e	30
Italy				
[1]Istituto Nazionale di Fisica Nucleare, Rome	electron	360 cm	e	1 000
Japan				
[1]Osaka Prefectural University, Osaka	electron	14 cm	e	30
[1]Tohoku University, Sendai	electron	25 cm	e	40
	electron	30 cm	e	60
[1]Tokyo, University, Faculty of Science, Tokyo	electron	100 cm	e	200
[1]Tokyo, University, Institute of Nuclear Study, Tokyo	electron	400 cm	e	1 000
[1]Tokyo Institute of Technology, Tokyo	electron	15 cm	e	25
Netherlands				
[1]Delft Institute of Technology, Delft	proton	3.25 m	p	1 000
Sweden				
[1]Fysiska Institutionen, Lund	electron	3.65 m	e	1 200
	electron	20 cm	e	35
Switzerland				
[1]European Council for Nuclear Research	proton	100 m	p	25 000
[1]Roentgeninstitut, Inselspital, Bern	electron	29 cm	e	100
Union of Soviet Socialist Republics				
[1,6,7]Big Volga Laboratories, Bolshoya Volga	proton	28 m	p	10 000
[6,7]Leningrad	electron	n.a.	e	150
[6,7]Lebedev Institute, Moscow	electron	n.a.	e	240
	electron	n.a.	e	600
[6]Moscow Physical Institute, Moscow	nonferrous, electron	n.a.	e	200

Acknowledgments

The author sincerely appreciates the aid and encouragement that he has received from many sources during the preparation of this accelerator list. The aid of various members of the Technical Information Division staff has been invaluable. Special thanks are due to Dr. Edwin M. McMillan for suggesting the accelerator classification system used here.

NUCLEAR INSTRUMENTS 3 (1958) 201–203; NORTH-HOLLAND PUBLISHING CO. – AMSTERDAM

PROPOSAL FOR AN ANALOG-TO-DIGITAL ELECTRONIC CONVERTER SUITED FOR NUCLEAR PULSE HEIGHT ANALYSIS

A. ALBERIGI, C. BERNARDINI and I. F. QUERCIA

Istituto Nazionale di Fisica Nucleare – Laboratori di Frascati

Received 5 August 1958

An analog-to-digital converter is proposed based on the use of delay lines as codifying elements. Application of the converter to pulse height analyzers, with one or more channels, is discussed. Preliminary experimental work is briefly reported.

1. Introduction

This paper concerns a proposal on a pulse height analysing device. The basic idea is the following: if a short pulse, of amplitude V_0, is injected at the input A of a circuit like the one shown in fig. 1, the discriminator will be triggered by a series of pulses due to the reflections at the ends of the suitably terminated line L

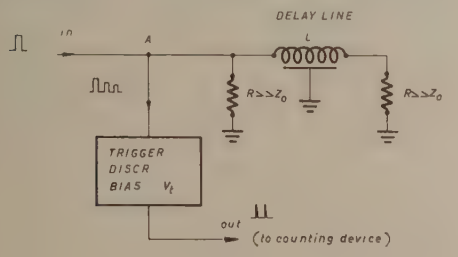

Fig. 1. Basic circuit.

and equally spaced in time by τ (the time delay of $2L$), until the characteristic attenuation of L reduces V_0 to a value less than V_t, the discriminator threshold.

If γ is the attenuation coefficient per unit length and L is the line length, the amplitude of the n-th pulse reaching the discriminator input is:

$$V_0 \, e^{-2n\gamma L} \qquad (n = 0, 1, 2, \ldots)$$

while the amplitude of the last triggering pulse is such that

$$V_0 \, e^{-2n\gamma L} > V_t > V_0 \, e^{-2n\gamma L} \, e^{-2\gamma L} \, .$$

In principle this device could work as an analog-to-digital converter, the number n characterising a digit (a channel) on a logarithmic scale for the input amplitudes[1]).

It is easily shown that the fractional channel width of such a pulse analyzer would be constant, namely that:

$$\text{fractional channel width} = e^{2n\gamma L} - 1 \, .$$

Conventional pulse height analyzers have a constant channel width, rather than a constant fractional channel width. We shall see in § 3 that it is possible to modify the basic circuit to fulfill this requirement.

In § 2 we shall show an immediate application of the basic circuit to a window-type discriminator[2]).

2. Window-Type Discriminator

Let us start by introducing the "last pulse triggering" (LPT) circuit.

Let a series of n equally spaced pulses be

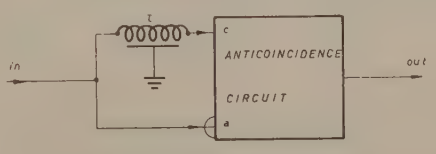

Fig. 2. Last pulse triggering circuit.

[1]) B. Åström, Nuclear Instruments **1** (1957) 143.

[2]) The use of a delay line for a one channel pulse height analyzer has been already proposed by: E. Gatti and F. Piva, Nuovo Cimento **10** (1953) 984.

injected at the input of the circuit shown in fig. 2 starting at time $t = 0$; the last pulse of the series (the n-th) is the only one that triggers the anticoincidence if the time delay τ of the line is just equal to the pulse spacing. Thus, only one pulse appears at the output of the device at the time $(n + 1)\,\tau$.

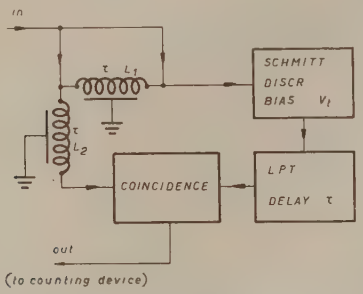

Fig. 3. Window discriminator block diagram.

Let us consider the circuit of fig. 3: we shall show that it works as a window discriminator. The circuit operates in the following manner:

(a) if two pulses trigger the Schmitt discriminator, one coming directly from the input and its τ-delayed partner coming from the line L_1, the LPT fires at the time 2τ: this pulse however is blocked by the coincidence because a pulse appears at the other input of the latter at the time τ, due to the delay line L_2. This happens if

$$V_0\, e^{\gamma L_1} > V_t\,.$$

(b) if $V_0 < V_t$ the Schmitt does not fire at all.

(c) if, however, the input pulse but not the attenuated one triggers the discriminator, then the LPT fires at time τ; at the same time there is a pulse at the other input of the coincidence through the delay line L_2 and a pulse is produced at the output.

The circuit selects those pulses the height of which lies in the interval.

$$V_t < V_0 < V_t\, e^{\gamma L_1}\,.$$

The width of the window, $V_t\,(e^{\gamma L_1} - 1)$ is not constant but varies proportionally to the discriminator bias V_t.

3. Multi-Channel Analyzer

Returning to the constant-width pulse height analyzer, it is easy to see that one can obtain any desired combination of delay and attenuation by means of a network like the one shown in fig. 4; the attenuation is obtained by the dividers (R_k, r_k) together with the characteristic attenuation of the delay lines. Now, it is possible to arrange things so that a pulse, of amplitude V_0, injected at A_k, appears at the output at the time $k\tau$ with an amplitude $V_0/(k + 1)$ (k being an integer ranging from 0 to n).

Let us consider the following diagram (fig. 5):

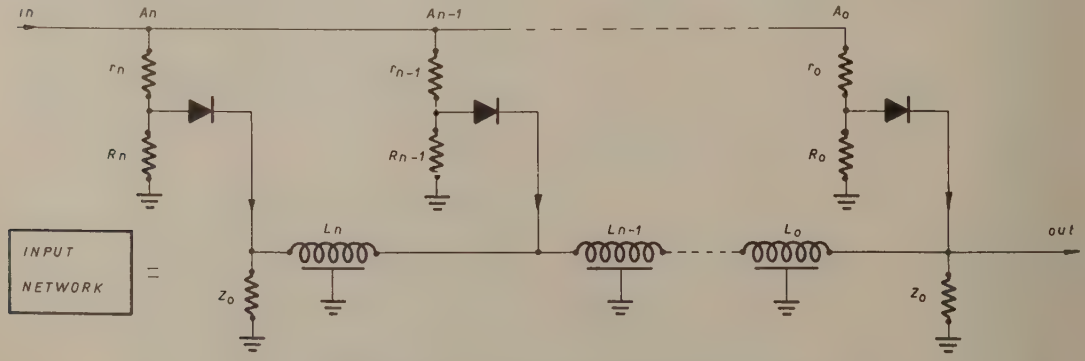

Fig. 4. Basic network for linear amplitude to-delay conversion.

Writing $V_0 = (k_0 + \varepsilon)\,V_t$, where k_0 is an integer and $0 < \varepsilon < 1$, a standard pulse appears at the LPT output at the time $(k_0 + 1)\,\tau$. This is the last pulse which has triggered the discriminator since the succeeding pulse at the discriminator input has an amplitude:

$$\frac{V_0}{k_0+1} = \frac{k_0+\varepsilon}{k_0+1} V_t = \left(1 - \frac{1-\varepsilon}{1+k_0}\right) V_t < V_t \ .$$

Fig. 5. Block diagram of the analog to digital converter

The "first digit" k_0 of the input pulse has been converted in this way into a time delay $(k_0 + 1)\,\tau$. The pulse can now be conveyed to the k-th counting channel of a storage system according to the diagram of fig. 6.

A four-channel network has been tested using a "Hochental type HH 2 500" delay line (characteristic impedence $Z_0 = 2.700$ ohm, delay 1.9 μs/m, $\gamma = 0.055$ m^{-1}). The lines L_0, L_1, L_2, L_3, all of the same length were adjusted for 2 μs delay. The pulse injected at the input network had a length of 1 μs, and rise and fall times < 0.1 μs. The four output pulses have been carefully checked as regards the amplitude ratios: these ratios were observed to remain accurately constant (within 1%) for large variations of the input amplitudes. Reflections

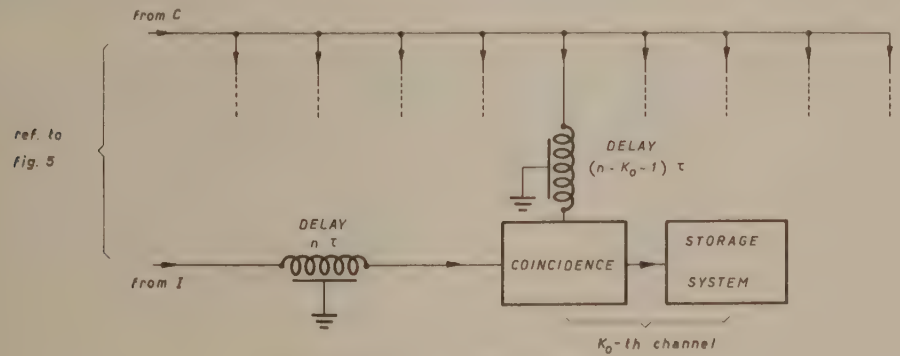

Fig. 6. Decoding and storage system.

Only that coincidence the input of which is delayed by $(n - k_0 - 1)\,\tau$, is triggered by the input pulse delayed by $n\tau$, and by the analyzed pulse delayed by $(k_0 + 1)\,\tau$.

In this way pulses are collected in the channels

$$V_t < V_0 < 2V_t;\ \ 2V_t < V_0 < 3V_t;\ \ldots\ (n-1)\,V_t < V_0 < nV_t$$

that is, the analyzer has $n - 1$ channels of constant width V_t.

4. Preliminary Experimental Work

Preliminary experimental tests have been made of the "Input network" shown in fig. 4. at injection points were found to be completly negligible.

A 16-channel linear pulse height analyzer, and a window analyzer of the types described in §§ 2 and 3 are now being designed. Satisfactory tests of elementary circuits, e.g. the LPT circuit, have been performed. Up to now we have tested the circuits in the 1 μs range, because of the speed limitations of the conventional Schmitt circuits employed as discriminators. To reach shorter analyzing times we need faster discriminators; at present we are studying the latter.

NUCLEAR INSTRUMENTS 3 (1958) 204–206; NORTH-HOLLAND PUBLISHING CO. – AMSTERDAM

SCHNELLER RINGZÄHLER ALS ELEKTRONISCHER SCHALTER

WOLFGANG GRUHLE

Institut für Physik im Max Planck-Institut für med. Forschung, Heidelberg

Received 12 August 1958

An improved ring counter is described which can be extended to any number of stages. The use of modern switching tubes allows counting rates up to 1 Mc/s, every stage giving separate output pulses without loading effect on the cycling process. For program switching application more than one state may simultaneously pass around the ring.

Abweichend von den üblichen Untersetzerschaltungen, bei denen bistabile Multivibratoren (Flipflop-Kreise) in Serie liegen, wurde erstmalig von Regener[1]) eine Ringform beschrieben. Die Flipflop-Paare sind so zu einem Ring verkettet, dass stets die Hälfte aller Röhren in einer Gruppe von direkt aufeinander folgenden Stufen leitet. Bei N Stufen (mit $2N$ Röhrensystemen) wandert der leitende Zustand einer Gruppe von N Röhren bei jedem Steuerimpuls um eine Stufe weiter, bis er nach N Impulsen in die Anfangslage zurückgekehrt ist. Eine Anzahl von Zähldekaden[2,3]) in verschiedenen Abwandlungen wurde beschrieben: ein doppelter Durchlauf eines Fünfer-Ringes[4]), sowie die Durchlaufmöglichkeit in beiden Ringrichtungen[5]). Spezielle Schaltröhren wurden ebenso selten verwendet[6]) wie ihre direkte Steuerung durch einen Ringzähler[7]).

Soll jeweils nur eine Ringstufe leiten (sperren)[8]), so muss dafür gesorgt werden, dass die Durchlaufrichtung im Ring eindeutig ist bzw. die vorhergehende Stufe zurückgestellt wird. Auch mit Transistoren lassen sich Ringzähler aufbauen[9]). Die in neuerer Zeit entwickelten Schaltröhren EH90, EH900S (E91H), H80E, 6BN6 u.a. erlauben den Aufbau von erheblich schneller arbeitenden Ringen. Da sich bei diesen Röhren das Teilsystem G_3-Anode unabhängig vom übrigen Röhrensystem als Schalt-Tor verwenden lässt, können von jeder Ringstufe rückwirkungsfrei saubere Rechteckimpulse abgenommen werden, die zum Steuern elektronischer Bausteine geeignet sind. Ein so aufgebauter Ring hat folgende Eigenschaften:

1. Von N Stufen liegt normalerweise nur eine einzige im leitenden (bzw. gesperrten) Zustand, der bei jedem Triggerimpuls auf die nächstfolgende weiterspringt. Die Ablesung des Zustandes, etwa durch Glimmlampen, ist wesentlich vereinfacht, da die Widerstandsnetzwerke der normalen Untersetzer vermieden werden.

2. Der Ring lässt sich auf nahezu beliebig viele Stufen erweitern. Die Grenze wird nur durch den mit wachsender Stufenzahl ansteigenden Steuerleistungsbedarf (zunehmende kapazitive Last) gesetzt, der bis zu 100 Stufen aber leicht aufzubringen ist. Auf diese Weise lassen sich beliebige ungerade Untersetzungsverhältnisse erzielen.

3. Mit besonderen Schaltröhren lassen sich die Impulse mit ihrer Gleichspannungskomponente rückwirkungsfrei auch ohne Kathodenfolger auskoppeln.

4. Unter einer später genannten Bedingung kann der ganze Ring in einen Anfangszustand gesetzt werden, bei dem mehrere Stufen den

[1]) V. H. Regener, Rev. Sc. Instr. **17** (1946) 185.
[2]) L. Seren, Rev. Sc. Instr. **18** (1947) 654.
[3]) B. Åström, Rev. Sc. Instr. **21** (1950) 323.
[4]) R. Baker, Journ. Sc. Instr. **25** (1948) 127.
[5]) V. H. Regener, Rev. Sc. Instr. **17** (1946) 375.
[6]) B. J. Moore, Rev. Sc. Instr. **21** (1950) 337.
[7]) N. A. Moerman, Electronics **19**/4 (1946) 150.
[8]) T. K. Sharpless, Electronics **21**/3 (1948) 122.
[9]) A. W. Lo, Proc. I.R.E. **40** (1952) 1559.
[10]) R. Weissmann, Electronics **22**/5 (1949) 84.

ausgezeichneten Zustand annehmen. Diese Konfiguration wandert unverändert durch den ganzen Ring.

Abb. 1 zeigt drei Stufen eines solchen Ringes. Jedes übereinander gezeichnete Röhrenpaar bildet mit den ersten beiden Gittern (als Trioden) einen bistabilen Multivibrator. Die Eigenart der Schaltröhren erlaubt die Sperrung des Anodenstroms durch Gitter 3, ohne dass der Triodenteil K-G_1-G_2 davon beeinflusst wird.

Steuerimpuls lässt den gleichen Vorgang über die beiden nächsten Stufen ablaufen, bis der ganze Ring durchwandert ist.

Die Anoden der unteren Röhrenreihe sind zur (rückwirkungsfreien) Abgabe von Impulsen frei. Sie liegen im Ruhezustand (leitend) auf etwa +100 Volt, im aktiven Stufenzustand (gesperrt) auf etwa +200 Volt. Es lassen sich daher Rechteckimpulse von 100 Volt Amplitude abgreifen, wobei ebenfalls die Gleichspannungs-

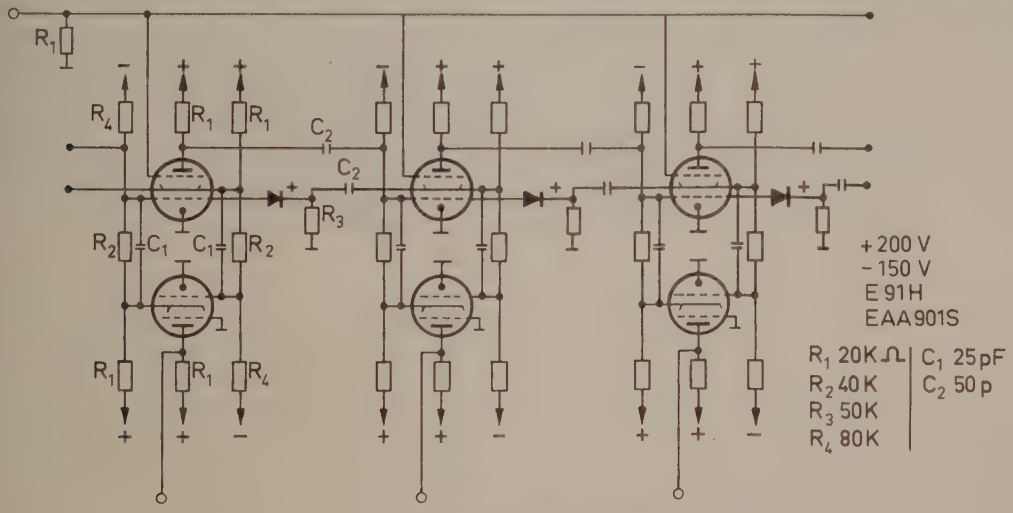

Abb. 1. Drei Stufen des Ringzählers.

Die mittlere Stufe sei im ausgezeichneten Zustand, d.h. ihre obere Röhre sei leitend, die untere gesperrt, während alle übrigen Röhren der oberen Reihe gesperrt seien. Trifft jetzt ein (negativer) Impuls auf den Eingang des Ringes (Gitter 3 aller oberen Röhren), so wirkt er nur auf die mittlere Stufe. Ihr Anodenstrom wird in der oberen Röhre unterbrochen und der positive Impuls an der Anode wird auf das Gitter 1 der nächstfolgenden Stufe geführt. Dadurch kippt diese um und nimmt den bisherigen Zustand der mittleren Stufe an. Diese selbst wird durch einen negativen Impuls zurückgestellt, der an Gitter 2 der oberen Röhre der folgenden Stufe afgenommen wird. Die Einkopplung führt jeweils über eine Diode, damit nicht beim Zurückkippen einer Stufe die davor liegende wieder gezündet wird. Jeder folgende

komponente entnommen werden kann, ohne die Funktion des Ringes zu stören. Mit umgekehrter Polung der Impulse gilt das gleiche für die Anoden der oberen Röhren, mit der Einschränkung, dass hier auf Rückwirkungen geachtet werden muss. Diese werden vermieden, wenn Röhren mit zwei Anoden (H80E) verwendet werden.

In der unteren Reihe sind alle Gitter 3 geerdet. Sie lassen sich aber auch zur getrennten Einspeisung von Steuerimpulsen verwenden. Durch eine Unterbrechertaste kann der Ring in den Anfangszustand (Stufe 1 leitend) versetzt werden (Abb. 2). Analog lassen sich andere Anfangsgruppierungen wählen, bei denen mehrere Stufen gleichzeitig den ausgezeichneten Zustand besitzen. Diese Gruppierung wandert bei jedem Steuerimpuls um eine Stufe im Ring

weiter. Jedoch können infolge der Rückwärtslöschung zwei unmittelbar hintereinander liegende leitende Stufen nicht bestehen bleiben. Die Vielzahl der möglichen Kombinationen gestattet auch komplizierte Programm-Steuerungen.

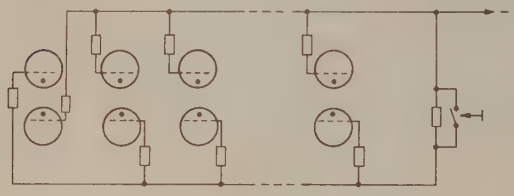

Abb. 2. Rückstellung in eine Anfangslage.

Der Ring benötigt negative Steuerimpulse von rund 10 Volt und einigen 100 nsec Anstiegszeit, die zweckmässig über einen Kathodenfolger eingekoppelt werden. Bei sehr hohen Zählraten sind steilere Impulse (Anstiegszeit maximal 100 nsec) notwendig. Positive Impulse bleiben wirkungslos. Mit den angegeben Werten in Abb. 1 haben die Flanken der abgenommenen Rechteckimpulse etwa 0.7 μsec Anstieg und 0.3 μsec Abfall. Kleinere Arbeitswiderstände verringern diese Zeiten, jedoch wächst dabei der Stromverbrauch des Ringes. Der über die Röhrenkapazitäten noch an den Ausgang gelangende Rest-Impuls von der nächst folgenden Stufe liegt unter einem Prozent der Impulsamplitude. Die Anodenspannung (+200 V) und die negative Spannung (— 150 V) werden elektronisch geregelt. Eine von ihnen wird auf den Wert eingestellt, der einen stabilen Arbeitspunkt sichert. Der Stromverbrauch pro Stufe (Abb. 1) beträgt etwa + 16.5 mA und —3.5 mA.

NUCLEAR INSTRUMENTS 3 (1958) 207–212; NORTH-HOLLAND PUBLISHING CO. – AMSTERDAM

RELATIVE SCINTILLATION EFFICIENCIES OF NOBLE GAS MIXTURES†

J. A. NORTHROP and JUDITH C. GURSKY

University of California, Los Alamos Scientific Laboratory, Los Alamos, New Mexico

Received 20 August 1958

An investigation has been made of the relative amounts of scintillation light emitted from mixtures of the noble gases during the 0.5 μsec interval following the stopping of an α-particle. A bellows pump and a hot uranium furnace in a closed circulation system maintained gas purity. A diphenyl stilbene coating on the photomultiplier tube and the walls of the scintillation volume acted as a wavelength shifter for the primary ultraviolet radiation. Data on the efficiency of various proportions of binary combinations of xenon, krypton, argon, neon, and helium are presented. They show a characteristic large drop in the light for mixtures containing a small proportion of the heavier gas in a major fraction of the lighter. These results may be qualitatively interpreted in terms of noble gas molecular ion formation. The large light output of the 10% Xe–90% He mixture might be useful in constructing a neutron spectrometer of high efficiency using the $He^3(n,p)H^3$ reaction.

1. Introduction

The noble gases have recently proven useful as scintillation detectors because of their short decay times, constancy of light output per unit energy independent of ionization density, relatively large light output when used in conjunction with an appropriate wavelength shifter, availability in a wide range of Z, and suitability in either a gaseous or condensed state[1]). Although the emission of light following the passage of a charged particle through a noble gas should be rather easily understood compared to the complex phenomena taking place in other scintillators, no adequate description of the process seems to exist. Such an understanding would greatly assist further improvement of these detectors. Since most of the primary scintillation light lies in the far ultraviolet, direct observations of the fundamental processes are difficult to make. The investigation of binary gas mixtures described in this paper was undertaken in the hope of finding an efficient combination of a heavy gas wavelength shifter in a cheaper light gas. Although this particular result was not attained, the data are of interest in other applications of gas scintillation counters as well as providing information about energy transfer and radiation processes.

† Work performed under the auspices of the U. S. Atomic Energy Commission.

2. Counter and Gas System

A sketch of the gas scintillation counter is shown in fig. 1. It consisted essentially of a hollow aluminium cylinder through which the gas was continuously circulated. A photomultiplier tube (DuMont 6292) was sealed to one end and a U^{234} α-particle source to the other end, using Myvaseal O-rings. The collimator transmitted only particles having a direction such that they ended their range in the gas. The face of the phototube was coated with 30 $\mu g/cm^2$ of diphenyl stilbene by vacuum evaporation[2]). This phosphor acted as a wavelength shifter, absorbing the ultraviolet light of the primary scintillation and radiating it in a spectral region more nearly matching the spectral sensitivity of the photocathode. The cylinder wall was smoked with a thick layer of MgO by burning magnesium

[1]) C. Eggler and C. M. Huddleston, Nucleonics **14**, No. 4 (1956) 34;
A. Sayres and C. S. Wu, Rev. Sci. Instr. **28** (1957) 758;
R. A. Nobles, Rev. Sci. Instr. **27** (1956) 280;
M. Forte, Nuovo Cimento (Ser. 10) **3** (1956) 1443;
J. A. Northrop and R. Nobles, Nucleonics **14**, No. 4 (1956) 36;
IRE Trans. on Nuclear Sci. **NS-3**, No. 4 (1956) 59.

[2]) J. A. Northrop, Rev. Sci. Instr. **29** (1958) 437.

ribbon and subsequently coated with an evaporated layer of 200 $\mu g/cm^2$ of diphenyl stilbene. Such a system was shown to be optically very efficient in that large variations in gas pressure

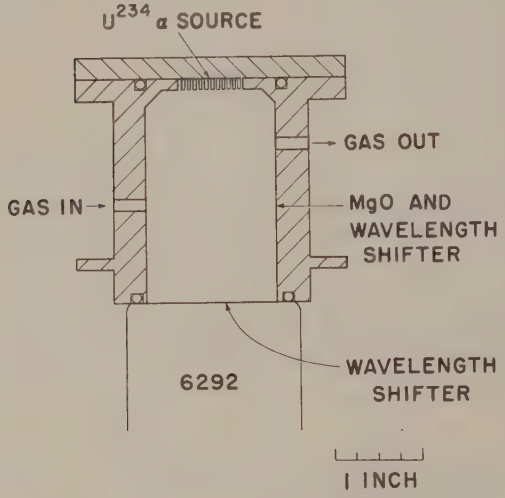

Fig. 1. Scale drawing of the gas scintillation counter.

which radically changed the distance between photocathode and the centroid of the scintillation light, had but little effect on the signal output from the phototube.

Gas scintillators are particularly susceptible to the poisoning effects of contaminants arising from poorly outgassed systems. The poisoning time constant for this system when the gas was isolated in the counter was several days. A metal bellows pump and a check valve system provided unidirectional flow of the gas over a uranium metal purifier, into the counter, and back to the pump. The flow rate was such as to change the volume of gas in the counter every few seconds. The pump had two bellows sections, operating out of phase, which maintained a constant volume, and hence pressure, in the system. The purifier was a stainless steel tube initially loaded with 50 g of uranium metal turnings imbedded in steel wool. Following assembly of the complete gas system, the metal was made finely divided and reactive by first converting to uranium hydride by admitting hydrogen gas and heating, and subsequently reducing the hydride back to the metal. In operation the input end of the tube was held at 800°C and the outlet end kept at room temperature for hydrogen absorption. Such a purifier is efficient in removing gross quantities of contaminants such as H_2, O_2, N_2, and CH_4. However, the ultimate vapor pressure of such contaminants is determined by the balance between the rate of evolution from the walls of the system and the rate of reaction with the uranium, and was not known for this equipment. When gas circulation was restored following poisoning by natural gas evolution from the walls, the light signal returned to its equilibrium value in about five seconds. An initial filling of new gas took about ten minutes to be purified to maximum pulse height.

The collimated source of U^{234} α-particles produced a rate of 600 counts per minute in the gas volume. The regulated photomultiplier voltage was continuously compared to a standard cell and corrected for small drifts to maintain constant phototube gain. The amplifier, which had a clipping time constant of $RC = 0.5$ μsec, drove a ten-channel pulse-height analyzer. Following each run, the gain of the amplifier-analyzer system was measured, using a standard pulser.

3. Gas Mixture Measurements

The noble gases used for these measurements were spectro-grade supplied by Linde[3]). However, it should be noted that the uranium purifier was operated at all times so that the quantities of contaminants, other than the noble gases, were controlled by the purifier rather than by the quantities present initially in the gas. The supplier's analysis indicates 500 ppm krypton were present in the xenon.

Tanks of all five gases were attached to the system through a simple manifold. The krypton and xenon tanks were of thin-walled steel so that these gases could be recovered from the system back into the tank by immersing the tank in liquid nitrogen. A diffusion pump with a liquid air trap reduced the pressure in the complete pump, purifier, and counter system to

[3]) Linde Air Products Company, Tonawanda, New York.

10^{-5} mm Hg between fillings. Gas mixtures in which each fraction had a partial pressure > 1 mm were measured by conventional pressure gauges. Very small concentrations were subsequently obtained by multiple dilutions with the predominant gas, followed by thorough mixing in the circulation system. The adequacy of such a technique was verified by comparing the results obtained from, for example, three successive 2:1 dilutions with that from a single 8:1 dilution. Except for the case of small concentrations obtained by multiple dilution, gas mixtures not containing krypton or xenon were discarded after each run. Significant amounts of the latter gases were recovered into their storage tanks by freezing, and the lighter gas fraction (argon, neon, or helium) was removed with the pumping system. Separation of xenon from krypton by this method of freezing and pumping was so incomplete as to require new gas to be used for each of the very limited number of data points obtained for this mixture.

In this series of measurements in which the stopping power of the gas varies, it was not clear whether the pressure or the ionization density along the track should be kept constant. The latter case was chosen since it had the added advantage of constant light geometry. Thus, even though the amount of light at the photocathode was very insensitive to the location of the scintillation pulse in the gas volume, indicating an efficient reflector and small self-absorption, the pressure of each gas mixture was adjusted to maintain constant α-particle range. The absolute pressures used were such that the α-particle range was about two-thirds the length of the cylinder. The extreme pressures were 30.4 cm Hg for xenon and 300 cm Hg for helium.

The light outputs for various fractional mixtures are shown in fig. 2. The data have been normalized to the pulse height obtained for pure xenon gas. The light outputs for the pure gases relative to xenon are

$$\text{Xe:Kr:A:Ne:He} = 1.0:0.52:0.16:0.043:0.33.$$

One does not observe a monotonic change in the light output in going from one pure gas to another. In all cases there is a pronounced decrease in light with small amounts of the heavier gas in a major fraction of the lighter one. These parts of the curves are shown in more detail in the inserts having a logarithmic abscissa. The Kr-Xe and one of the A-Kr curves (bottom two in fig. 2) were obtained with a quaterphenyl wavelength shifter on both the phototube face and MgO reflector. The similarity of the shapes of the A-Kr curves for diphenyl stilbene (top left) and quaterphenyl (bottom left) suggests that these resonant effects are independent of the specific wavelength shifter used. It seems probable that the slight increase in light in going from pure xenon to the 90% He-10% Xe mixture is associated with the radical variation of absolute pressure over this range. It is also to be noted that pure neon has less light output than is obtained at the minimum of the Ne-Xe and Ne-Kr curves.

TABLE 1

Partial pressures and relative scintillation light output at the point of minimum light output in binary noble gas mixtures

Mixture	Total absolute pressure of mixture (mm Hg)	Fraction (by atoms) of heavier gas at the minimum	Scintillation light at minimum relative to pure xenon
He-Ne	2.23×10^3	1×10^{-1}	0.016
He-A	2.86×10^3	1×10^{-2}	0.014
He-Kr	2.95×10^3	2.5×10^{-3}	0.018
He-Xe	3.00×10^3	3×10^{-4}	0.044
Ne-A	6.64×10^2	3×10^{-2}	0.035
Ne-Kr	6.65×10^2	1.5×10^{-2}	0.053
Ne-Xe	6.66×10^2	5×10^{-3}	0.082
A-Kr	5.25×10^2	5×10^{-2}	0.109
A-Xe	5.29×10^2	1×10^{-2}	0.097
Kr-Xe[a]	6.06×10^2	1.5×10^{-2}	0.24

[a] Quaterphenyl wavelength shifter. All others are for diphenyl stilbene.

Table 1 lists the pressure and the amplitude of the light signal at the point of minimum light output for each binary mixture. The data are again normalized to the value for pure xenon. Since these minima are generally quite broad, it

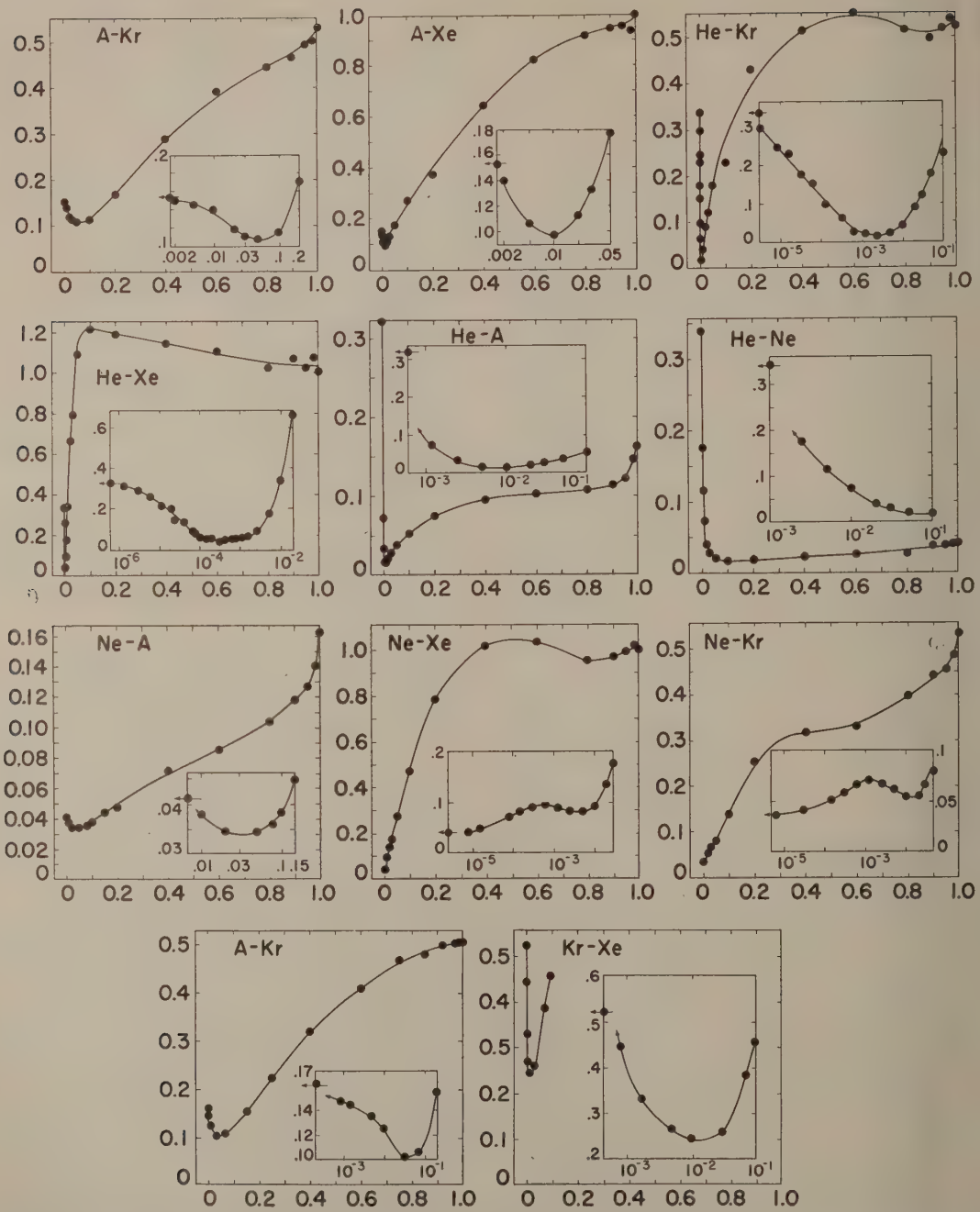

Fig. 2. Scintillation light output of binary noble gas mixtures for U^{234} α-particles detected by a 6292 photomultiplier tube and amplified by an electronic system having $RC = 0.5$ μsec clipping. The ordinates have been normalized to the light obtained from pure xenon. The abscissas are the fraction by pressure of the heavier gas in the mixture. The semilog inserts show the detail of the left part of each curve. All data were obtained using diphenyl stilbene as a wavelength shifter except for the bottom two (A-Kr and Kr-Xe), for which quaterphenyl was used.

is rather difficult to locate the precise percentage mixture at these points. However, a systematic trend is evident in that a larger difference in the number of closed electronic shells of the two constituent gases in any mixture leads to a smaller light output at the minimum and a smaller fractional pressure of the heavy gas at which the minimum light occurs.

4. Discussion

The relative importance of the various modes of decay of excited noble atoms in producing a fast scintillation pulse is not clearly understood. The slowing of a fast charged particle leaves energy in the form of ions, neutral excited atoms, and atoms which are both ionized and excited. The energy level diagrams of the neutral and singly ionized noble gases are characterized by a very high lowest excited state, typically of the order of two-thirds of the ionization energy. The most common mode of de-excitation is thus a direct radiative transition to the ground state, having decay times of the order of 10^{-8} sec, with lines in the visible part of the spectrum arising from transitions ending on excited levels relatively less important. However, radiation arising from a transition to the ground state will be resonance-trapped, thus leading to somewhat longer times for the actual escape of the energy from the volume of the gas[4]). That part of the primary energy deposited in metastable states in most cases can be transferred by thermal collisions to resonance levels which frequently lie within several kT's of the metastable levels[5]). Radiation arising from the de-excitation of excited ions is not resonance-trapped and escapes directly.

The data of this paper are interpretable largely in terms of the remaining process, the energy released by electron-ion recombination. Biondi has investigated the recombination times of noble gas atomic and molecular ions using microwave techniques in which the electron density is measured as a function of time following a microwave discharge[6]). These techniques allowed him to deduce the following series of events. Direct recombination of an atomic ion with a thermal electron in a radiative capture is relatively improbable since radiation times are long compared to collision times. In a pure noble gas the primary atomic ions first form stable molecular ions in collisions with normal atoms. Such molecular ions have an electron recomination coefficient much larger than that for an atomic ion, since electron capture followed by dissociation into excited neutral atoms is a nonradiative process. In a mixture containing a small quantity of a heavier gas in a major fraction of a lighter one, such as the He-A mixture (0.1 percent argon) investigated by Biondi, the positive charge is transferred in collisions from helium to argon since the heavier gas always has the lower ionization potential. The low density of argon prevents the formation of argon molecular ions in argon ion-argon atom collisions from taking place at an appreciable rate. Thus, in pure argon at several millimeters pressure electrons disappear at a rate characteristic of a recombination loss, while in the He-A mixture recombination follows ambipolar diffusion of the ions to the walls of the microwave cell. These data allow Biondi to estimate that the atomic ion recombination coefficient is at least a factor of 10^3 smaller than the molecular ion coefficient.

A quantitative comparison of the present measurement to Biondi's data is difficult because of the higher pressures used and inadequate estimates of equivalent electron volume densities for the case of an ionized track. A numerical value for the electron density could be used in conjunction with his estimate of a limiting value of the recombination coefficient for atomic ions to give a minimum recombination time. But it is clear that the reduction in scintillation

[4]) A. C. G. Mitchell and M. W. Zemansky, Resonance Radiation and Excited Atoms (The Macmillan Company, New York, 1934);
T. Holstein, Phys. Rev. **72** (1947) 1212; and **83** (1951) 1159.

[5]) A. V. Phelps and J. P. Molnar, Phys. Rev. **89** (1953) 1202;
P. Avivi and S. G. Cohen, Phys. Rev. **108** (1957) 972.

[6]) M. A. Biondi and S. C. Brown, Phys. Rev. **76** (1949) 1697;
M. A. Biondi and T. Holstein, Phys. Rev. **82** (1951) 962;
M. A. Biondi, Phys. Rev. **83** (1951) 1078.

light output for small admixtures of a heavy noble gas is produced by the longer recombination times for the atomic ions, leading to scintillation decay times longer than the electronic clipping time. The ambipolar diffusion loss of electrons is independent of ion density and may be calculated for the present He-A mixture using Biondi's value of the diffusion coefficient of A^+ in helium of $D_a p = 900$ (cm²/sec) — (mm Hg), where $p = 2.86 \times 10^3$ mm. The characteristic diffusion length of our counter is $\Lambda = 0.74$ cm and leads to a decay constant $T = \Lambda^2/D_a = 2\ \text{sec}^{-1}$. Thus it is clear that at the pressures used here, as opposed to the low-pressure microwave measurements, the light remaining at the bottom of the mixture curve does not arise from ion diffusion to the walls. It may well come from de-excitation of He^{+*} in which the radiation to the ground state of He^+, since it is not resonance radiation, can escape trapping in the gas.

A possible use of these gas mixture data that may be of considerable interest would be the application of the 10% Xe-90% He mixture to a gas scintillation neutron spectrometer of high efficiency using the $He^3(n,p)H^3$ reaction. Such a spectrometer, using a proportional counter filled with He^3, Kr, and CO_2, has been described by Batchelor *et al.*[7]). Their choice of krypton for the gas to be added to the helium was dictated by a compromise between two desired properties. The heavier gas xenon, having a higher atomic stopping power, would have reduced wall effects, thus reducing anomalous low-energy pulses arising from some of the H^3 reaction particles striking the walls. A lighter gas such as argon would have been preferable in allowing faster electron collection in the proportional counter. An equivalent device which used a helium-xenon mixture at high pressure for a scintillation gas would have the advantages of reduced wall effect and very fast pulses, as well as increased overall efficiency for neutron capture due to the higher pressure of He^3, but at a sacrifice in resolution. If one extrapolates the resolution of a gas scintillator as measured by Sayres and Wu[1]) by the usual square-root law to, for example, capture of a 600 keV neutron by He^3, about 9.5% resolution could be expected. This is to be compared to the $2.7 \pm 0.3\%$ spread obtained by Batchelor *et al.* in their proportional counter.

These mixture data also indicate the desirability of removing trace amounts of heavy noble gases when filling a scintillator with a lighter gas. Particular care must be taken to adequately pump out any hot calcium or uranium purifier that may be used with the scintillator. Although the results of the present work may be used as a guide, the exact shapes of the dips in light output will probably depend on absolute pressure of the gas mixture and the electronic clipping time in the amplifier.

The authors are indebted to Mrs. Lois K. Schlacks, who made many of the preliminary measurements.

[7]) Batchelor, Aves and Skyrme, Rev. Sci Instr. **26** (1955) 1037.

NUCLEAR INSTRUMENTS 3 (1958) 213–217; NORTH-HOLLAND PUBLISHING CO. – AMSTERDAM

ZUR HERSTELLUNG SEHR DÜNNER ELEKTRISCH LEITENDER PRÄPARAT-UNTERLAGEN FÜR ABSOLUTE β-ZÄHLUNG

E. HUSTER und W. RAUSCH

Physikalisches Institut der Universität Marburg

Received 1 August 1958

Absolute β-counting with radioelements of low decay-energy is difficult because of absorption losses in the source and its backing. If moreover the half-life is very high, extended sources are necessary. It has been furthermore shown, that backings must be electrically conducting to prevent charging of the source and thereby distortion of the electric field of the counter, if counting is done with the source in the interior of the counter.

A method is described for preparing electrically conducting formvar foils of 85 × 30 mm² with an overall thickness of 10 μg/cm². The conductivity is attained by first exposing the foil to a glow discharge in a hydrocarbon atmosphere and then evaporating silver on it.

1. Einleitung

Absolutmessungen von β-Aktivitäten sind um so schwieriger, je geringer die Zerfallsenergie und je grösser die Halbwertszeit des Strahlers ist. Misst man im Zählrohr in 2π-Geometrie, so wird die Messung durch zwei gegenläufige Effekte gefälscht, durch Absorption im Präparat und durch Rückstreuung aus der Unterlage. Welcher Effekt überwiegt, ist oft schwer zu entscheiden. Misst man in 4π-Geometrie (Fig. 1), so treten Zählverluste auf infolge von Absorption in Präparat und Unterlage. Bei β-Strahlern geringer Zerfallsenergie oder bei solchen, deren β-Spektrum einen hohen Bruchteil von Elektronen niedriger Energie enthält, muss man deshalb versuchen, Präparat und Unterlage möglichst dünn zu machen. Wenn zu der geringen β-Energie noch eine hohe Halbwertszeit hinzukommt (wie z.B. beim Rb^{87}), so benötigt man grossflächige Präparate, um ausreichende Zählraten zu erhalten. Ausserdem muss die Präparatunterlage eine so hohe elektrische Leitfähigkeit haben, dass sie die beiden Zählrohre elektrostatisch völlig trennt, oder, mit anderen Worten, Zählrohrkathode und Präparat müssen stets auf gleichem Potential liegen. Im anderen Falle lädt sich die Folie in der Zählrohrentladung positiv auf, und energiearme β-Teilchen werden nicht angezeigt[1]).

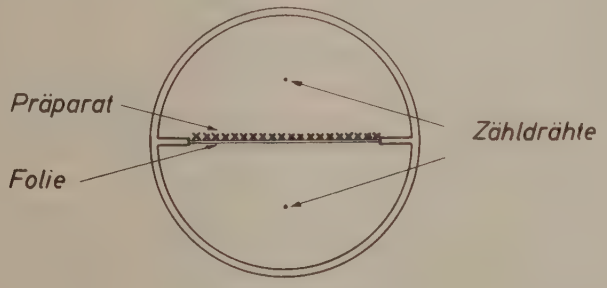

Fig. 1. 4π-Zählrohr.

Zur Absolutmessung der β-Aktivität langlebiger energiearmer Strahler werden also als Präparatunterlagen relativ grossflächige Folien

[1]) I. Geese-Bähnisch und E. Huster, Naturwiss. **41** (1954) 495; I. Geese-Bähnisch, Z. f. Physik **142** (1955) 565

hoher elektrischer Leitfähigkeit benötigt. Im allgemeinen werden organische Folien mit aufgedampfter Metallschicht benutzt. Im Rahmen unserer Untersuchungen an energiearmen β-Strahlern haben wir versucht, solche Folien mit möglichst geringer Massenbelegung herzustellen. Da sich zeigte, dass hierfür allgemeineres Interesse besteht, teilen wir im folgenden die Herstellungsmethode mit.

2. Herstellung der Trägerfolien

Zunächst wurde versucht, die Folien aus Zaponlack herzustellen. Es zeigte sich jedoch, dass Zaponfolien, die den anschliessenden Bedampfungen mit Metall und Präparat gewachsen sind, relativ dick sein müssen. Bei gleicher Dicke ist Formvar† mechanisch und thermisch weitaus höher belastbar als Zapon.

Dünne Formvarfolien lassen sich relativ einfach in folgender Weise herstellen:

(a) Man reinigt eine Glasscheibe, die etwas grösser ist als die benötigte Folie, erst in destilliertem Wasser, dann in einer Äther-Alkohol-Lösung, und wischt sie danach gründlich mit einem Fensterleder ab.

(b) Man taucht die Glasscheibe bis etwa 10 mm unterhalb ihres oberen Randes senkrecht in eine Lösung von Formvar in Dichloräthylen. Die erforderliche Konzentration der Lösung richtet sich nach der gewünschten Schichtdicke (Angaben darüber bei P. Barreau *et al.*[2]).

(c) Man zieht die senkrecht gehaltene Scheibe aus der Lösung heraus. Die Dicke der anhaftenden Formvarschicht hängt ausser von der Konzentration der Lösung beträchtlich von der Geschwindigkeit ab, mit der man die Scheibe herauszieht. Man kann daher durch Verändern dieser Geschwindigkeit die Schichtdicke über die Länge der Folie variieren und Schichten mit einer Art von Querrippen herstellen.

(d) Nach wenigen Minuten ist das Lösungsmittel verdunstet. Man ritzt jetzt die Formvarschicht einige mm vom Rand der Scheibe entfernt ringsherum mit einem weichen Metalldraht (Cu oder Al) ein. (Eine Rasierklinge beschädigt die Oberfläche der Glasscheibe. Diese kann danach nicht erneut benutzt werden.) Anschliessend schwemmt man die Folie in destilliertem Wasser ab, indem man die Scheibe möglichst flach langsam unter die Wasseroberfläche schiebt.

(e) Wenn die Folie frei auf dem Wasser schwimmt, taucht man den Rahmen, auf den sie aufgebracht werden soll, unter die Wasseroberfläche und zieht ihn dann vorsichtig in senkrechter Stellung so wieder heraus, dass ein Rand der Folie am oberen Rand des Rahmens haften bleibt. Sehr dünne Folien können leicht durch die Oberflächenspannung des Wassers oder durch das Gewicht anhaftender Wassertröpfchen zerstört werden. Es empfiehlt sich daher, den Rahmen zunächst nur so weit anzuheben, bis sich ein Streifen der Folie von nur 1 bis 2 mm oberhalb der Wasseroberfläche befindet. Wartet man dann einige Sekunden, so reisst der Wasserfilm an beiden Seiten des Rahmens ab. Anschliessend muss der Rahmen so langsam herausgezogen werden, dass die von der Wasseroberfläche abgezogene Folie an ihrer Unterseite keinen Wasserfilm (oder Tröpfchen) mitnehmen kann. Hier wirken die unter (c) erwähnten Querrippen sehr günstig, wenn sie in der Richtung liegen, in der die Folie von der Wasseroberfläche abgezogen wird.

Bei sorgfältiger Beachtung besonders der unter (e) genannten Vorsichtsmassregeln gelang es, Folien bis herab zu 0.9 $\mu g/cm^2$ bei einer freitragenden Fläche von 85×30 mm^2 von freier Hand herzustellen, ohne Verwendung des von Barreau *et al.* beschriebenen mechanischen Tisches. (Die mittlere Massenbelegung der Folien wurde mit einer Mikrowaage bestimmt.)

3. Metallbedampfung der Folien

Frau Geese[1]) erreichte ausreichende Leitfähigkeit der Zaponfolie in ihrem 4π-Zählrohr (Fig. 1) meist nur mit einem Silberbelag von je 30 $\mu g/cm^2$ auf jeder Folienseite. Nur in Ausnahmefällen genügten dünnere Schichten. Ob

† Formvar wird z.B. unter der Bezeichnung Polyvinylformal E 220444 von den Farbwerken Hoechst hergestellt.

[2]) P. Barreau, P. Léger, J. Moreau und P. Prugne, Journ. Phys. et Rad. 15 (1954) 4A.

eine einseitige Bedampfung ausgereicht hätte, wurde nicht geprüft.

Dass ausreichende Leitfähigkeit erst bei so hohen Schichtdicken eintritt, liegt an der relativ hohen Oberflächenbeweglichkeit der Silberatome. Sie hat zur Folge, dass sich das Silber zunächst in Form voneinander isolierter Inselchen niederschlägt. Wachsen diese Inseln beim Bedampfen bis zur gegenseitigen Berührung, so steigt die Leitfähigkeit oft innerhalb einer Zunahme der mittleren Massenbelegung von nur 1 bis 2 $\mu g/cm^2$ um mehrere Zehnerpotenzen. Einen eindeutigen Zusammenhang zwischen Aufdampfbedingungen und Leitfähigkeit der Schicht konnte Frau Geese nicht feststellen.

Es ist jedoch bekannt, dass die Oberflächenbeweglichkeit beim Aufdampfen mit steigender Schmelztemperatur des Metalls abnimmt und mit steigender Temperatur der Unterlage zunimmt[3]). Die dünnen Folien zu kühlen, ist schwierig. Sie werden beim Bedampfen naturgemäss erheblich wärmer als etwa Glasplatten, bei denen deshalb gute Leitfähigkeit schon bei erheblich dünneren Metall-Aufdampfschichten eintritt. Es blieb die Möglichkeit, die Folien entweder mit einem Metall hohen Schmelzpunktes zu bedampfen oder wenigstens zu "bekernen". Es genügt, die Folie mit einer weniger als monoatomaren Schicht des schwer schmelzbaren Metalls zu bedampfen, um damit für die folgende Bedampfung mit einem Metall niedrigen Schmelzpunktes Kondensationskerne zu schaffen[4]). Deshalb wurde zunächst versucht, nach dem von Brochard *et al.*[5]) angegebenen Verfahren Platin oder Wolfram durch Elektronenbeschuss zu verdampfen. Das gelang auch, doch wurden die Folien durch die Wärmestrahlung des verdampfenden Metalls zerstört.

Die Bekernung gelang jedoch mit Kohlenstoff, der wegen seines sehr hohen Schmelzpunktes sehr geeignet erschien. Dünne Kohlenstoffschichten lassen sich durch eine Glimmentladung in einem gasförmigen Kohlenwasserstoff erzeugen. Die in einer solchen Entladung entstehenden C-Ionen werden im elektrischen Feld je nach ihrer Ladung zur Anode oder Kathode beschleunigt. Die Folien wurden deshalb einer Glimmentladung in Naphtalindampf von einigen 10^{-3} Torr ausgesetzt. Die Folien wurden dabei isoliert etwa 10 cm vor der Kathode angebracht. Die der Anode zugewandte Seite war durch ein Blech abgedeckt, so dass nur eine Seite der Folie bekernt wurde. Bei einer Spannung von 1000 V und einem Entladungsstrom von 10 mA nahm die Massenbelegung der Folie um etwa 1.3 $\mu g/cm^2$ je Minute Glimmdauer zu (Mikrowaage).

Zum Vergleich wurden nun (durch 10 sec Glimmentladung) bekernte und unbekernte Formvarfolien mit Silber bedampft und die elektrischen Widerstände verglichen. Das Silber wurde bei einem Druck von etwa 1×10^{-5} Torr von einem elektrisch geheizten Tantalblech durch eine Blende von 5 mm Durchmesser hindurch auf die etwa 20 cm vom Blech entfernte Folie aufgedampft. Gegen Wärmestrahlung war soweit als möglich abgeschirmt. Die Aufdampfzeit betrug je nach Heizstromstärke und gewünschter Ag-Schichtdicke 5 bis 15 sec.

Nach dem Aufdampfen wurde die Schichtdicke durch Wägung ermittelt und danach die Folie auf einen Glas-Objektträger† aufgebracht, wo eine solche dünne Folie von selbst festklebt. Nachdem an beiden Enden des Objektträgers zusätzlich je eine dicke Silberschicht als Kontakt aufgedampft war, konnte der Widerstand zwischen diesen beiden Kontakten mit einer Messbrücke bestimmt werden.

Der elektrische Widerstand einer solchen Schicht ist

$$R = \varrho \frac{a}{b\,d},$$

wenn ρ der spezifische Widerstand, a der Abstand der Kontakte, b die Breite und d die

[3]) H. Mayer, Physik dünner Schichten, Band 2 (Wissenschaftliche Verlagsgesellschaft m.b.H., Stuttgart, 1955) S. 98 ff.

[4]) ib., S. 102. Für entsprechende Hinweise noch vor Erscheinen des Buches möchten wir dem Verfasser herzlich danken.

[5]) J. Brochard, P. Giacomo und P. Jacquinot, Journ. Phys. et Rad. **12** (1951) 632.

† Die Objektträger müssen völlig glatt und frei von Kratzern sein. Schon eine Scharte, die man mit einer Rasierklinge in die Glasoberfläche einritzt, kann den Widerstand einer *danach* aufgebrachten Folie von etwa 100 auf etwa 1000 Ohm erhöhen.

Dicke der Schicht ist. Für $a = b$, d.h. für quadratische Schichten erhält man also

$$R = \frac{d}{\varrho}.$$

Diesen von Ausdehnung und Form der Schichten nicht mehr abhängenden Ausdruck nennen wir "Flächenwiderstand". Er ist für unbekernte und bekernte Folien in Fig. 2 dargestellt. (Wegen des beschränkten Messbereichs der verwendeten Brücke wurden nur Widerstände $R < 10^7$ Ohm gemessen.) Die Kurven zeigen den erwarteten steilen Abfall von R, der innerhalb weniger $\mu g/cm^2$ über mehrere Zehnerpotenzen geht. Ohne Bekernung beginnt der steile Abfall unter 10^7 Ohm bei etwa 12 $\mu g/cm^2$, mit Bekernung schon bei etwa 6 $\mu g/cm^2$.

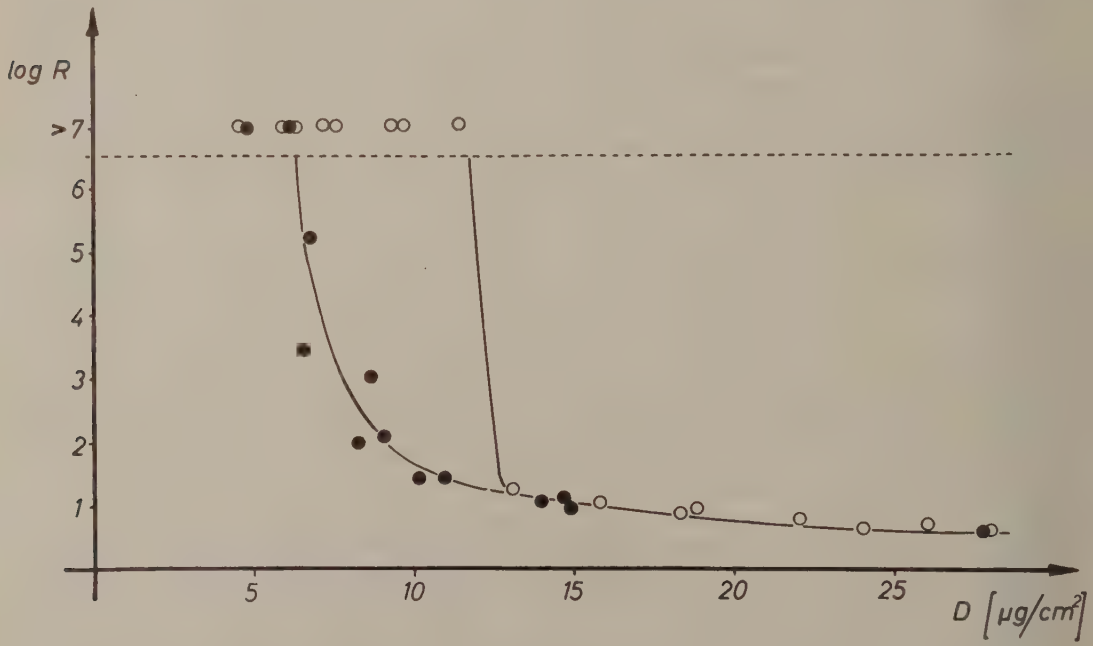

Fig. 2. Flächenwiderstand aufgedampfter Ag-Schichten auf bekernten (●) und unbekernten (○) Folien.

Weiter wurden mit und ohne Bekernung aufgedampfte Silberschichten im Elektronenmikroskop untersucht. Um bei völlig gleichen Aufdampfbedingungen vergleichen zu können, wurden die Folien bei der Bekernung zur Hälfte abgedeckt, so dass nur eine Hälfte der Entladung ausgesetzt war. Die Figuren 3 und 4 zeigen den Strukturunterschied der anschliessend aufgedampften Silberschichten.

Das Silber hebt sich dunkel von der Folie ab. Auf unbekernten Folien schlägt es sich zunächst in Form unregelmässig geformter Tröpfchen nieder, aus denen bei weiterer Bedampfung verästelte, aber noch immer voneinander isolierte Bereiche entstehen (Fig. 3a). Erst bei etwa 12 $\mu g/cm^2$ wird die Schicht einigermassen zusammenhängend (Fig. 4a). Bei bekernten Folien erfolgt dieser Ubergang viel früher (Fig. 3b). (Schon bei nur 3.5 $\mu g/cm^2$ ist hier der Zusammenhang besser als bei 8.4 $\mu g/cm^2$ in Fig. 3a.) Ab etwa 10 $\mu g/cm^2$ sind die Schichten auf bekernten Folien nahezu homogen wie in Fig. 4b.

4. Prüfung im im 4π-Zählrohr

Ob eine Folie ausreichend leitet, lässt sich leicht im 4π-Zählrohr prüfen (Fig. 1). Man legt an einen der Zähldrähte Zählspannung und zählt. Wenn die Zählrate sich nicht ändert, wenn man die Spannung am anderen Draht

von Null bis kurz unter die Einsatzspannung variiert, so sind die beiden Rohre elektrostatisch völlig voneinander getrennt. Bei bekernten Folien von etwa 2 $\mu g/cm^2$, die einseitig mit etwa gedampfte RbCl zwischendurch zweimal durch Untertauchen der Folie in destilliertem Wasser abgespült wurde.

Es ist also möglich, für Aktivitätsmessungen

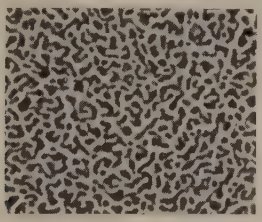

Fig. 3a. 8.4 $\mu g/cm^2$ Ag, unbekernte Folie.

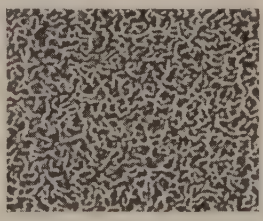

Fig. 3b. 8.4 $\mu g/cm^2$ Ag, bekernte Folie.

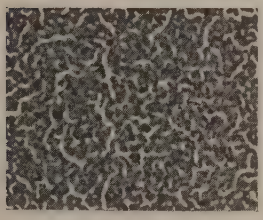

Fig. 4a. 11.5 $\mu g/cm^2$ Ag, unbekernte Folie.

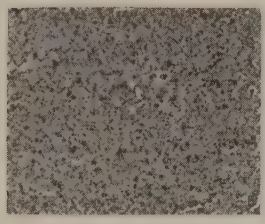

Fig. 4b. 11.5 $\mu g/cm^2$ Ag, bekernte Folie.

Fig. 3a, 3b, 4a, 4b. Elektronenmikroskopische Aufnahmen von Ag-Aufdampfschichten auf Formvarfolien. (Vergrösserung 1:60 000).

8 $\mu g/cm^2$ Silber bedampft waren, war das der Fall.

Die ausserordentliche Festigkeit derartiger Präparatunterlagen ersieht man aus der Tatsache, dass es gelungen ist, eine Formvarfolie von 3.0 $\mu g/cm^2$, die mit 9.3 $\mu g/cm^2$ Ag bedampft war, insgesamt neunmal mit verschiedenen RbCl-Schichten zu bedampfen, wobei das auf-

in Zählrohren ausreichend leitende Präparatunterlagen herzustellen mit einer mittleren Massenbelegung von nur 10 $\mu g/cm^2$ und einer freitragenden Fläche von mindestens 85 × 30 mm^2. Gegenüber den von Frau Geese verwendeten Folien von 50 bis 100 $\mu g/cm^2$ bedeutet dies einen nennenswerten Gewinn.

NUCLEAR INSTRUMENTS 3 (1958) 218–222; NORTH-HOLLAND PUBLISHING CO. – AMSTERDAM

MEASUREMENT AND AUTOMATIC CONTROL OF THE ENERGY OF A 31 MeV BETATRON

U. FARINELLI, F. FERRERO and R. MALVANO

Istituto di Fisica dell'Università di Torino, Istituto Naz. Fisica Nucleare, Sez. di Torino

Received 1 July 1958

A simple method to control the energy of a betatron is proposed. It compares a signal proportional to the average e.m.f. during the acceleration period derived from a measuring loop to a suitable reference voltage, and derives an error signal which operates small changes in the expansion time.

1. Introduction

Several methods have been proposed and realized in order to measure and control accurately the energy of the electrons impinging on the target of a betatron and hence the maximum energy of the bremsstrahlung X-rays. In all cases the energy measurement is made by evaluating the integrated e.m.f. induced in a measuring coil by the accelerating magnetic field, the integration being extended from the moment the electrons are injected in the doughnut to the moment they hit the target. If the magnetic field at the coil is equal (or proportional) to the field on the path of the electrons, this quantity is a measurement of the energy gained by the electrons in the doughnut. When an automatic energy control is used, the integrated signal from the coil can conveniently be employed, through a sensitive discriminator, to trigger the expansion circuit of the betatron[1]) as it was firstly done by the Saskatchevan group, or else the energy can be controlled by varying the overall a.c. voltage applied to the magnet, in order to keep at long range the energy at the desired value[2]).

In our case, the second type of control would have implied major changes in the installation while the first one, apart from involving a somewhat critical circuitry for the discriminator, operates satisfactorily only with a much better defined expansion pulse than the one we have; the uncertainties in shape and delay of the actual pulse, such as it is now, introduce a large error, expecially at low energies.

The line we followed was therefore to use a signal proportional to the average over a certain number of cycles of the integrated e.m.f. in the measuring coil such as given by the B.B.C.† megavoltmeter, and to derive from it an error signal by comparison with a reference voltage, with which to operate small phase changes in the inductor controlling the triggering of expansion. The correction is thus prompt to within a few cycles, and since energy fluctuations in single cycles have been observed to be negligible, the system has no practical disadvantage with respect to other systems performing the integration of each cycle.

2. Measurement of the Energy

As we mentioned, the B.B.C. megavoltmeter gives an output proportional to the time average (with a time constant of the order of a few cycles) of the value of the integrated e.m.f. induced in the measuring coil, between the time of injection and the moment the electrons hit the target, which is determined by the X-ray burst detected by a scintillator and photomultiplier. This provides a more direct and reliable measurement than triggering with

[1]) B. W. Katz *et al.*, Phys. Rev. **94** (1954) 763; see also e.g. D. Jamnik, Nuclear Instruments **1** (1957) 327.

[2]) R. Basile and C. Shuhl, J. Phys. Radium **16** (1955) 372.

† Brown Boveri Co., Baden (Switzerland).

the expansion pulse, since delays in expansion do not affect the result. Unfortunately, the output of the megavoltmeter is proportional not only to the energy of the electrons but also to the frequency of repetition cycles (being a time average with a fixed time constant). For the B.B.C. betatron, this frequency is just the frequency of the line, which cannot be considered a constant in most countries, when a high accuracy, for instance of the order of 1/1000, is required (in Italy frequency variations of the order of $\pm$ 1% from the nominal value of 50 cycles/sec are not uncommon). In order to get rid of these limitations, the signal from the megavoltmeter is compared with a predetermined fraction of a reference voltage, which is exactly proportional to the frequency of the line.

The principle of the circuit used to obtain a voltage proportional to the frequency of the line is shown in fig. 1a. Its main feature lies in that the frequency dependence is added as a correction term to a constant voltage: since the frequency varies very little about a fixed value, the correction term may be of order of 1%; errors even as big as 10% in this term introduce an overall error not greater than 1/10000 at most in the reference voltage, provided the d.c.

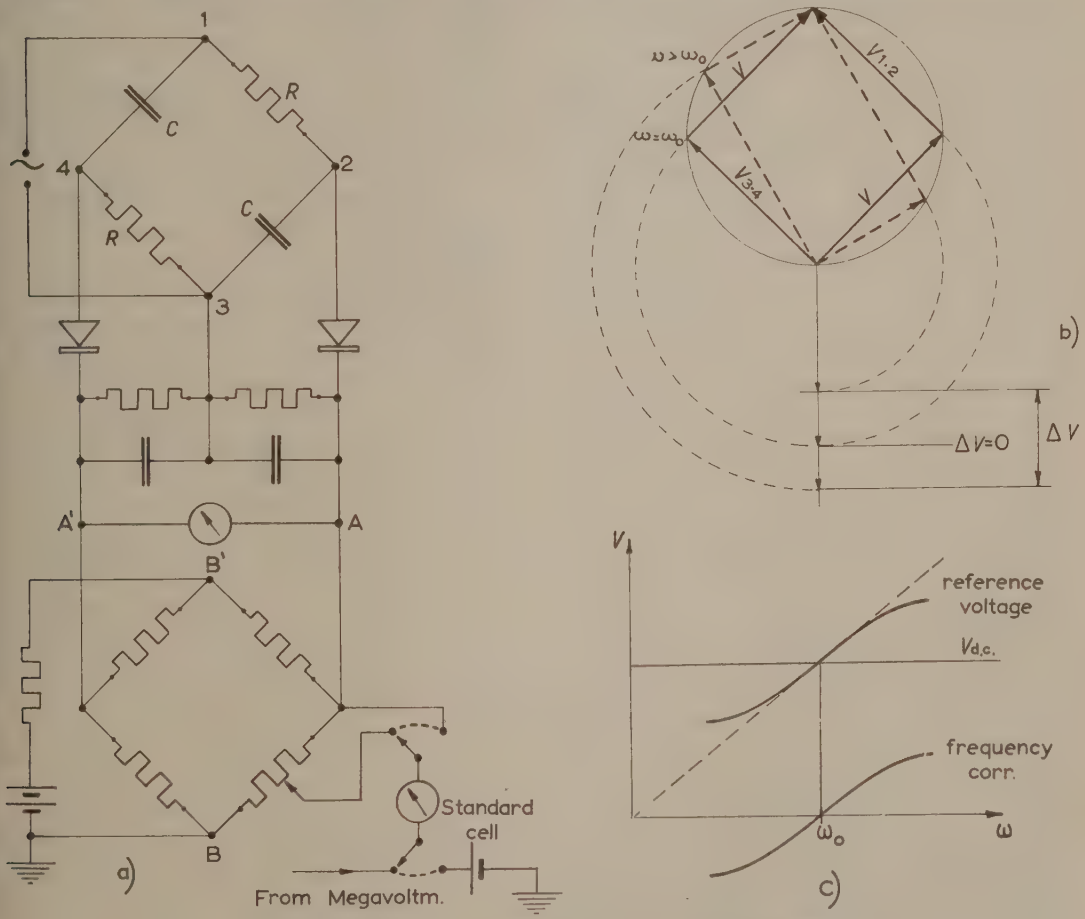

Fig. 1. (a) Measuring bridge (schematic diagram). (b) Voltages across the bridge sides. (c) Reference voltage *vs.* line frequency.

voltage is constant to better that 1/1000; this in turn is obtained by periodically checking the d.c. voltage against a standard cell. The frequency term is derived from the upper bridge in fig. 1a. R and C are adjusted to match the nominal frequency of the line ($RC = 3.12 \times 10^{-3}$ sec). The correction signal is obtained by comparing the absolute value of the voltage drops across the lower sides of the bridge by means of two rectifiers. Apart from differences in the rectifiers, A and A′ are at the same potential when the frequency of the line has its nominal value; displacements from this value give potential differences of either sign, as can be seen from fig. 1b, which shows the voltage across the sides of the bridge in various conditions. In the range to be covered, the signal may, at all effects, be considered linear with frequency. The instrument between A and A′, with central zero corresponding to the nominal frequency, provides an accurate measurement of the frequency itself.

The correction term is added to the constant voltage by means of the lower bridge in fig. 1a. The sensitivity of the system to frequency is checked by varying of a small known amount the characteristic frequency of the upper bridge (practically by shorting a fraction, about 1%, of one of the resistors R), and measuring the variation of potential difference between A and B. This sensitivity must be adjusted (for instance by regulating the a.c. voltage applied to the upper bridge) so that when linearly extrapolated to zero frequency, the voltage given by the frequency correction term exactly compensates the constant voltage applied to the lower bridge. In these conditions, the resulting voltage between A and B will be not only a linear but also an homogeneous function of frequency (see fig. 1c).

It was found necessary to feed the upper bridge through a filter that elimates from the line the harmonics that are always present in a variable quantity, since harmonics tend to give a spurious correction term, always of the same sign.

The value of $V_A - V_B$ for $\omega = \omega_0$ is equal to the maximum voltage given by the megavoltmeter (i.e. to the signal corresponding to the maximum energy of the betatron). AB is actually a Helipot potentiometer, so that a fraction of the voltage, corresponding to the desired fraction of the maximum energy, can be derived from its centre point C. If the frequency deviates from its nominal value, V_c varies accordingly, but always represents the voltage that should be given by the megavoltmeter if the energy is to be constant. By comparing V_c with the output of the megavoltmeter, V_m, one has an error signal $V_c - V_m$ that can be dispayed on a galvanometer, or used for an automatic control of the energy as we shall presently see.

A practical variation of the circuit of fig. 1a is shown in fig. 2. The introduction of a vacuum tube, used as a cathode differential amplifier, has

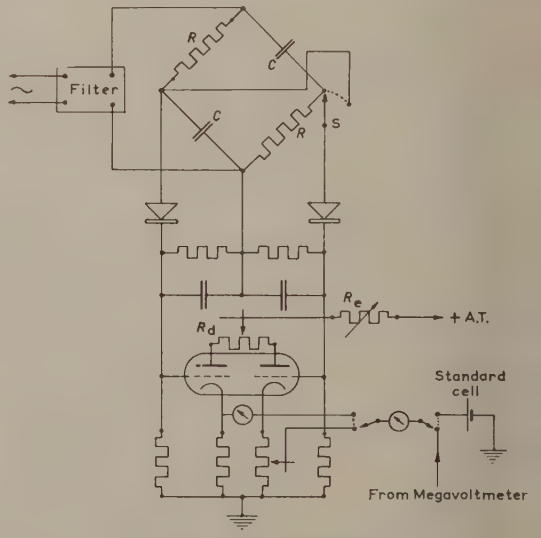

Fig. 2. Measuring bridge (actual circuit).

the main advantage of completely separating the frequency measuring bridge from the output, and allows an easy matching of impedences. By connecting with a switch S the two rectifiers to the same end of the frequency bridge, one can check the zero of the frequency meter. When deviations occur, due to changes in the rectifiers characteristics or in the two

sections of the tube, or in the cathode resistors, they can be compensated with fine variations of the potentiometer R_d, controlling the relative potential of the two anodes, so that when the frequency correction is absent, $V_A = V'_A$. Another check is made by comparing V_A (always in absence of frequency correction) with the voltage from a Weston standard cell, through the same galvanometer used to display the error signal; a variable resistor R_e allows fine regulations of V_A.

3. Manual and automatic Control of the Energy

The error signal obtained by comparing the voltage V_c with the output of the megavoltmeter V_m can be used by the operator to control manually the energy of the betatron, or it can be used directly for an automatic control. In each case, the variations of energy are obtained with a simple and prompt way of displacing finely the moment of expansion.

In the B.B.C. betatron, the moment of expansion is controlled by the monophase secondary coil of a three phase inductor. When the voltage of the secondary passes through zero, a starting pulse is fed to the expansion circuit. The moment of expansion and hence the energy of the beam are normally controlled by mechanicaly rotating the secondary coil of the inductor with respect to the primary be means of a servomotor. This procedure is not apt to produce rapid changes in the expansion phase; fine changes are also difficult to obtain with the necessary accuracy. Another method has therefore been developped that consists in varying the relative phases of the primary and secondary coils of the inductor by shifting the phase of the center of the primary (that has a star-type connection). This can be done by means of a variable impedence on one of the branches of the star.

In the case of a fine manual regulation, this only involves an ordinary variable resistor on one of the branches. A first energy control was thus achieved keeping as steadily as possible on the zero position the needle of the galvanometer displaying the error signal by manual operation of the variable resistor.

The result obtained in this way are satisfactory for most purposes. This system takes care sufficiently well of relatively slow variations and of long term drifts. Very fast fluctuations of energy are practically absent in most cases.

However, in order to have a better time response, and also to avoid continous manual operation, an automatic system was studied. With this system, the variable resistor is substituted by an equivalent vacuum tube. The variations are made by applying to the grid of this tube the error signal that operated the galvanometer in the manual control system, properly amplified by a d.c. amplifier. If the amplification if high, the energy stability depends only on the accuracy of the megavoltmeter output and the reference signal. The system has a large negative feedback, the loop being closed through the expansion of the betatron and the megavoltmeter.

The zero drift admissible for the d.c. amplifier can be of the same order as that of the output of the tube in the reference signal circuit of fig. 2. The d.c. amplifier is therefore not very critical, and the importance of zero drifts in the reference voltage circuit is limited, since applied voltage (including megavoltmeter output) can be of the order of one or a few volts, and slow drifts in the millivolt range such as one meets in a selected tube—do not greatly disturb. A zero check is anyway advisable from time to time (we performed it about every ten minutes) and is easily done with the same system seen in section 2. In this case, though, the instrument will be connected at the output of the d.c. amplifier, so as to show drifts both of the reference system and the amplifier.

4. Calibration of Energy

Several nuclear reactions have been employed to calibrate energy scales up to 20 MeV; no very well known point, on the other hand, can be used in the region from 20 to 30 MeV; the calibration has therefore to be extrapolated in this region. However, there is no reason why

the energy scale should not be strictly linear. The points we used for an absolute calibration were the threshold of (γ, n) reactions in Cu (at 10.71 MeV) and Si (at 16.8 MeV), and C at (18.73 MeV) measured by the activitation method. A straight line through these points passes through—0.51 MeV within experimental errors; what gives confidence in the linearity of the scale (see fig. 3). Other thresholds subsequently measured gave results in good agreement with previous experiments.

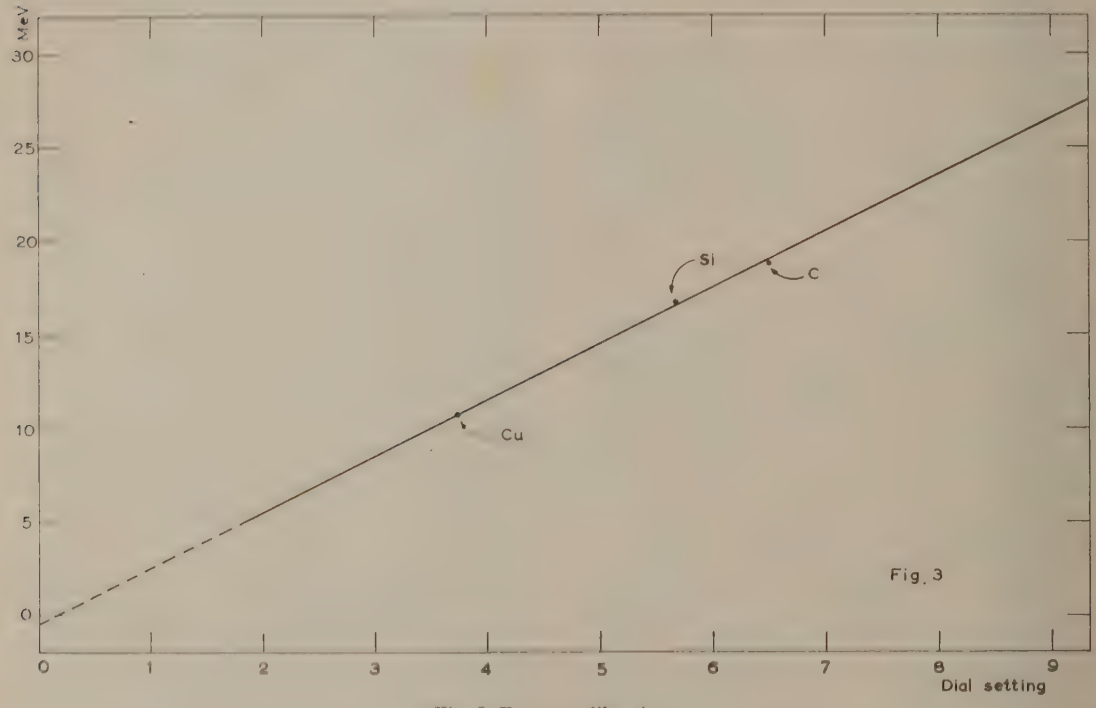

Fig. 3. Energy calibration.

With other conventional methods, the long term stability of the system was investigated, and no significant drift was observed greater than the 1/1000 stability presently obtainable with this simple system.

NUCLEAR INSTRUMENTS 3 (1958) 223–228; NORTH-HOLLAND PUBLISHING CO. · AMSTERDAM

CHOICE OF COLLIMATORS FOR A CRYSTAL SPECTROMETER FOR NEUTRON DIFFRACTION

G. CAGLIOTI, A. PAOLETTI† and F. P. RICCI

Comitato Nazionale per le Ricerche Nucleari, Roma

Received 1 July 1958

In this paper we establish some criteria for the choice of the collimators for a crystal spectrometer for neutron diffraction in order to achieve a good compromise between luminosity and resolution.

General expressions for the full width at half maximum and for the luminosity of the diffraction peaks are developed for powder sample. The advantage of the parallel arrangement is also computed.

1. Introduction

The diffraction pattern obtained with a neutron crystal spectrometer shows several peaks due to Bragg reflections of the crystalline sample.

The full width at half maximum and the luminosity of these peaks are related to the angular divergence of the spectrometer collimators and to the crystal mosaic spread.

The purpose of this paper is to show how to choose the most convenient values for the angular divergences of the collimators in order to obtain a good compromise between resolution and luminosity.

2. The Soller Collimators and the Crystal Mosaic Spread

2.1. THE SOLLER COLLIMATORS

In a crystal spectrometer for neutron diffraction, there are three collimators: the first collimator is located inside a beam hole in the reactor shielding, the second one is in the monochromatic beam between the monochromating crystal and the sample, the third one is on the rotating arm, between the sample and the BF_3 detector.

We shall assume the three collimators to be of the Soller type[1]); the horizontal angular divergence α_i $(i = 1, 2, 3)$ of the i-th collimator is determined by the ratio $\alpha_i = s_i/l_i$ of the width s_i to the length l_i of its Soller elements.

We shall also assume, in accordance with Sailor *et al.*[2]), that the i-th collimator reduces the intensity of the incident neutron beam by a factor

$$A(\phi_i) = \exp \cdot (\phi_i/\alpha'_i)^2 \qquad (1)$$

where ϕ_i is the angle made by the projection on a horizontal plane, of any individual ray with the centerline of the i-th collimator††, and $\alpha'_i = \alpha_i/2(\ln 2)^{\frac{1}{2}}$. The sign of ϕ_i is chosen so that $+\phi_i$ would tend to increase the Bragg angle of the ray.

It can be shown that, by providing a coarse vertical collimation, any effect due to the vertical angular divergence of i-th collimator can be neglected.

2.2. THE CRYSTAL MOSAIC SPREAD

We shall assume[2]) that the monochromating crystal is actually composed of mosaic blocks, each individually perfect, oriented in a gaussian distribution of the type

$$\Theta(\eta) = K \exp -(\eta/\beta')^2 \qquad (2)$$

where K depends on the properties of the crystal under consideration[2]), η is the angular displacement from the mean of the projection of the

† Present address: Brookhaven National Laboratory, Upton, L.I., N.Y.

†† Such an angle is given by $\sigma - \phi_3$ (see sect. 3. eq. (71)) for the third collimator.

[1]) W. Soller, Phys. Rev. **24** (1924) 158.

[2]) V. L. Sailor, H. L. Foote, Jr., H. H. Landon and R. E. Wood, Rev. Sci. Instr. **27** (1956) 26.

normal to the reflecting planes of any block upon a horizontal plane, and β' is related to the full width at half maximum of the distribution β, by eq. $\beta' = \beta/2(\ln 2)^{\frac{1}{2}}$. The sign of η is chosen so the Bragg angle would be increased when η is positive.

3. Derivation of the Full Width at Half Maximum and of the Luminosity of the Diffraction Peaks; Powder Sample

In order to calculate the shape and the full width at half maximum of the experimental diffraction peaks due to a powder sample, it will be useful to establish some relations between the angles ϕ_i, the Bragg angles of the monochromating crystal and the Bragg angles of the sample.

Let θ_0 be the Bragg angle for a central ray incident upon the monochromating crystal with $\phi_1 = 0$ and $\eta = 0$, and let θ be the Bragg angle for any individual ray. Hence we have[2]):

$$\theta - \theta_0 \equiv \delta = \phi_1 + \eta \tag{3}$$

$$\phi_2 = \delta + \eta \,. \tag{4}$$

Furthermore, let d be the interplanar distance of the monochromating crystal, and let d_B and θ_B be the interplanar distance and the Bragg angle of the sample respectively; setting:

$$a = \frac{(\mathrm{d}\lambda/\mathrm{d}\theta)_{\text{monochromating crystal}}}{(\mathrm{d}\lambda/\mathrm{d}\theta)_{\text{sample}}} = \frac{d \cos\theta_0}{d_B \cos\theta_{B0}}\,, \dagger \tag{5}$$

in the "parallel position" we get:

$$\phi_3 = 2a\delta - \phi_2 \,\dagger\dagger. \tag{6}$$

For any Bragg angle θ_B, let ρ be the angular displacement of the axis of the BF_3 detector with respect to the angle $2\theta_{B_0}$ (for which the diffracted ray intensity has a maximum).

Let us now consider a neutron of wavelength $(\lambda,\ \lambda + \mathrm{d}\lambda)$ and, therefore, having a value of $\theta - \theta_0$ equal to $(\delta,\ \delta + \mathrm{d}\delta)$. The probability $J(\rho, \phi_1, \delta)\,\mathrm{d}\phi_1\,\mathrm{d}\delta\,\mathrm{d}\rho$ of such neutron going through the first collimator with an angle $(\phi_1,\ \phi_1 + \mathrm{d}\phi_1)$, being reflected by the monochromating crystal with a Bragg angle given by $(\delta,\ \delta + \mathrm{d}\delta)$, going through the second collimator, being reflected by the sample and then finally reaching the BF_3 detector whose axis makes an angle $(\rho,\ \rho + \mathrm{d}\rho)$ with the direction $2\theta_{B_0}$, is given by:

$$J(\rho, \phi_1, \delta)\,\mathrm{d}\phi_1\,\mathrm{d}\delta\,\mathrm{d}\rho = H \exp -\left[\left(\frac{\phi_1}{\alpha'_1}\right)^2 + \left(\frac{\eta}{\beta'}\right)^2 + \left(\frac{\phi_2}{\alpha'_2}\right)^2 + \left(\frac{\rho - \phi_3}{\alpha'_3}\right)^2\right] \mathrm{d}\phi_1\,\mathrm{d}\delta\,\mathrm{d}\rho \tag{7}$$

where H is a constant.

Taking into account eqs. (3), (4), and (6), we get for the total number, $I(\rho)\,\mathrm{d}\rho$, of neutrons reaching the BF_3 detector at the angular position $(\rho,\ \rho + \mathrm{d}\rho)$:

$$I(\rho)\,\mathrm{d}\rho = H\,\mathrm{d}\rho \int_{-\infty}^{+\infty}\mathrm{d}\phi_1 \int_{-\infty}^{+\infty}\mathrm{d}\delta \exp -\left[\left(\frac{\phi_1}{\alpha'_1}\right)^2 + \left(\frac{\delta - \phi_1}{\beta'}\right)^2 + \left(\frac{2\delta - \phi_1}{\alpha'_2}\right)^2 + \left(\frac{\rho - \phi_1 + 2\delta\,(1-a)}{\alpha'_3}\right)^2\right]. \tag{8}$$

In eq. (8) we extend the limits of integration to $\pm\,\infty$ since this doesn't appreciably affect the value of $I(\rho)\,\mathrm{d}\rho$.

By applying the relation:

$$\int_{-\infty}^{+\infty} \exp(-px^2 \pm qx)\,\mathrm{d}x = \left(\frac{\pi}{p}\right)^{\frac{1}{2}} \exp\frac{q^2}{4p} \tag{9}$$

twice, we obtain from eq. (8):

$$I(\rho)\,\mathrm{d}\rho = M\,\mathrm{d}\rho\, \frac{\alpha_1\alpha_2\alpha_3\beta}{\left[\alpha_1^2\alpha_2^2 + \alpha_1^2\alpha_3^2 + \alpha_2^2\alpha_3^2 + 4\beta^2(\alpha_2^2 + \alpha_3^2) - 4a\alpha_2^2(\alpha_1^2 + 2\beta^2) + 4a^2(\alpha_1^2\alpha_2^2 + \alpha_1^2\beta^2 + \alpha_2^2\beta^2)\right]^{\frac{1}{2}}} \tag{10}$$

$$\cdot \exp -\left\{\rho^2 \frac{(4\ln 2)(\alpha_1^2 + \alpha_2^2 + 4\beta^2)}{\left[\alpha_1^2\alpha_2^2 + \alpha_1^2\alpha_3^2 + \alpha_2^2\alpha_3^2 + 4\beta^2(\alpha_2^2 + \alpha^2{}_3) - 4a\alpha_2^2(\alpha_1^2 + 2\beta^2) + 4a^2(\alpha_1^2\alpha_2^2 + \alpha_1^2\beta^2 + \alpha_2^2\beta^2)\right]}\right\}.$$

† The quantity a takes into account the fact that in the crystal spectrometer for neutron diffraction, the dispersion of the sample in any Bragg position is, in general, different from the dispersion of the monochromating crystal.

†† In the "antiparallel position" we get: $\phi_3 = 2a\delta + \phi_2$. (6′)

In eq. (10), M contains numerical factors connected with the nature of the monochromating crystal and the sample, the structure factors of their Bragg reflections under consideration, etc.

Eq. (10) shows that any diffraction peak, centered about an angle $2\,\theta_{B_0}$ related to a by eq. (5), has a gaussian shape with the full width at half maximum $A_{\frac{1}{2}}$ given by:

$$A_{\frac{1}{2}} = \left[\frac{\alpha_1^2\alpha_2^2 + \alpha_1^2\alpha_3^2 + \alpha_2^2\alpha_3^2 + 4\beta^2(\alpha_2^2 + \alpha_3^2) - 4a\alpha_2^2(\alpha_1^2 + 2\beta^2) + 4a^2(\alpha_1^2\alpha_2^2 + \alpha_1^2\beta^2 + \alpha_2^2\beta^2)}{\alpha_1^2 + \alpha_2^2 + 4\beta^2} \right]^{\frac{1}{2}}. \quad (11)$$

By integration of eq. (10) with respect to ρ, we find for the luminosity L':

$$L' = P \frac{\alpha_1\alpha_2\alpha_3\beta}{(\alpha_1^2 + \alpha_2^2 + 4\beta^2)^{\frac{1}{2}}} \quad (12)$$

where P is a constant factor related to M in a simple way.

We will refer to the quantity $L \equiv L'/P$ as the spectrometer luminosity.

4. Preliminary Discussion of the Results for the Particular Case $\alpha_1 = \alpha_2 = \alpha_3 = \beta \equiv \alpha$

It may be useful to study first the behaviour of $A_{\frac{1}{2}}$ and L, in a particular case of practical interest: i.e. for the case with $\alpha_1 = \alpha_2 = \alpha_3 = \beta \equiv \alpha$.

From eqs. (11) and (12), we obtain for this case:

$$A_{\frac{1}{2}} = \alpha \left(\frac{11 - 12a + 12a^2}{6} \right)^{\frac{1}{2}} \quad (11')$$

$$L = \alpha^3/(6)^{\frac{1}{2}}. \quad (12')$$

We see, therefore, that for any Bragg angle, the full width at half maximum of the diffraction peaks is proportional to α, while the luminosity is proportional to α^3. This fact implies a comparatively large sacrifice of luminosity when resolution has to be improved.

Furthermore, we see that the quantity $A_{\frac{1}{2}}/\alpha$, expressed as a function of a, has a minimum at $a = 0.5$, and then increases with a in a way almost proportional to a.

In fig. 1, curve U shows how $A_{\frac{1}{2}}/\alpha$ should vary with a. We compared this theoretical behaviour with the values of $A_{\frac{1}{2}}/\alpha$ obtained from diffraction peaks by Corliss *et al.*[3,4]), who used $\alpha \cong 20$ min·arc. Our theoretical values of $A_{\frac{1}{2}}/\alpha$ are in accordance within about 15% with experimental values of $A_{\frac{1}{2}}/\alpha$ obtained from fig. 3 of ref.[4]). The small deviations of our theoretical values from the experimental widths could be partly attributed to our having neglected in the calculations any effect of total reflection of neutrons against the walls of the steel collimators.

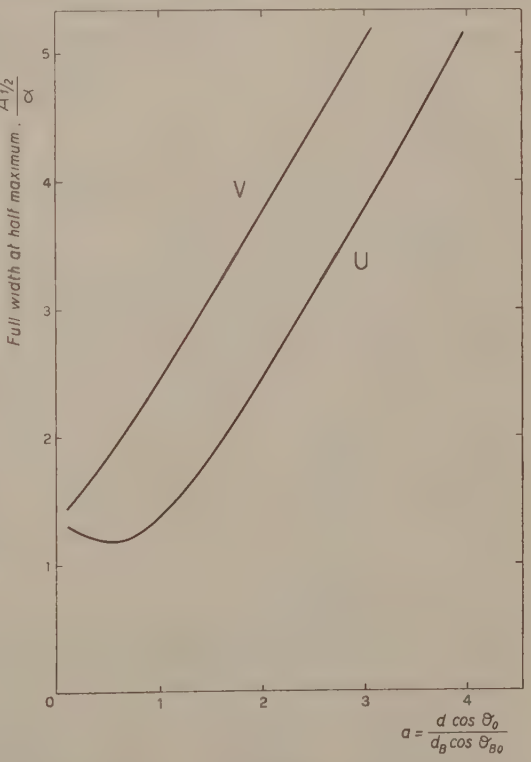

Fig. 1. Full width at half maximum $A_{\frac{1}{2}}$, divided by the horizontal angular divergence of the collimators α, as a function of $a = d \cos \vartheta_0/d_B \cos \vartheta_{B_0}$, for the particular case $\alpha_1 = \alpha_2 = \alpha_3 = \beta \equiv \alpha$. Curves U and V refer to the parallel and antiparallel positions respectively.

[3]) Pasternack, McReynolds, Weiss and Corliss, Phys. Rev. **81** (A) (1951) 326.

[4]) L. M. Corliss, J. M. Hastings and F. G. Brockman, Phys. Rev. **90** (1953) 1013.

It may be interesting to note that, taking into account eqs. (3), (4), (6′) and (7), in the antiparallel position we get:

$$A_{\frac{1}{2}}\,(\text{antiparallel}) = \alpha\left(\frac{11 + 12a + 12a^2}{6}\right)^{\frac{1}{2}} \quad (11'')$$

$$L\,(\text{antiparallel}) = \alpha^3/(6)^{\frac{1}{2}}\,. \quad (12'')$$

Eqs. (11′–12″) show that, the luminosity being the same, $A_{\frac{1}{2}}$ (antiparallel) $> A_{\frac{1}{2}}$ for any a.

In fig. 1, curve V is a plot of eq. (11″). Curves U and V show the focusing action due to the parallel position; they are in satisfactory agreement with experimental results[5]).

5. Discussion

With reference to eqs. (11) and (12), we may state that:

(1) The luminosity L is a symmetrical function of α_1, and α_2.

(2) The luminosity L is a linear function of α_3, so that a convenient way of obtaining a larger luminosity is to increase α_3.

(3) The function $A_{\frac{1}{2}}{}^2$ is a sum of three quantities: the first, which is independent of a, gives the largest contribution to $A_{\frac{1}{2}}{}^2$ for small values of a (or $2\theta_B$). The first term is the only one which depends on α_3, so that an increase in the luminosity as suggested in (2) causes a broadening of the diffraction peaks mainly for small values of a (or $2\theta_B$).

The third term is a symmetrical function of α_1 and α_2, so that α_1 and α_2 are equally important in broadening the diffraction peaks for large values of a (or $2\theta_B$).

In order to show the features of the various possible choices of the horizontal angular divergences of the collimators with reference to L and $A_{\frac{1}{2}}$, we found it convenient to plot in the $(L, A_{\frac{1}{2}})$ plane, for each choice of the values of α_1, α_2, α_3, the three points of co-ordinates $L\,(\alpha_1, \alpha_2, \alpha_3; \beta)$ and $A_{\frac{1}{2}}\left(\alpha_1, \alpha_2, \alpha_3; \beta; \begin{smallmatrix} a=3 \\ a=1.5 \\ a\to 0 \end{smallmatrix}\right)$.

Obviously we will obtain a convenient situation for the points $(L, A_{\frac{1}{2}})$ which lie near the lower right corner of the plot.

We have calculated the quantities L and $A_{\frac{1}{2}}$ for about 150 groups of the values $(\alpha_1, \alpha_2, \alpha_3; a)$ and for the value of practical interest $\beta = 20$ min arc[3]).

In fig. 2 we report typical results.

Looking at fig. 2, we may further observe that for two ordered groups

(4)	(5)	(6)
$\underline{\alpha}^{(1)} = (\alpha_1, \alpha_2, \alpha_3)$	$\underline{\alpha}^{(3)} \equiv (\alpha_1, \alpha_2, \alpha_3)$	$\underline{\alpha}^{(5)} \equiv (\alpha_1, \alpha_2, \alpha_3)$
$\underline{\alpha}^{(2)} \equiv (\alpha_2, \alpha_1, \alpha_3)$	$\underline{\alpha}^{(4)} \equiv (\alpha_1, \alpha_3, \alpha_2)$	$\underline{\alpha}^{(6)} = (\alpha_3, \alpha_2, \alpha_1)$
for which		
$\alpha_1 < \alpha_2\,,$	$\alpha_2 < \alpha_3\,,$	$\alpha_1 < \alpha_3\,,$
we have:		
$L(\underline{\alpha}^{(1)}) = L(\underline{\alpha}^{(2)})$	$L(\underline{\alpha}^{(3)}) > L(\underline{\alpha}^{(4)})$	$L(\underline{\alpha}^{(5)}) > L(\underline{\alpha}^{(6)})$
$A_{\frac{1}{2}}(\underline{\alpha}^{(1)}) < A_{\frac{1}{2}}(\underline{\alpha}^{(2)})$	$A_{\frac{1}{2}}(\underline{\alpha}^{(3)}) < A_{\frac{1}{2}}(\underline{\alpha}^{(4)})$	$A_{\frac{1}{2}}(\underline{\alpha}^{(5)}) < A_{\frac{1}{2}}(\underline{\alpha}^{(6)})$

where the eqs. for $A_{\frac{1}{2}}(\underline{\alpha})$ hold for a large part of the range of a, and hold definitely as a increases.

On the basis of the above remarks, we believe it would be wise in general to discard a group $(\alpha_1, \alpha_2, \alpha_3)$ for which $\alpha_1 > \alpha_2 > \alpha_3$ (see for example the points (30, 20, 10) and (10, 20, 30) in fig. 2).

We also think it would be convenient to choose a comparatively small value of α_1, which allows us to obtain both a small $A_{\frac{1}{2}}$ (by reducing L), and a comparatively large value of the luminosity (without a big loss of resolution), by changing only α_2 and/or α_3 (see for example the points (10, 10, 10) and (10, 60, 60) in fig. 2).

In figs. 3 and 4, we show the behaviour of other groups of the values $(\alpha_1, \alpha_2, \alpha_3)$; each plot is obtained by varying only the value of α_2.

6. Conclusion

In this paper we have established some criteria which should be of some help in the designing and operation of a crystal spectrometer for neutron diffraction.

In particular we found that the simple choice of three identical collimators may not be the most convenient one, when a good compromise between resolution and luminosity has to be achieved. Instead a suitable choice of the values

[5]) G. E. Bacon, Neutron Diffraction (Oxford at the Clarendon Press, 1955) p. 88, fig. 34.

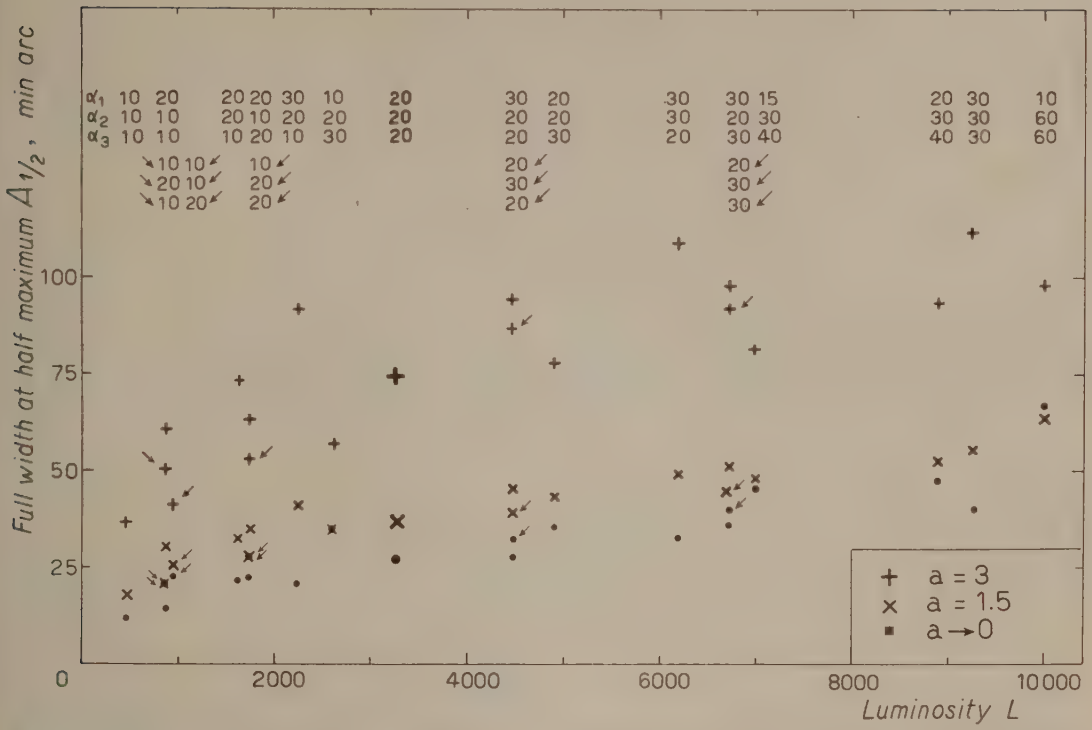

Fig. 2. Full width at half maximum $A_{\frac{1}{2}}$ (min·arc) *vs.* luminosity L for various choices of the horizontal angular divergences (α_1, α_2, α_3) of the three collimators, and for the values $a \to 0$, $a = 1.5$, and $a = 3$. All the points are calculated for a monochromating crystal mosaic spread $\beta = 20$ min·arc.

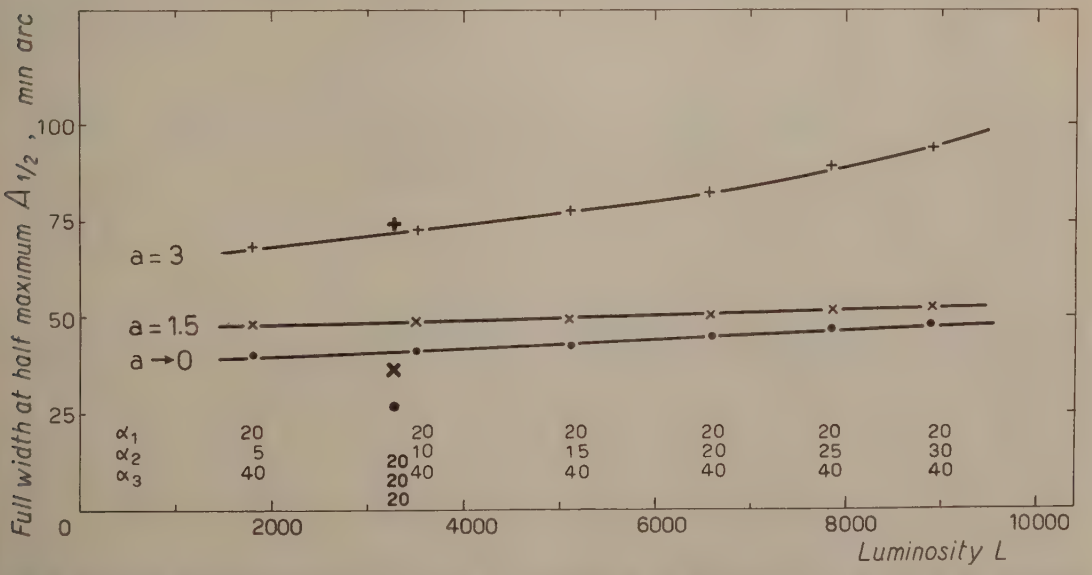

Fig. 3. Full width at half maximum $A_{\frac{1}{2}}$ (min·arc) *vs.* luminosity L, for the choices (20, α_2, 40) of the horizontal angular divergences of the three collimators, and for the values $a \to 0$, $a = 1.5$, $a = 3$, $\beta = 20$ min·arc. Points $\left[L\,(20, 20, 20), A_{\frac{1}{2}}\left(20, 20, 20; \begin{smallmatrix} a=3 \\ a=1.5 \\ a\to 0 \end{smallmatrix}\right)\right]$ are also reported.

$(\alpha_1, \alpha_2, \alpha_3)$ of the horizontal angular divergences of the first, second, and third collimators seems to be one for which $\alpha_1 < \alpha_2 < \alpha_3$.

approximation, and could be useful for those cases for which one is interested in a comparison between a possible group of values $(\alpha_1, \alpha_2, \alpha_3)$

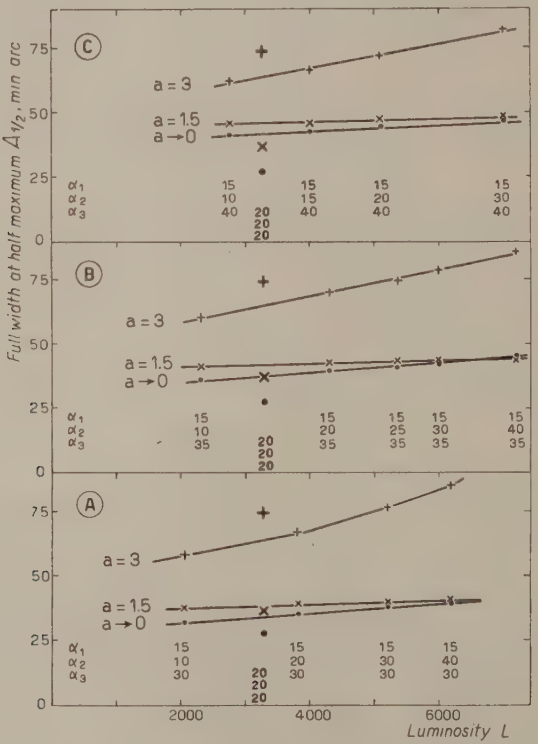

Fig. 4. Full width at half maximum $A_{\frac{1}{2}}$ (min·arc) *vs.* luminosity L, for the following choices of the horizontal angular divergences of the three collimators: (15, α_2, 30), (15, α_2, 35), (15, α_2, 40) respectively in sections A, B, and C, and for the values $a \to 0$, $a = 1.5$, $a = 3$, $\beta = 20$ min·arc. Points $\left[L\,(20, 20, 20), A_{\frac{1}{2}}\left(20, 20, 20; \begin{smallmatrix} a=3 \\ a=1.5 \\ a\to 0 \end{smallmatrix} \right) \right]$ are also reported.

Further, we evaluated the focusing action due to the parallel position.

Our calculations refer to collimators in which total reflection of neutrons can be neglected. Nevertheless, the criteria we established can be thought of as holding in general as a first and a group of values (for instance the group (20, 20, 20)) of known experimental behaviour[4]).

7. Acknowledgments

We wish to thank Professor E. Amaldi for the interest shown in this work.

NUCLEAR INSTRUMENTS 3 (1958) 229–232; NORTH-HOLLAND PUBLISHING CO. – AMSTERDAM

INTERNALLY REFLECTING ČERENKOV COUNTER FOR HIGH ENERGY PROTONS

N. E. BOOTH, F. L. HEREFORD and G. W. HUTCHINSON

Department of Physics, University of Birmingham

Received 15 July 1958

A high energy proton detector is described, which utilises multiple internal reflections of Čerenkov radiation to achieve a sharp energy threshold. The detector is capable of accepting a charged particle beam of cross section comparable to that of the radiator. A preliminary version of the counter has been studied experimentally in the 500–900 MeV proton energy range. The performance of the detector agrees with that expected, when allowance is made for various factors which limit the resolution.

1. Introduction

Čerenkov counters have been widely used in recent years for the detection of relativistic charged particles[1]). In a number of instances sensitivity to the energy of the detected particles has been achieved with optical systems which involve the directional properties of the Čerenkov radiation. In at least two instances[2]) internal reflection of the radiation at a surface of the radiator has been used to this end.

We have recently constructed and tested a simple proton counter which utilises internal reflection to achieve a relatively sharp energy threshold. Although only a preliminary version of the device has been studied experimentally at this time, it seems expedient to report the results in view of a shutdown of the Birmingham Proton Synchrotron, which will delay further experiments for a few months.

2. Description and Theory

In the detector studied (fig. 1) monoenergetic protons of velocity β traversed a series of plane faced slabs of a radiator material with thin sheets of black paper interspersed in the air gaps between adjacent slabs. Consider the emitted cone of Čerenkov radiation of a given wavelength λ, to which there correspond refractive indices n_1 for the radiator and n_2 for air. For a proton incident normal to the slab faces, this cone will strike each radiator-air interface at the angle $\theta_c = \cos^{-1}(1/\beta n_1)$. With increasing proton velocity this angle will approach the critical angel $\theta_R = \sin^{-1}(n_2/n_1)$, beyond which all light will be internally reflected, (i.e. for $1/\beta^2 \leqslant n_1^2 - n_2^2$). Since the electric vector of the radiation is in all cases in the plane of incidence, the probability of reflection rises very steeply[3]) near the angle θ_R. In the detector tested the reflected light was detected by a pair of 5″ Dumont photomultipliers, which viewed the radiators from the sides as shown in fig. 1. Hence, detection necessitated multiple internal reflections, in which

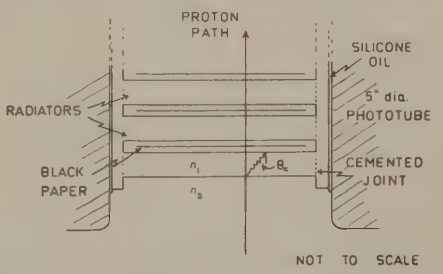

Fig. 1. Schematic diagram of detector. The edges of the radiators parallel to the plane of the paper were polished to improve the light collection efficiency. In the detector studied the radiator consisted of twenty-one 2″ × 3″ slabs of polystyrene $\frac{1}{8}$″ thick.

[1]) For a review of the various techniques employed see J. Marshall, Annual Review of Nuclear Science Vol. 4 (Annual Reviews, Inc., Stanford, 1954) p. 141.

[2]) V. Fitch and R. Motley, Phys. Rev. **101** (1956) 496; L. van Rossum, U.C.R.L. Report No. 391 (1957).

[3]) A. Sommerfeld, Optics (Academic Press, New York, 1954) p. 27.

case the detection probability vs. θ_c approaches a unit step function at θ_R.

For an optically perfect radiator and a unidirectional proton beam, one can compute the expected efficiency of such a counter as a function of proton energy. Initially the influence of multiple scattering and energy loss of the proton will be neglected.

The "detectable" Čerenkov radiation emitted per unit path length of a proton of velocity β will have a spectral distribution determined by the emitted Čerenkov spectrum, weighted by the transmissivity of the radiator medium and the spectral sensitivity of the photomultiplier. We assume the refractive index of air to be 1 and use the dispersion curve for the medium to express the spectral distribution as a function of n[1] (called n, hereafter). Let

$I(n)\mathrm{d}n$ = number of "detectable" photons for which the relative refractive index lies between n and $n + \mathrm{d}n$.

The probability of several internal reflections of the radiation can be approximated as,

$$P(n) = \begin{cases} 1, & \text{for} \quad n \geqslant \dfrac{\sqrt{1+\beta^2}}{\beta} \ (\text{i.e., } \theta_c \geqslant \theta_R) \\ 0, & \text{for} \quad n < \dfrac{\sqrt{1+\beta^2}}{\beta} \ (\text{i.e., } \theta_c < \theta_R) . \end{cases}$$

The expected pulse height for a proton of velocity β is then proportional to the total number of photons reaching the photomultiplier, and is given in arbitrary units by,

$$V(\beta) = \int_0^\infty I(n)\, P(n)\, \mathrm{d}n = \int_{\frac{\sqrt{1+\beta^2}}{\beta}}^{\infty} I(n)\, \mathrm{d}n . \qquad (1)$$

For a given radiator design and photocathode efficiency one can compute the average absolute number of photoelectrons produced in the photomultiplier per counted proton. This number defines the statistical width of the pulse height distribution for protons of a given velocity β, which distribution will exhibit a peak at $V(\beta)$ as given in eq. (1). The distributions for a number of values of β can be represented by Gaussian distributions peaked at $V(\beta)$ and of appropriate width. Integration of the portion of each distribution beyond a chosen bias level then yields the expected detector efficiency (η) vs. proton energy (E).

We have carried through this calculation for the detector studied, which consisted of twenty-one $\frac{1}{8}''$ thick slabs of polystyrene. The result which is shown by the solid curve in fig. 2

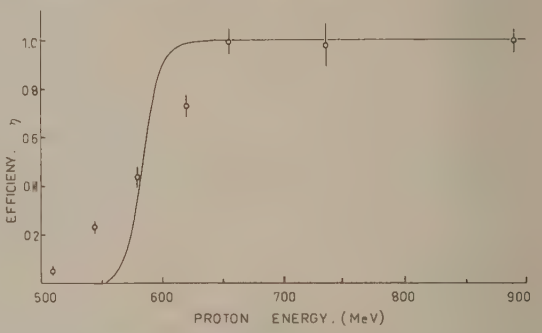

Fig. 2. Efficiency of the detector as a function of proton energy. The solid curve is computed as discussed in the text. The experimental points are shown. The position of the energy scale is uncertain to $\pm$ 10 MeV, but relative energies are much more accurate.

represents the optimum energy resolution of the detector as determined by the dispersion of the radiator medium and by statistical fluctuations.

3. Experimental Results

The detector was studied experimentally in the 500–900 MeV energy range, using the internally scattered proton beam emerging from the synchrotron. A quadrupole lens, heavy alloy collimators, and two $\frac{1}{2}''$ diameter plastic scintillators defined a unidirectional beam to within 0.1 degree. The Čerenkov counter was placed between the two scintillators and carefully oriented with slab faces normal to the proton beam to within 0.25 degree (estimated total error). The signals from the two 5″ photomultipliers were added and displayed on a multi-channel kicksorter, which was gated by triple coincidences of the two scintillation counters and the Čerenkov counter. Pulse height spectra were observed at various proton energies which were selected by expansion of the circulating beam to strike an internal carbon target at different times during the acceleration cycle.

At energies above the threshold region, the spectra exhibited well defined peaks, which deteriorated into continuous distributions over a 75 MeV region near the threshold. Two pulse height spectra for proton energies in the threshold region and just above it are shown in fig. 3.

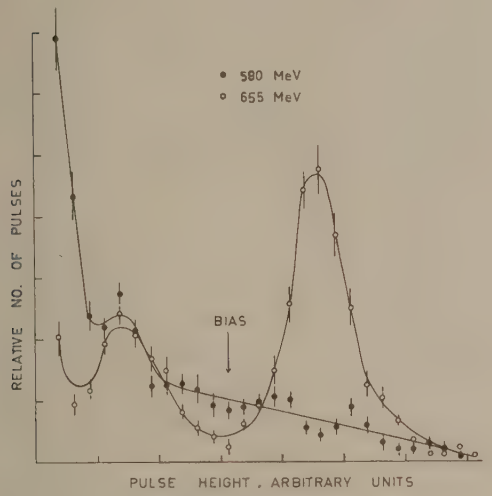

Fig. 3. Pulse height distributions from the polystyrene counter for proton energies of 580 and 655 MeV.

The detection efficiency for various proton energies was determined by integration of the portions of the observed spectra beyond the bias level indicated in fig. 3. The results are shown in fig. 2. It is clear that the detector has a well defined threshold, but the increase of efficiency with energy is less sharp than that predicted by the idealised calculation above.

4. Factors Limiting the Resolution

We discuss now the several reasons for the limited resolution and the extent to which improved design can yield a sharper threshold.

4.1.

Multiple scattering of the protons and possible misalignment of the radiator will result in a broadening and a tilting of the Čerenkov cone with respect to the radiatorair interface. For a sufficiently large angle of tilt this effect would seriously impair the dependence of pulse height upon energy, since approximately one half of the photons would be reflected over a considerable range of energies. However, for small angles the effect is less severe. As stated, the estimated possible error in alignment of the detector tested was 0.25°. The root mean square scattering angle for 700 MeV protons traversing the radiator was 0.35°. The most serious angular error was due to the poor optical quality of the polystyrene used, the faces of which contained ripples of estimated magnitude 0.5°. These factors result in a total angular error of approximately 1°, for which the corresponding uncertainty in energy is about 40 MeV. This results in a decrease in the slope of the computed curve $\eta(E)$. In particular the intercept with $\eta = 0$ will be lowered by 40 MeV and the intercept with $\eta = 1$ raised by 40 MeV. It can be seen (fig. 2) that this correction will bring the computed and observed slopes into rough agreement.

4.2.

The energy loss of protons in the radiator causes a progressive decrease in the Čerenkov angle and a corresponding loss of energy resolution. For the counter tested the proton energy loss was 16 MeV which is not significant relative to the factors discussed immediately above. Actually this energy loss can be corrected for by using gases of progressively lower refractive index in the spaces between the slabs. For example, the difference in refractive indices of pentane and helium at atmospheric pressure is 0.0017, corresponding to a difference in energy threshold of 12 MeV, which would have adequately corrected the detector employed.

4.3.

The ultimate limit of energy resolution is determined by the dispersion of the radiator medium (1) relative to that of the medium (2) between interfaces. For a proton of velocity β and for emitted radiation of wavelength λ, critical reflection occurs for

$$1/\beta^2 = [n_1(\lambda)]^2 - [n_2(\lambda)]^2 . \qquad (2)$$

Thus, an achromatic detector results if this quantity is constant for all wavelengths, that is if,

$$[n_1(\lambda_1)]^2 - [n_2(\lambda_1)]^2 = [n_1(\lambda_2)]^2 - [n_2(\lambda_2)]^2$$

or if

$$[n(\lambda_1)]^2 - [n(\lambda_2)]^2$$

is the same for the two media. Examination of the refractive properties of all possible combinations of materials for which data could be found indicated that a glass of low dispersive power with a gas (e.g. air) between slabs comes closest to satisfying this achromatic criterion.

A second detector consisting of good optical quality slabs of plate glass is under construction and will be tested shortly. This counter should have an energy threshold at about 920 MeV and should yield an energy resolution closely approaching the limit set by dispersion. The increased effect of multiple scattering due to the higher atomic number of the glass will be minimised by use of smaller scintillation counters to define the beam.

For the design of similar counters for use at higher proton energies and with other charged particles, a curve relating $n_2\beta$ and n_1/n_2 for the critical condition is shown in fig. 4. This shows, for example, that a perspex-air counter would have a proton threshold at $\approx$ 1100 MeV and a pion threshold at $\approx$ 165 MeV. At higher energies multiple scattering is less severe; also, smaller differences are required between n_1^2 and n_2^2. The latter fact might make it possible to choose materials giving some measure of achromatism. However, there is also a loss of energy resolution at very high energies due to the fact that $d\beta/dE$ approaches zero.

In some experiments (e.g. anti-proton detection) it is important to use thin counters. Detectors of the type described herein could be made quite thin. The reduction in the number of emitted photons could be partially overcome by adjusting n_1 to yield a large value of θ_c and a correspondingly larger number of photons. At the same time n_2 could be chosen to yield any threshold energy consistent with the considerations in the preceding paragraph.

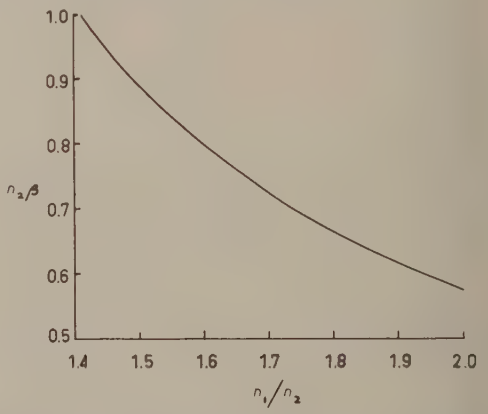

Fig. 4. Plot of $n_2\beta$ *vs.* n_1/n_2 from eq. (2). For $n_2 = 1$ (air) the curve gives the relation between n_1 and β over the range of available optical materials.

Acknowledgments

One of us (N.E.B.) is indebted to I.C.I. for a research fellowship, another (F.L.H.) to the U.S. Educational Commission for a Fulbright Award.

NUCLEAR INSTRUMENTS 3 (1958) 233–236; NORTH-HOLLAND PUBLISHING CO. – AMSTERDAM

NEW TYPE OF ANGULAR-DISTRIBUTION CHAMBER

R. L. CLARKE

Physics Division, Atomic Energy of Canada Limited, Chalk River, Ontario

Received 1 August 1958

A chamber to be used in the observation of charged particles from nuclear reactions is described. This chamber allows observations to be taken over the continuous range — 25° to + 145° with respect to the incident beam without opening the vacuum system.

1. Introduction

When one studies angular distributions of charged particles from a nuclear reaction, a problem that must be met is that of rotating the detection apparatus around the target without breaking the vacuum. The problem becomes somewhat more difficult if the accelerator produces a horizontal beam and the detector accepts outgoing particles lying in a horizontal plane. This is the situation at the Chalk River electrostatic accelerator where the beam is bent by the deflecting magnet on to a horizontal path and the detector, a 180° double-focussing magnet of the type described by Snyder *et al.*[1]), has an approximately horizontal inlet port. This magnet is mounted on a carriage which allows it to rotate around a vertical axis. This axis passes through the beam of the accelerator and the object position of the magnet.

The problem of providing a reaction chamber for similar situations in other laboratories has been met in a number of ways. In the "zipper" chamber devised by Cook[2]), the continuous rotation is achieved by passing the outlet tube through a shaped foot which moves laterally between inflated rubber diaphragms. These gaskets comprise part of the chamber wall, sealing both to each other and to the foot at rest or during motion. Since a large area of rubber is exposed to the system the vacuum attainable is severely limited. In the design used at M.I.T.[3]), Liverpool, and Harwell[4]), the outlet tube is carried by a flat spring-steel strip which forms part of the chamber wall. During rotation the strip moves past fixed gaskets, unrolling from a surplus roll maintained at one end and rolling on to a similar roll at the other. A design in which the continuous rotation is accomplished by lateral deformation of large bellows has been used at Rochester but has a restricted angular range[5]). At Brookhaven[6]) a device somewhat similar to the chamber described in the present work has been built. It uses only rotating seals and permits observations over a range of angles from + 116° to — 116°.

The chamber to be described represents an improvement over the other designs because it allows greater backward angles, — 25° to ± 145°, and because it achieves its motion with the use of only rotating seals, as opposed to sliding seals. These in general give fewer troubles with the vacuum and are easier to move.

2. Kinematical Principles

The kinematical principles of the chamber are illustrated in fig. 1.

[1]) Snyder, Rubin, Fowler and Lauritsen, Rev. Sci. Instr. 21 (1950) 852.

[2]) C. J. Cook, Bull. Am. Phys. Soc. 29 (1954) 24.

[3]) W. W. Buechner, private communication.

[4]) R. Middleton, Harwell, private communication to D. A. Bromley, Atomic Energy of Canada Limited.

[5]) D. A. Bromley, private communication.

[6]) E. N. Hatch, private communication.

In the lower part of the figure the dashed line represents the incoming beam which is horizontal. The solid line OA represents the outgoing beam. If observations are to be carried out at various angles the point A must move on the horizontal circle shown.

limit of the motion of A is reached when $< AOB = \pm 90°$, at which condition C lies in the plane of the circle. These limits correspond to the points M and N in the figure.

The conversion of this system of moving triangles to a mechanical system can be seen

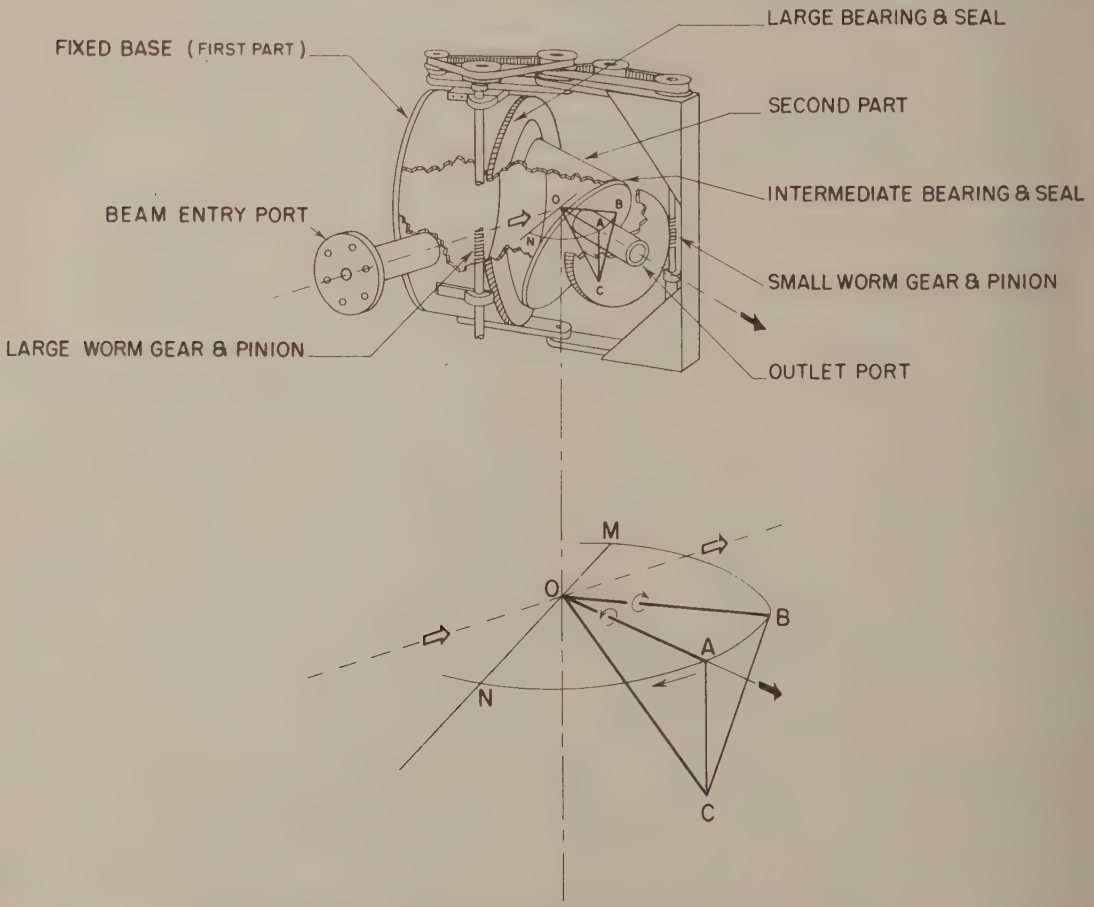

Fig. 1. Kinematical diagram and sketch of the angular-distribution chamber.

The triangles OAC and OBC are constructed so that C lies below the plane of the circle with $< AOC = < BOC = 45°$, and hence AC = BC. The following properties are then obvious. As the point A moves about the circle with B fixed, the planes of the triangles rotate about the axes OA and OB, equally, but in opposite directions. Also, the triangles rotate with respect to each other along the line OC. The

with the aid of the upper portion of fig. 1. The axis OB of the system of triangles is identified with the axis of the large bearing and seal which are mounted on the first (fixed) part of the mechanism. The second part of the mechanism is carried on the large bearing and it in turn carries the intermediate bearing and seal. This intermediate bearing is located so that its axis corresponds to the line OC. Thus, the second

part of the mechanism, having axes OA and OC fixed on it, can move so that it is fixed relative to the triangle BOC. The intermediate bearing carries the third portion which has in it the outlet port. The outlet port is mounted with its axis along OA. Since this third portion has axis OA and OC fixed on it, it can move so that it is fixed relative to triangle AOC. If then the parts associated with the triangles move in the manner of the triangles, as described above, the point A (outlet port) will move in a circle whose plane contains the incoming beam.

It will be seen that all these parts, when assembled, make a vacuum-tight cap over the open side of the stationary part of the chamber.

The property of the triangles, referred to above, of rotating equally in opposite directions makes it possible to provide a motor-actuated drive for the chamber. The system of belts seen at the top of the chamber couple together the two worm gears which are seen to drive the largest and smallest seals. The system shown here does not provide in principle an exactly equal rotation for the two seals. As the axis OA traverses around the horizontal circle MBN, the worm gear driving the pinion attached to the outlet port turns through the same angle as the worm gear driving the large pinion, relative to a fixed co-ordinate system. However, the exact kinematical requirement is that the rotation of the small worm gear (and the small pinion) should be the same in a co-ordinate system fixed along axis OA, as the rotation of the large worm gear (and pinion). The error so introduced has been made negligible by the use of a large number of teeth in the pinions.

This system provides, then, an outlet port whose axis moves in a horizontal plane through an angle of 180° about point O within the chamber. It is to be noted that this point is not in the plane of the large bearing but lies in this figure to the right of the bearing. This, of course, is the position of the target. The angle between the incident beam and the plane of the large bearing has been chosen to be 30° so that the chamber can scan the range $-30°$ to $+150°$ relative to the beam.

3. Description

In the final form of the apparatus the target hangs from an arm which is supported from the back face of the chamber. A manually-operated gearing mechanism allows the target to be turned about the same axis as the outlet port.

Fig. 2 shows the actual apparatus. In fig. 2 the moving parts, outlet port, drive belts and gears, motor, etc. can all be seen. The target mounting is insulated so that the target current can be measured. Although the target lies inside the irregularly shaped intermediate piece, there is enough room around the target for a cage to supress secondary electrons from it. The mounting for the target system has a number of adjustable stops so that it can be removed and replaced without disturbing the alignment once established.

The drive motor seen below the chamber is connected to a system of switches so that as the analysing magnet is moved around its circular track the chamber follows automatically. There are also limit switches which limit the motion to the range $-25°$ to $+144°$.

4. Performance

It was found that due to the flexing of the parts of the chamber as it is moved under vacuum the outlet port moves up and down by as much as $\frac{1}{4}$ in. This is larger than anticipated and could be reduced by more rigid design of the yoke that holds the outlet port. However it is well within the tolerances of the bellows used, and the diameter of the outlet port is such that it does not at any time shadow the beam, provided the limiting aperture is set by the analysing magnet. When the chamber has been used with other detecting systems suitable collimators have been provided.

An effort was made to find a change in pressure within the system as the chamber and analysing magnet traversed several times over their complete range. During these tests the system was pumped in the normal manner by the pumps on the accelerator and the analysing magnet. No measureable change of pressure could be seen at the accelerator.

5. Conclusions

The chamber has been in use intermittently, for a period of several months with the analysing magnet, as originally intended and with a high-pressure ion chamber[7]). On the whole it has performed satisfactorily. In spite of the somewhat irregular geometry of the system it has not proved difficult to align. In future designs the mechanical system should be made more rigid as most of the troubles encountered came from this feature. Due to the massive and rather bulky nature of the chamber it is not well adapted for use when it is necessary to observe gamma rays or neutrons from the target as well as charged particles. This shortcoming could be avoided to a large extent by changing the target mounting and sacrificing some of the monitor ports.

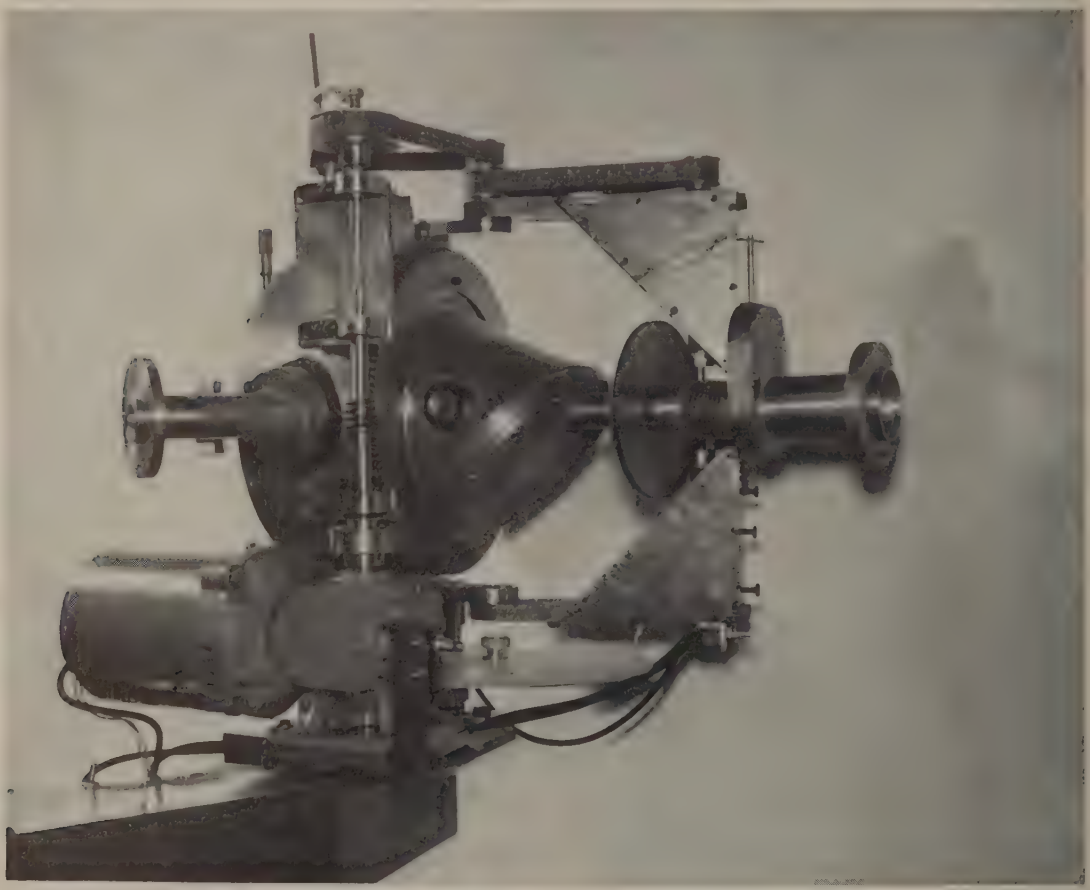

Fig. 2. View of the chamber from the outlet-port side. The analysing magnet, beam collimator, and connection to the accelerator have been removed. The valve and bellows connecting the chamber and the analysing magnet can be seen on the righthand side. The moving parts, viz. the intermediate section and the cover which carries the outlet port, are seen on the right. Also visible are the driving mechanism and supporting yoke for the small worm gear and pinion. The drive motor is below. The beam inlet flange is seen to the left of the body of the chamber.

The design of this chamber arose from experience at Chalk River, and the writer is indebted to his colleagues for many discussions of the requirements of such an angular distribution chamber. During the transition from an idea into a piece of apparatus the co-operation of C. A. Crawford, G. C. Duff, and W. W. Beale of the Chalk River engineering staff was much appreciated.

[7]) D. A. Bromley, to be published.

NUCLEAR INSTRUMENTS 3 (1958) 237–244; NORTH-HOLLAND PUBLISHING CO. – AMSTERDAM

STUDIES OF NEUTRON PRODUCTION IN LINEAR DEUTERIUM PINCHES†

P. OHLIN, K. SIEGBAHN, T. SUNDSTRÖM and S. SVENNERSTEDT

Institute of Physics, Uppsala

Received 22 June 1958

With the experimental set-up, described earlier[8]), further studies of high current linear deuterium pinches have been made. The stabilizing effect of an external magnetic field has been investigated. This effect has appeared in two ways. Firstly, peaks in the voltage curves and dips in the current curves, which are interpreted as due to sausage instabilities, disappear at $B_z > 400$ gauss. Secondly, the number of subsequent pinches is increased by the field and as many as six consecutive pinches have been observed. The dependence of the neutron yield on the magnetic field has been found to be very weak, the yield decreasing only by a factor of 2/3 for 760 gauss. The influence of the gas pressure on the number of neutrons produced has been studied in the region 9 to 30 microns. For $B_z = 0$ a slight decrease in the neutron yield with increasing pressure has been observed. With the field applied the yield seems to be almost independent of the pressure. The resistance of the discharge has been found to decrease to 0.01 ohm within the first tenths of the discharge period. The results are discussed in connection with the results of other investigators.

During the last years fusion reactions in heavy deuterium discharges have attracted a considerable and increasing interest and several publications in this field have appeared, especially on linear discharges[1–23]). One main problem is the stabilization of the pinch and another one is the nature of the mechanism producing fusions.

Two kinds of instabilities are well known, kink instabilities, causing a bending of the discharge channel, and sausage instabilities, which tend to cut off the discharge. A coaxial return conductor, surrounding the discharge tube, has a stabilizing influence on the kink instabilities. If the discharge channel bends and moves towards the tube wall, eddy currents are developed in the return conductor which counteract the kinking. The sausage instabilities may be eliminated by an axial magnetic field. Due to skin effect the discharge starts as a thin sheet close to the tube wall. The magnetic field thus becomes surrounded by a highly conducting plasma layer which moves inwards during the pinch. Since the field is almost unable to penetrate the conducting gas sheet during the time of the discharge it is trapped inside the cylindrical plasma column and thus compressed by the pinch. The result is an increased inner magnetic pressure which prevents the formation of sausage instabilities. According to calculations of, among others, Rosenbluth[20]) and Tayler[18]) a straight cylindrical discharge may under certain conditions be stabilized by a coaxial return conductor and an axial magnetic field. Similar results concerning the effect of a magnetic field have recently been arrived at theoretically by Kruskal and Tuck[23]). According to these authors the field stabilizes the short wave perturbations but leaves some long wave perturbations unstabilized.

The sausage instabilities cause large local rates of increase in inductance giving a potential drop $V = I \cdot \mathrm{d}L/\mathrm{d}t$ across each constriction of the discharge. Such local voltage drops accelerate groups of ions to considerable energy. During their passage through the gas the high energy ions may give rise to a large number of neutrons. This explanation was proposed by Artsimovich *et al.*[4]) and by Colgate[6]), who investigated the phenomenon experimentally and theoretically. In Colgate's experiments the neutron yield was 10^8 or more per discharge at currents of the order of 150 kA. This number is

† References are placed at the end of the article.

much too high to be consistent with a thermonuclear origin of the neutrons. Measurements of recoil proton energies in photographic emulsions clearly showed that the neutrons originated from deuterons with an average energy of about 50 keV colliding with deuterons at rest. Colgate Thus Dunaway (LADC 2943, to be published) reports a vanishing of the neutrons for 100 gauss, Hagerman and Mather[11]) a decrease by a factor of 6 for 23 gauss and Hagerman and Mather[11]), using a bigger condenser bank, a decrease to ½ for 125 gauss. On the other hand

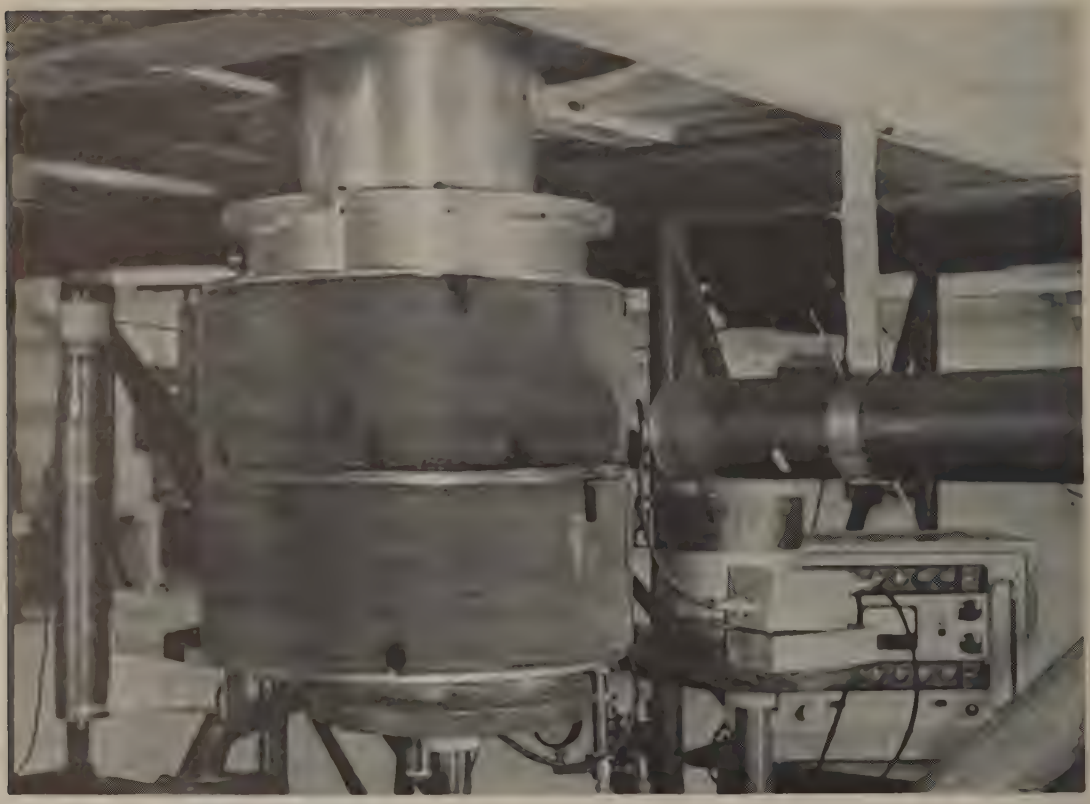

Fig. 1. Straight discharge arrangement, showing aluminium coaxial return conductor, field coils, potential divider (to the left), shielded scintillation counter (to the right) and GM counter in lead shield, containing silver foil and paraffin. Below, deuterium gas inlet.

estimates the diameter of the constrictions necessary to produce such electric fields to a few tenths of a millimeter. This is consistent with the strong dependence of the neutron yield on an axial magnetic field. Colgate found a decrease of the neutron production by a factor of 10 for a field strength of 100 gauss and a factor of 40 for 140 gauss. Similar results concerning the influence of an axial magnetic field have been found by a number of investigators. Bodin and Reynolds[9]) have found a much weaker influence of the magnetic field. In their case the neutron yield, being on the average 10^5 per pulse, decreases only by a factor 10 for a field strength as high as 1000 gauss. Burkhardt and Lovberg[12]) have observed neutrons at B_z-fields as high as 1750 gauss. The yield is, however, very small, of the order of 10^3. An interesting feature is that the neutrons are observed during a period of 4 microseconds around the current

maximum. Such lack of correlation between neutron yield and magnetic field is supposed to be an indication of suppression of sausage instabilities, i.e. the neutrons should not in these cases originate in such instabilities. The mechanism generating the reactions in these cases, is however, not clearly understood.

Investigations of linear pinches in deuterium from part of the fusion program of the Institute of Physics at Uppsala. The apparatus used for experiments of that kind has been described earlier[8]) and will be mentioned only briefly here. The energy is stored in a coaxially wired condenser bank (60 μF, 50 kV) of extremely low inductance (6 mμH). Porcelain discharge tubes of various dimensions have been used. The best results have been obtained with tubes of 60 cm length and 28 cm diameter and the investigations reported in this paper are carried out with tubes of this size. Flat aluminium electrodes which form the ends of the tube are used and the tube is surrounded by a close-fitting aluminium cylinder, forming the return conductor. The whole circuit, including the spark gap and discharge tube, has a minimum inductance of 70 mμH, which can be increased to 520 mμH by means of a series inductance. The voltage across the tube, dI/dt and the neutron bursts are recorded with oscillographs. Absolute measurements of the neutron yield are made by activation of silver foils, which are calibrated by means of a Ra-Be source of known strength (fig. 1).

The present investigation mainly deals with the stabilization of the discharge by an external axial magnetic field and the neutron yield dependence on various factors such as external magnetic field strength, pressure and voltage. The magnetic field is produced by a solenoidal coil surrounding the tube ($B_{max} = 750$ gauss). The work has been carried out in the voltage region 20–32 kV, corresponding to currents from 300 to 500 kA. At higher voltages the pinches decrease gradually and disappear completely at about 40 kV. The pressure has been varied from 9 microns, which is the lowest value at which the discharge starts, to 30 microns. At higher pressures the pinches are less pronounced. A peculiar effect which has been observed in a few percent of the discharges may be mentioned briefly, though its origin is not understood. It consists of an almost undamped oscillation which is seen both in the voltage and in the dI/dt oscillograms. Fig. 2 shows such a voltage oscillogram. During the

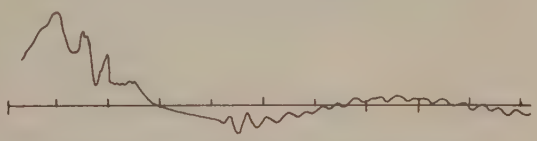

Fig. 2. Voltage oscillogram showing a high frequency oscillation (1.4 Mc/s) starting at the end of the first half period of the discharge (i.e. at $I = 0$. The period of the discharge is 13 μs).

first quarter period of the discharge the oscillogram has a normal shape with several peaks and dips corresponding to compressions and expansions of the plasma (in this case four pinches). At the end of the period the voltage has dropped to zero and starts to increase with reversed sign. When the voltage during this half period has reached its maximum (the current then being zero) a high frequency oscillation starts. This oscillation has the considerable amplitude (about 5 kV, peak to peak) and is nearly undamped, lasting until the main oscillation (the discharge) is damped out. The frequency and the amplitude are nearly constant (at least after a few cycles), the frequency being 1.4 Mc/s. Furthermore the frequency and amplitude, within the errors of measurements, have turned out to be independent of pressure and magnetic field strength. The frequency lies in the region of the positive ion oscillations. At the moment it is, however, not clear if the oscillation observed is really due to positive ion oscillations. An indication of the plasma origin of the oscillation has been obtained as follows. The porcelain tube was taken away and a brass tube mounted in its place, the gas discharge part of the total circuit thus being substituted by a metallic conductor. Hundreds of shots were made under these conditions but the oscillation did not appear.

The general appearance of the oscillograms is

seen in fig. 3 which shows voltage and dI/dt curves and the current as integrated from the dI/dt curve. In fig. 3 three successive pinches

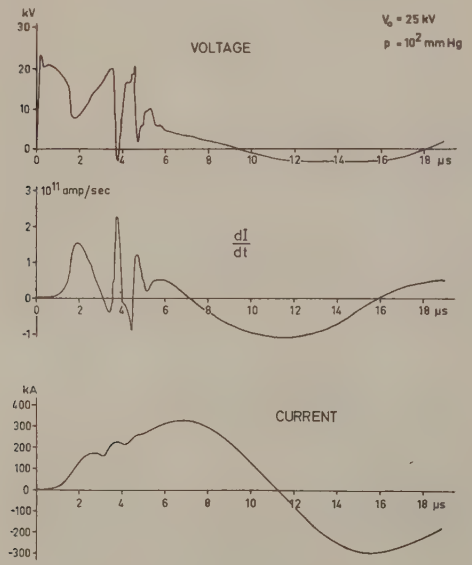

Fig. 3. Voltage and dI/dt oscillograms showing three successive pinches. At the second pinch an instability peak in the voltage curve and the corresponding dip in the dI/dt curve is seen.

are seen during the first quarter cycle of the discharge. They appear as maxima in the voltage diagrams and minima in the dI/dt and current diagrams. If the B_z field is zero or comparatively weak ($<$ 400 gauss) peaks in the voltage and dips in the dI/dt oscillograms are seen in many cases. Such peaks and dips are visible in fig. 3 at the second pinch. They are interpreted as being due to sausage instabilities since such instabilities grow very rapidly and cause a sudden increase in the inductance of the discharge. Another reason for this explanation of the peaks and dips is that they are always accompanied by much heavier neutron bursts than usual. Fig. 4 shows a dI/dt diagram with a very pronounced dip occurring about 3.5 μsec after the start of the discharge (at the second pinch). The lower part of the figure is the oscillogram of the corresponding big neutron burst as recorded with a scintillation counter. As much as 3×10^7 neutrons per discharge has been observed in such cases. This should be compared to 5×10^5–10^6, the number occurring at regular discharges with sufficiently strong magnetic fields. Finally

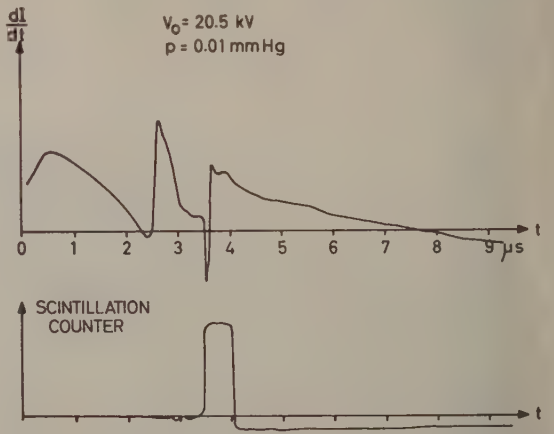

Fig. 4. dI/dt oscillogram showing a large instability dip at the second pinch (upper curve) and the accompanying big neutron burst (lower curve).

the peaks and dips gradually decrease with increasing B_z field and they have never been found for $B_z > 400$ gauss. This in turn indicates that the discharge is stable against sausage

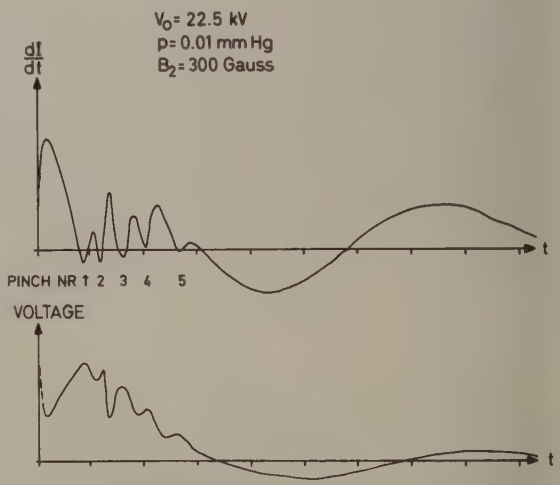

Fig. 5. dI/dt and voltage oscillograms of a discharge with five consecutive pinches.

break-up for an axial field larger than 400 gauss. The stabilizing effect to the magnetic field is seen in another way as well. While the number

of pinches usually is three for $B_z = 0$ it increases with increasing field and for strong fields ($B_{z\,max} = 750$ gauss) five successive pinches are rather common (fig. 5). In a single case as many

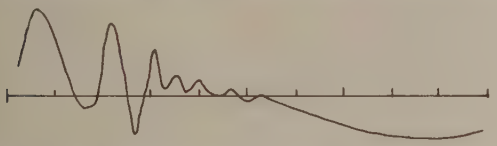

Fig. 6. dI/dt oscillogram showing six successive pinches. $p = 0.009$ mm Hg, $B_z = 750$ gauss, sweep 1 μs/cm, $V_0 = 23$ kV.

as six pinches have been observed, which, as far as we know, has not been reported before. In the dI/dt oscillogram of fig. 6 they are seen as six successive minima occurring during the whole first quarter cycle of the discharge. From the figure it can also be seen that the pinches gradually become less pronounced, the last one occurring immediately before dI/dt definitely passes zero (i.e. current maximum).

Due to the very low inductance in the discharge circuit the period of the discharge is as short as 13 μsec. In order to get a longer period the above mentioned series inductance of maximum 450 mμH was put in, giving a maximum period of 34 μsec. On the whole the phenomena earlier observed remained. The fast dips in the dI/dt oscillograms, associated with big neutron bursts, turned out to be a little more reproducible and more pronounced; one of the heaviest bursts of neutrons ever observed in this work was registered under these conditions. The series inductance, however, introduced a new phenomenon particularly in discharges where comparatively low bank voltages were used. Under these conditions pinches were observed not only in the first quarter period but in several subsequent half periods. Five half periods are seen in fig. 7 and in every one is an indication of the pinch effect. In the last half waves the effect is very small, as can be expected from the decreasing mean current. In fig. 7 the pinches are not very pronounced even in the first half period, probably due to low power, the initial bank voltage being 16 kV. The phenomenon also appeared at higher voltages and was then associated with stronger pinches, though not in so many periods.

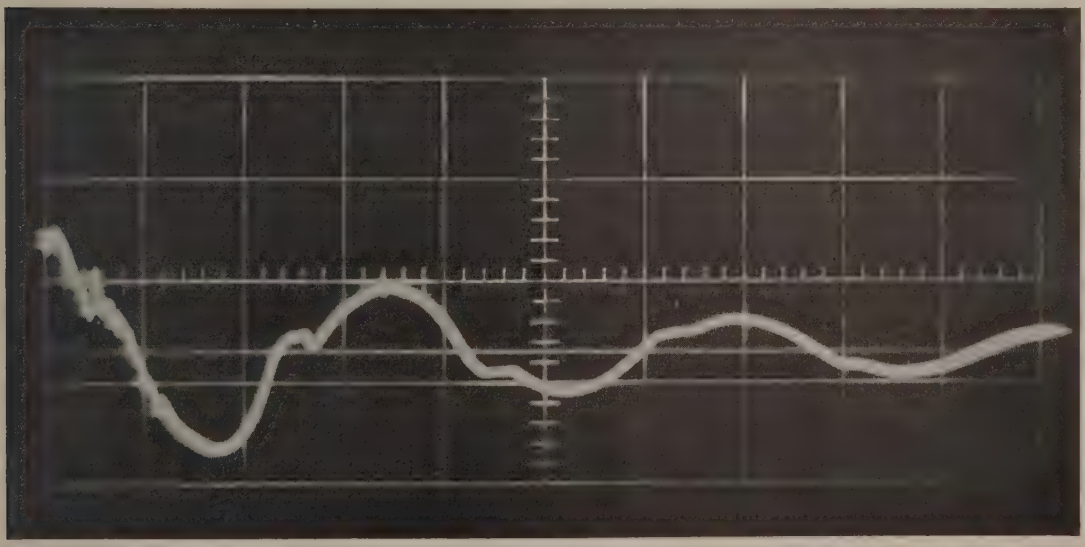

Fig. 7. dI/dt oscillogram showing pinches in the three first half cycles. $p = 0.009$ mm Hg, sweep 10 μs/cm, $V_0 = 66$ kV.

As already mentioned several investigators have found a strong dependence of the neutron yield on the external axial magnetic field. In the present work, however, this influence is found to be rather weak. Fig. 8 shows diagrams of the

neutron yield as a function of B_z at 32 kV and 22.5 kV, the pressure being 9 microns. At 32 kV the yield is 10^6 neutrons/discharge for $B_z = 0$ and it decreases linearly with increasing B_z, and is about 6.5×10^5 for $B_z = 750$ gauss. At 22.5 kV the yield decreases from 7.5×10^5 to 5×10^5 for the same change in B_z. In both cases a field

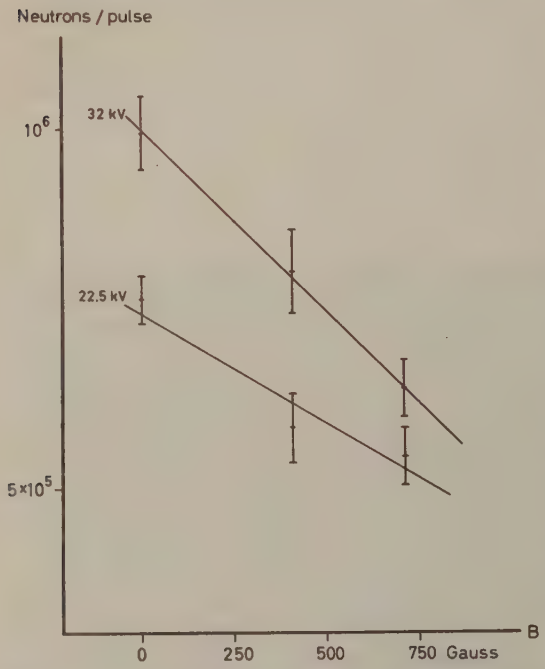

Fig. 8. The neutron yield as a function of externally applied axial magnetic field. $p = 0.009$ mm Hg.

as strong as 750 gauss thus quenches only 1/3 of the neutron production. This weak field dependence, together with the fact that the peaks in the voltage oscillograms and the dips in the dI/dt curves disappear for $B_z > 400$ gauss, indicates that the neutrons generated at such strong fields are not of sausage instability origin. The question whether the neutrons are generated by sausage instabilities, accelerating groups of deuterons, can be settled by measurements of the neutron energy distribution. Such measurements have been made by Colgate *et al.*[13]) who found a neutron energy anisotropy indicating that the neutrons where generated by 50 keV deuterons colliding with deuterons at rest. These measurements were performed without a stabilizing magnetic field. Similar results have been obtained by Hagerman and Mather[11]) who observed a neutron energy distribution corresponding to deuteron energies of about 20 keV. For their measurements a stabilizing field of 200 gauss was used. In both these experiments the neutron yield was very high, of the order of 10^7–10^8, in itself indicating instabilities. In the present work determinations of the neutron energy distribution have not been successful so far owing to the comparatively small number of neutrons. If, however, we assume that the neutrons in our experiments are not due to sausage instabilites, the possibility remains that they are generated by kinking of the discharge. In fact, Colgate[13]) has observed a neutron yield of the order of 10^5 in a linear deuterium pinch, partially stabilized by an axial magnetic field. He recognized the kinking by observing the sudden decrease in the external magnetic field due to the wrapping of the pinch into a helix. Such measurements of the external field have not been performed in the present work but the frequent occurrence of as many as five subsequent pinches make the existence of kink instabilities less probable.

The influence of the deuterium pressure on the neutron production has been studied by some investigators. Thus Colgate[6,13]) found a maximum at 200 microns, the yield being one order of magnitude smaller at 50 microns than at 500 microns. Contrary to this Hagerman and Mather[11]) observed a linear increase of the yield by a factor of 2.3 when the pressure was raised from 70 microns to 200 microns. The neutron yield dependence on the pressure, found in our investigation, is seen in fig. 9. For $B_z = 0$ the number of neutrons per discharge decreases linearly from about 7.7×10^5 to 6×10^5 in the pressure region 9–30 microns. For an external magnetic field of 375 and 750 gauss the yield is about 6×10^5 and remains almost constant within the pressure region in question. It is interesting to note the different course of the yield when the field is off and on, respectively. In the first case it shows, within the

limit of errors, a clearly decreasing tendency. In the second case, on the other hand, it starts from a lower value but seems to be independent of the pressure.

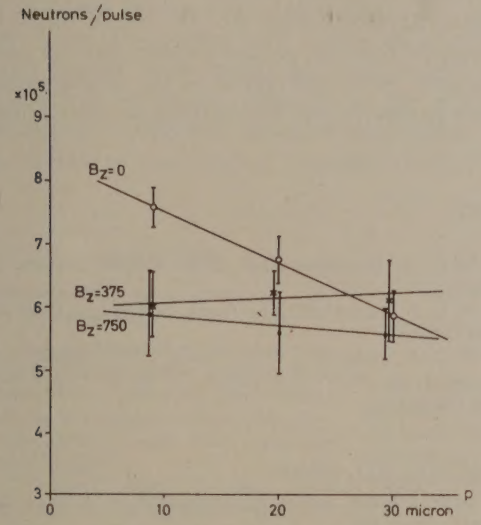

Fig. 9. The neutron yield as a function of the pressure for different values of the external magnetic field.

A calculation of the discharge resistance has been made. The voltage across the tube is given by

$$V = RI + I\mathrm{d}L/\mathrm{d}t + L\mathrm{d}I/\mathrm{d}t\,,$$

where all quantities refer to the discharge tube and its coaxial return conductor only. If a stable pinch of radius r is assumed and the radius of the return conductor is R_0, the inductance of the tube is given by $L = (\mu\mu_0 l/2\pi) \times \ln (R_0/r)$ henry (l = length if the tube). From the equation of motion of the plasma it is possible to find r, the radius of the discharge, rather precisely, especially during the first microsecond. The agreement with the measured time to the first pinch is sufficiently good. From this $\mathrm{d}L/\mathrm{d}t$ and R are calculated. The result is seen in fig. 10. At the start of the discharge R is practically infinite. It drops within 0.5 μs to 10 Ω and, after 1.8 μs, is 0.01 Ω. After this time the method of calculation is not applicable. In fig. 10 the corresponding voltage oscillogram is drawn. From this it is seen that the voltage has a minimum at 1.8 μs and thereafter rises due to the increase in inductance. In the case illustrated, the period of the discharge was 17 μs. Within one tenth of the first period the gas resistance thus drops to a very low value, indicating a fast ionization of the gas.

The result of the present investigation may be summarized as follows: An axial magnetic field has a stabilizing effect on the discharge. The sausage instabilities which are seen as peaks in the voltage oscillograms and dips in the $\mathrm{d}I/\mathrm{d}t$ oscillograms and are always accompanied by very heavy neutron bursts, decrease with rising field and disappear for $B_z > 400$ gauss. The number of neutrons per discharge (as a mean of several shots) is reduced by only one third of the initial value when B_z is increased from zero to 750 gauss. This is not in accordance

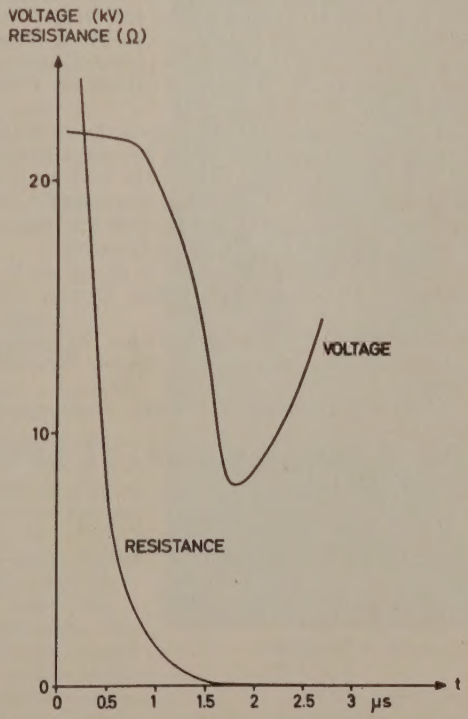

Fig. 10. Variation of the gas resistance during the discharge.

with the results obtained by the majority of investigators, who have observed a much stronger quenching of the neutron production

by a magnetic field. Without a magnetic field the neutron yield shows a slight decrease when the pressure is raised from 9 to 30 microns. With the field applied the yield seems to be independent of the pressure in the region investigated. In this respect different researchers have obtained different results. The resistance of the gas during the first 1.8 μs of the discharge (that is the first tenths of the period) has been calculated and found to drop to 0.01Ω within this time, indicating a fast ionization of the gas during the first stage of the discharge.

Finally it should be mentioned that, due to different geometry, different properties of the electrical circuits used etc., the results found by different research groups are not directly comparable. Such differences in the arrangements may naturally give rise to different phenomena.

References

EXPERIMENTAL WORK

[1]) I. V. Kurchatov, Atomnaya Energiya **1** (1956) 65; J. Nucl. Energy **4** (1957) 193.

[2]) L. A. Artsimovich, A. M. Andrianov, O. A. Bazilevskaya, Y. G. Prokhorov and N. V. Filippov, Atomnaya Energiya **1** (1956) 76; J. Nucl. Energy **4** (1957) 203.

[3]) M. A. Leontovich and S. M. Osovets, Atomnaya Energiya **1** (1956) 81; J. Nucl. Energy **4** (1957) 209.

[4]) L. A. Artsimovich, A. M. Andrianov, E. I. Dobrokhotov, S. Y. Lukyanov, I. M. Podgronyi, V. I. Sinitsyn and N. V. Filippov, Atomanya Energiya **1** (1956) 84; J. Nucl. Energy **4** (1957) 213.

[5]) A. L. Bezbatchenko, I. N. Golovin, D. P. Ivanov, V. D. Kirillov and N. A. Yavlinsky, Atomnaya Energiya **1** (1956) 26; J. Nucl. Energy **5** (1957) 71.

[6]) O. A. Andersson, W. R. Baker, S. A. Colgate, F. C. Gilbert, J. Ise, R. V. Pyle and R. S. White, Paper at Conference on Plasma Physics, Venice (June 1957).

[7]) K. W. Allen, H. A. B. Bodin, S. C. Curran, R. A. Fitch, Paper at Conference on Plasma Physics, Venice (June 1957).

[8]) S. Berglund, R. Nilsson, P. Ohlin, K. Siegbahn, T. Sundström and S. Svennerstedt, Nuclear Instruments **1** (1957) 233.

[9]) H. A. B. Bodin and L. A. Reinolds, Engineering **184** (1957) 538.

[10]) L. C. Burkhardt, R. H. Lovberg and J. A. Phillips, Nature **181** (1958) 224.

[11]) D. C. Hagerman and J. W. Mather, Nature **181** (1958) 226.

[12]) L. C. Burkhardt and R. H. Lovberg, Nature **181** (1958) 228.

[13]) O. A. Andersson, W. R. Baker, S. A. Colgate, H. P. Furth, J. Ise, R. V. Pyle and R. E. Wright, Phys. Rev. **109** (1958) 612.

THEORETICAL WORK

[14]) M. Kruskal and M. Schwarzschild, Proc. Phys. Soc. A **223** (1954) 348.

[15]) V. D. Shrafranov, Atomnaya Energiya **1** (1956) 38; J. Nucl. Energy **5** (1957) 86.

[16]) J. E. Allen, Proc. Phys. Soc. B **70** (1957) 24.

[17]) R. J. Tayler, Proc. Phys. Soc. B **70** (1957) 31.

[18]) R. J. Tayler, Proc. Phys. Soc. B **70** (1957) 1049.

[19]) R. J. Bicherton, Paper at Conference on Plasma Physics, Venice (June 1957).

[20]) M. N. Rosenbluth, Paper at Conference on Plasma Physics, Venice (June 1957).

[21]) M. N. Rosenbluth and C. L. Longmire, Annals of Phys. **1** (1957) 120.

[22]) L. C. Burkhardt, R. E. Dunaway, J. W. Mather, J. A. Phillips, G. A. Sawyer, T. F. Stratton, E. J. Stovall Jr. and J. L. Tuck, J. Appl. Phys. **28** (1957) 519.

[23]) M. Kruskal and J. L. Tuck, Proc. Roy Soc. A **245** (1958) 222.

Spotlight on Industry

We take pleasure in introducing is this issue of *"Nuclear Instruments"* a new section that will appear each month and will feature various happenings of interest in the nuclear industrial world and objective information on products of the nuclear manufacturers. This new section is offered entirely as a service and all nuclear manufacturers are cordially invited to submit clearly objective and descriptive material on their endeavors and product developments for consideration for use in this section.

COUNTERS

Radiation Counter Laboratories, Inc., Nucleonic Park, Skokie, Illinois

Non-photosensitive, all glass halogen quenched geiger counters have transparent, patented, non-metallic conductive cathode surface. Thin glass walls permit high beta radiation transmission.

"Student proof" counters have infinite life; no hysteresis; 200 volt minimum plateaus with less than 3 per cent plateau slope; and can operate up to 280 degree centigrade for 250 days with no change in operating characteristics.

MAGNETIC MEMORY DRUM

Borg-Warner International Corporation, 36 South Wabash Avenue, Chicago 3, Illinois

A miniature memory device for laboratory data processing and computer system applications has been developed.

Designated as model 306, the miniature magnetic memory drum can store over 12 000 bits of data and associated clock and reference information.

The standard laboratory drum measures three and one-half inches in diameter and contains twelve data channels plus clock and fiducial channels. Each channel is 0.070 inch in width with a capacity of 1024 bits. Fiducial and clock channels are an integral part of the aluminium drum.

The drum is belt driven with speeds variable to 15 000 rpm. Runout is 0.0002 inch. Access time is approximately 1.25 millisec.

ACCELERATOR AT BRUSSELS FAIR

High Voltage Engineering Company, Burlington, Mass.

A 2 MeV Van de Graaff particle accelerator standing 9 feet in height dominated the exhibit of High Voltage Engineering Corporation in the International Science Hall of the Brussels World's Fair. To illustrate the actual operating conditions under which a conveyor belt would move when carrying products for irradiation, a rotating table was been installed to show the wide variety of products which can be treated by the machine's beam scanner.

TWIN CHANNEL PULSE GENERATOR

Marshall, The Airport, Cambridge, England

A Twin Channel Pulse Generator has been designed by Marshall of Cambridge as a universal instrument for the development and general testing of electronic equipment.

Extreme flexibility in use is achieved by virtue of the complete independence of the two channels apart from a common repetition frequency. The output pulses are fast-rising, of clean waveform, and at low impedance level.

Precise measurements of the resolution time of coincidence circuits, triggering characteristics of discriminators, and the overload performance of pulse amplifiers are readily made.

A pre-pulse is provided for the purpose of triggering auxiliary apparatus.

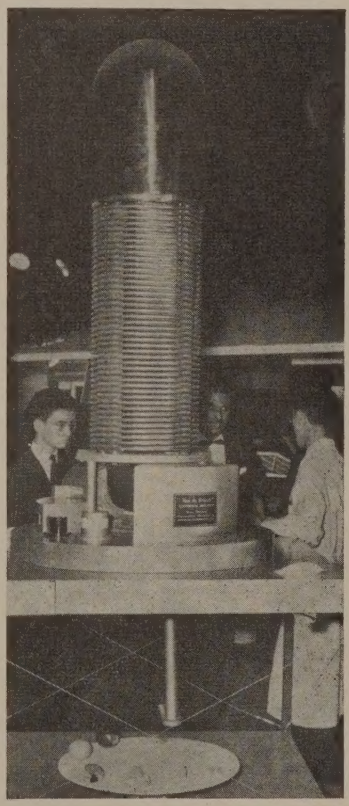

Accelerator at Brussels Fair

The "A" and "B" channel output pulses are independently variable in amplitude, duration, risetime, delay relative to the pre-pulse and polarity.

Pulses from the two channels may be additively mixed if desired so that they appear at a single terminal

A decade attenuator is provided, by

means of which pulses of small amplitude may be produced for injection into high gain amplifiers.

The delay between "A" and "B" pulses is indicated directly by a meter.

Pulse Repetition Frequency: 1 c/s to 100 kc/s from internal generator, any frequency from 100 kc/s downwards when driven by external sine or square wave generator.

Pulse Width: 0.2 to 1000 microseconds in twelve switched steps.

Rise Time: 0.05 to 100 microseconds time constant.

Amplitude: 0.50 volts adjustable by coarse and fine controls.

Polarity: Positive and negative simultaneously available.

Delay: 0.50 milliseconds in ten ranges.

Output Impedance: Positive output approximately 20 ohms, negative approximately 200 ohms. Attenuator impedance is 75 ohms.

Accuracy: The accuracy of continuously variable parameters is approximately $\pm$ 1% of full scale, and of switched quantities approximately $\pm$ 1% of the selected value.

ATOMIC EDUCATION EQUIPMENT

Nucleonic Corporation of America, 196 Degraw Street, Brooklyn 31, N.Y.

An expanded line of atomic education equipment for college and high school science instruction, as well as research, medical and industrial training programs, is now available. Some of this equipment was originally manufactured for the A.E.C.'s science training program and has been improved to perform actual research measurements.

Included are the following items:

Atomic Laboratory, featuring a precise scaler-ratemeter and accessories that permit not only simple or complex classroom experiments but actual research applications, too.

Atomaster, designed for high school and college lectures and demonstrations of elementary atomic principles, nuclear properties, and biological tracer studies.

Ray-Actor, a working reactor that behaves as a standard reactor in all important phases of reactor operation.

Rayotron, a safe electrostatic generator and particle accelerator that produces high voltages, X-rays, and many dramatic phenomena.

Raymaster, a diffusion cloud chamber that shows cosmic ray, alpha, and beta tracks.

EXPANSION AND CHANGES

Stone & Webster Engineering Corporation, 49 Federal Street, Boston, Mass.

This corporation announced expansion of its foreign operations in Europe with the formation of a Netherlands subsidiary and a further integration of its British, French and Australian subsidiaries.

The Dutch subsidiary will be known as Stone & Webster Engineering N.V. and will have headquarters in The Hague.

In Britain, E. B. Badger & Sons, Ltd. becomes Stone & Webster Engineering Limited. In France, the French subsidiary formerly known as Etablissements Badger, S.A., will be known as Stone & Webster Engineering S.A.

In Australia, the subsidiary company known as E. B. Badger & Sons Pty. Limited, will be known as Stone & Webster Pty., Limited.

NEW SYNCHRO-CYCLOTRON IN FRANCE

N.V. Philips' Gloeilampenfabrieken, Eindhoven, Holland

During June of this year a synchro-cyclotron built by N.V. Philips' Gloeilampenfabrieken of Eindhoven, Holland was put into operation and officially handed over to the University of Paris, Laboratoire de Physique Nucléaire in Orsay. During the testing programme carried out in the Laboratoire de Physique Nucléaire, the machine designed for a proton beam of at least 150 MeV, operated at 165 MeV. The internal beam current was found to exceed 5 μA. Work on the machine continues and additional parts for the oscillator will be installed, so that the machine can also supply a deuteron beam of 80 MeV. Furthermore, in the Philips factories in Eindhoven the construction of a beam extraction system is ready and these various parts will also be installed in the coming months. The whole project is scheduled to be delivered at the end of this year.

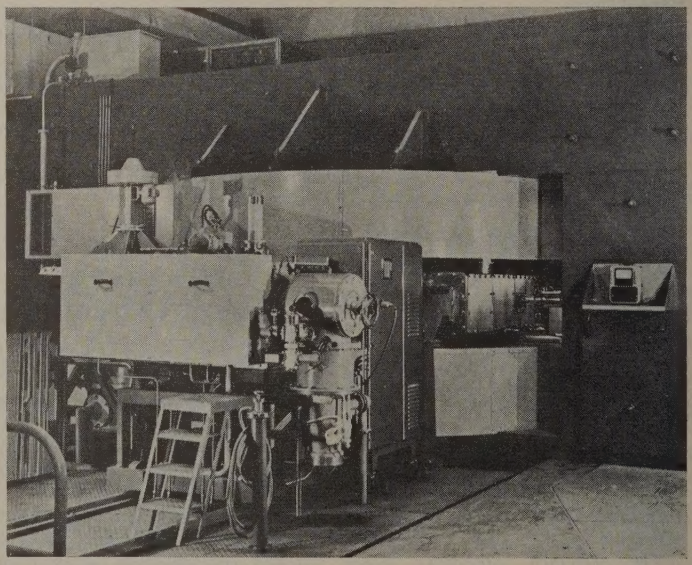

150 MeV synchro-cyclotron seen from the modulator end.